



Faculty of Graduate Studies

**Coordination Complexes of Transition Metals i.e. Zn(II) with
Rosmarinic Acid and Various Nitrogen Ligands. Synthesis,
Characterization, and Biological activity.**

معقدات جديدة ناتجة من تفاعل بعض العناصر الانتقالية مثل الزنك ثنائي الشحنة المرتبط مع حمض الروزمارينك والقواعد النيتروجينية المختلفة. التحضير، التركيب والنشاط البيولوجي.

**This Thesis is Submitted in Partial Fulfillment of the
Requirements for the Degree of Masters in Applied Chemistry at
the Faculty of Graduate Studies. Birzeit University, Ramallah,
Palestine.**

By

Fatima. I. Hamdan

**Under the Supervision of
Prof. Hijazi Abu Ali**

January, 2021

**Coordination Complexes of Transition Metals i.e. Zn(II) with
Rosmarinic Acid and Various Nitrogen Ligands. Synthesis,
Characterization, and Biological activity.**

By

Fatima. I. Hamdan

This thesis was defended successfully on 1/02/2021 and approved by:

Committee Members

Signature

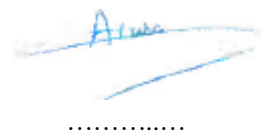
Prof. Hijazi Abu Ali



Supervisor

Department of Chemistry, Birzeit University

Dr. Arwa Abu Khweek

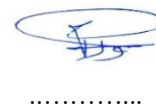


.....

Member of thesis committee

Department of Biology and Biochemistry, Birzeit University

Dr. Wadie Sultan



.....

Member of thesis committee

Department of Chemistry, Al-Quds University

ACKNOWLEDGMENTS

I would like express my special appreciation and thanks to many people for helping and supporting me during my study. I heartily thank my master thesis supervisor Prof. Hijazi Abu Ali. I have learned many things since I became Prof. Hijazi's student. I would like to thank you for encouraging my research and spending time instructing me how to write a paper and how to search literature. His friendly guidance and expert advice have been invaluable to me throughout all stages of this work. I am also grateful to thank my committee members, Dr. Wadie Sultan and Dr. Arwa Abu Khweek for spending their valuable time reading, discussing and providing useful suggestions about this thesis. Special appreciation and thanks to Dr. Arwa Abu Khweek, for helping me to do and complete the biological activity section of this work.

I sincerely thank all of the members of the Chemistry Department, especially Dr. Ibrahim Shalash, Mr. Azmi Dudin, Mr. Assem Mubarak, and Mr. Adi Qamhieh for their support, kindness, patience, and for providing excellent work conditions. Special thanks are given to Mr. Munther Matani and Mr. Rateb Mohammad for their help and patience in doing and completing the biological activity section of this work.

Last but not the least important, I owe more than thanks to my parents, brothers, sisters, family and friends for their encouragement and support throughout my life.

Birzeit, Jan, 2021

Fatima. I. Hamdan

TABLE of CONTENTS

ACKNOWLEDGMENTS.....	I
TABLE of CONTENTS.....	II
LIST of FIGURES.....	IV
LIST of TABLES.....	VII
LIST of SCHEMES.....	VIII
ABBREVIATIONS.....	IX
ABSTRACT.....	X
ملخص.....	XII
1. INTRODUCTION.....	1
1.1. General Principles.....	1
1.2. Zinc Metal Chemistry.....	3
1.3. Zinc Metal in the Human Body.....	4
1.4. Biological Role of Zinc.....	7
1.5. Natural Foods that Contain Zinc.....	9
1.6. Intake of Zinc.....	10
1.7. Excess of Zinc.....	11
1.8. Zinc Metal in Medicine.....	12
1.9. Coordination Chemistry of Zinc.....	16
1.10. Metal Carboxylates.....	17
1.10.1 Zinc Carboxylate Complexes.....	20
1.10.2 Zinc Complexes with Nitrogen Ligands.....	24
1.11. Rosmarinic Acid.....	27
1.12. Anti-bacterial Activity Study.....	31
1.13. Kinetic Measurements of BNPP Hydrolysis.....	33
1.14. Aim of the Project.....	37
2. EXPERIMENTAL.....	37
2.1. Chemicals, reagents, and biological species.....	37
2.2. Instrumentation.....	38

2.3. Synthesis and characterization of zinc with rosmarinic acid complexes	39
2.3.1 Synthesis of zinc with rosmarinic acid [Zn(RA)_n] (1)	39
2.3.2 Synthesis of zinc rosmarinic acid with 2-(methylamino) pyridine complex [Zn(RA)_n(2-(methylamino) py)_m] (2)	40
2.3.3 Synthesis of zinc rosmarinic acid with 2,2'-pyridine complex [Zn(RA)_n(2,2'-bipy)_m] (3)	41
2.3.4 Synthesis of zinc rosmarinic acid with 4,4'-pyridine complex [Zn(RA)_n(4,4'-bipy)_m] (4)	43
2.3.5 Synthesis of zinc rosmarinic acid with 2,9-dimethyl-1, 10-phenanthroline complex [Zn(RA)_n(2,9-dmp)_m] (5)	44
2.3.6. Synthesis of zinc rosmarinic acid with 2-aminopyridine complex [Zn(RA)_n(2-ampy)_m] (6)	45
2.4. In-vitro Biological Activity	46
2.4.1. Agar -well diffusion method	46
2.4.2. Tube dilution method	47
2.5. Kinetic studies of the hydrolysis reaction of BNPP	48
3. RESULTS AND DISSCUTION	49
3.1. Synthesis of zinc rosmarinic acid complexes	49
3.2. ¹H and ¹³C{¹H} NMR spectral results	54
3.3. Infrared spectra	67
3.4. Electronic Absorption Spectral Results	70
3.5. Bioassay Antibacterial Activity	73
3.6. Kinetic Measurements of BNPP Hydrolysis Results	80
4. CONCLUSIONS	89
5. REFERENCES	92
6. APPENDICIES	104
Appendix A: ¹H-NMR spectra of complexes 2-6	104
Appendix B: IR spectra of complexes 2-6	106
Appendix C: UV-Vis spectra of complexes 2-6	109

LIST of FIGURES

Figure 1. The Periodic Table of the elements highlighting those elements used by living organisms.	1
Figure 2. Schematic representation for the storage and distribution of zinc in the human body.	5
Figure 3. Catalytic, structural, and cocatalytic zinc binding sites in enzymes. The letters D, E and H refer to the amino acids, aspartic acid, glutamic acid and histidine, respectively.	5
Figure 4. The Zn ion (green), coordinated by two histidine side chains in Zn fingers.	7
Figure 5. Some of the key areas of medicinal inorganic chemistry.	14
Figure 6. Molecular structure of cisplatin (a) 2D, (b) 3D, respectively.	14
Figure 7. Role of zinc in diabetes with related disease conditions.	15
Figure 8. Coordination modes of carboxylate group: <i>syn</i> monodentate (1a), <i>anti</i> monodentate (1b), <i>syn-syn</i> symmetric chelate (2a), <i>syn-syn</i> asymmetric chelate (2b), chelating bridging (3), <i>syn-syn</i> bridging (4a), <i>syn-anti</i> bridging (4b), <i>anti-anti</i> bridging (4c), monoatomic bridging (5).	18
Figure 9. Overall structure and example of a Zn(II) site in a self-assembling protein crypt and templated by disulfide bonds. (a) Overlay of protein backbones of the apo and Zn(II)-bound forms of C81/C96 RIDC ₄ . (b) One of four ZnHis ₃ (H ₂ O) sites in A74/C81/C96 RIDC ₄	21
Figure 10. (a) Amino acid sequence of the zinc finger parent peptide. (b) Natural zinc finger fold ($\alpha\beta\beta$ structure) and (c) zinc finger $\alpha\beta\beta$ fold modified as a metallohydrolase.	21
Figure 11. Molecular structure of alkoxy zinc carboxylate.	22
Figure 12. The basic unit of (a) zinc benzoate structure. (b) zinc crotonate unit. (c) zinc crotonate polymer.	23
Figure 13. The bonding mode of carboxylates with metals (a) monodentate, [Zn(sul) ₂ .2H ₂ O] (b) bidentate chelate, [Zn(furo) ₂ (quin) ₂]. (sul = sulindac, furo= furosemide, quin= quinoline).	24

Figure 14. Heterocyclic N-donor ligands.	26
Figure 15. The chemical structure of rosmarinic acid (C ₁₈ H ₁₆ O ₈).	28
Figure 16. Potential functions of rosmarinic acid.	29
Figure 17. Structure of BNPP.	34
Figure 18. ¹ H-NMR spectra of complex 1	59
Figure 19. ¹³ C{ ¹ H}-NMR spectra of complex 1	59
Figure 20. IR spectra of RA (red), Na _{RA} (black), and complex 1 (blue).	69
Figure 21. UV-Vis spectra of RA and complex 1	71
Figure 22. Agar diffusion plates.	80
Figure 23. Plots of absorbance at 400 nm vs. time for BNPP hydrolysis by complex 1 in DMSO/HEPEs buffer solution with different temperature under the selected conditions (pH = 7.40, [complex 1] = 5.8 x 10 ⁻⁴ M, [HEPEs buffer] = 50 x 10 ⁻⁶ M and [BNPP] = 1x10 ⁻⁴ M).	81
Figure 24. Plots of absorbance at 400 nm vs. time for BNPP hydrolysis by complex 1 in DMSO/HEPEs buffer solution with different solution pH values under the selected conditions (T = 25 °C, [complex 1] = 5.8 x 10 ⁻⁴ M, [HEPEs buffer] = 50 x 10 ⁻⁶ M and [BNPP] = 1x10 ⁻⁴ M).	82
Figure 25. Plots of absorbance at 400 nm vs. time for BNPP hydrolysis by complex 3 in DMSO/HEPEs buffer solution with different temperature under the selected conditions (pH = 7.47, [complex 3] = 2.0 x 10 ⁻⁴ M, [HEPEs buffer] = 50 x 10 ⁻⁶ M and [BNPP] = 1x10 ⁻⁴ M).	83
Figure 26. Plots of absorbance at 400 nm vs. time for BNPP hydrolysis by complex 3 in DMSO/HEPEs buffer solution with different solution pH values under the selected conditions (T = 25 °C, [complex 1] = 2 x 10 ⁻⁴ M, [HEPEs buffer] = 50 x 10 ⁻⁶ M and [BNPP] = 1x10 ⁻⁴ M).	84
Figure 27. Plots of absorbance at 400 nm vs. time for BNPP hydrolysis by complex 3 in DMSO/HEPEs buffer solution with different concentration of complex 3 under the selected conditions (pH = 7.47, T = 37 °C, [HEPEs buffer] = 50 x 10 ⁻⁶ M and [BNPP] = 1x10 ⁻⁴ M).	85

- Figure 28.** Plots of absorbance at 400 nm vs. time for BNPP hydrolysis by complex **4** in DMSO/HEPEs buffer solution with different concentration of complex **4** under the selected conditions (pH = 6.99, T = 41 °C, [HEPEs buffer] = 50×10^{-6} M and [BNPP] = 1×10^{-4} M)..86
- Figure 29.** Second order rate for complex **3** with different [BNPP] under the selected conditions (pH = 7.91, temp = 37 °C and [complex 3] = 2×10^{-4} M).....87

LIST of TABLES

Table 1: Some of essential metal-containing biomolecules, examples and their functional biological system.	2
Table 2. Zinc content of some foods.	10
Table 3. A summary for some metals used in medicine.	13
Table 4. Stereochemistry of some Zn(II) compounds.	17
Table 5. Bioactive effects of rosmarinic acid.	31
Table 6. Analytical and physical data of the ligands and their complexes.	53
Table 7. ^1H NMR spectral data for 1 , Na_{RA} , and RA.	55
Table 8. ^{13}C -NMR spectral data for 1 , Na_{RA} , and RA.	57
Table 9. ^1H NMR spectral data for 2 , and 2-(methylamino)py.	60
Table 10. ^1H NMR spectral data for 3 , and 2,2'-bipy.	61
Table 11. ^1H NMR spectral data for 4 , and 4,4'-bipy.	62
Table 12. ^1H NMR spectral data for 5 , and 2,9-dmphen.	63
Table 13. ^1H NMR spectral data for 6 , and 2-ampy.	64
Table 14. Important IR spectral data of the RA, $\text{Na}_{(\text{RA})}$ and complex 1	68
Table 15. Important IR spectral data (in cm^{-1}) of complexes 2-6	70
Table 16. Electronic spectral data (nm) of the RA and complex 1	71
Table 17. Electronic spectral data (nm) of the ligands and their complexes.	72
Table 18. Results of antibacterial bioassay against Gram- positive bacteria (concentration used in 12 mg ml^{-1} of DMSO) ^a	75
Table 19. Results of antibacterial bioassay against Gram- negative bacteria (concentration used in 12 mg ml^{-1} of DMSO).	77
Table 20. In-vitro antibacterial activity data of complexes 1-6 at 18 mg/ml	79
Table 21. Kinetic parameters of the BNPP hydrolysis for complexes 1 , 3 and 4 at different BNPP concentrations.	88

LIST of SCHEMES

Scheme 1. The possible mechanism for the cleavage of BNPP catalyzed by mononuclear Zn(II):OH ⁻ complex of Zn:([12] aneN ₃).	36
Scheme 2. Proposed structure of [(Zn(RA) _n].	50
Scheme 3. Synthesis of complexes 2-4	51
Scheme 4. Synthesis of complexes 5 and 6	52

ABBREVIATIONS

RA	Rosmarinic acid
2-ampy	2-Aminopyridine
2,2'-bipy	2,2'-Bipyridine
4,4'-bipy	4,4'-Bipyridine
2,9-dmphen	2,9-Dimethyl-1,10-Phenanthroline
IR	Infrared
Ar	Aromatic
NMR	Nuclear Magnetic Resonance
DMSO	Dimethyl Sulfoxide
IZD	Inhibition Zone Diameter
MIC	Minimum Inhibition Concentration
NMR multiplicity	s = Singlet d = Doublet t = Triplet m = Multiplet dd = Doublet of doublet
m.p.	Melting point

ABSTRACT

Six Zn(II) complexes of rosmarinic acid and nitrogen-donor ligands, formulating as $[(\text{Zn}(\text{RA})_2)]$ (**1**), $[\text{Zn}(\text{RA})_2(2\text{-(methylamino)py})_2]$ (**2**), $[\text{Zn}(\text{RA})_2(2,2'\text{-bipy})]$ (**3**), $[\text{Zn}(\text{RA})_4(4,4'\text{-bipy})]$ (**4**), $[\text{Zn}(\text{RA})_2(2,9\text{-dmp})]$ (**5**), and $[\text{Zn}(\text{RA})(2\text{-ampy})_2]$ (**6**) were synthesized and characterized using IR, $^1\text{H-NMR}$, $^{13}\text{C}\{^1\text{H}\}\text{-NMR}$ and UV-Vis spectrometry and other physical properties.

The *in-vitro* antibacterial activity of the synthesized complexes was tested against Gram-positive (*S. epidermidis*, *M. luteus*, *B. subtilis*, *S. aureus*, and *E. faecalis*) and Gram-negative (*K. pneumonia*, *P. aeruginosa*, *E. coli*, and *P. mirabilis*) bacteria using agar diffusion method. All prepared complexes have exhibited considerable antibacterial activity against different Gram-positive and Gram-negative bacteria. Complex **1** has shown higher antibacterial activity against the tested bacteria of *P. aeruginosa* and *K. pneumonia* compared to RA. Complexes **5** and **6** have shown higher antibacterial activity than their parent ligands.

The rate of BNPP (bis(4-nitrophenyl)phosphate) hydrolysis was determined in order to study the effect of zinc complexes on the phosphate hydrolysis. According to the obtained results the hydrolysis

rate of BNPP for the **1**, **3**, and **4** complexes as follow: 5.2 at 25 °C, 4.2 at 37 °C, and 8.3 at 41 °C, respectively.

ملخص

يعرض هذا البحث تحضير مركبات جديدة من تفاعل أيون الزنك ثنائي الشحنة مع حمض الروزمارينك والقواعد النيتروجينية المختلفة :

$[(Zn(RA)_2]$ (1), $[Zn(RA)_2(2-(methylamino)py)_2]$ (2), $[Zn(RA)_2(2,2'-bipy)]$ (3), $[Zn(RA)_4(4,4'-bipy)]$ (4), $[Zn(RA)_2(2,9-dmp)]$ (5), and $[Zn(RA)(2-ampy)_2]$ (6).

تم تشخيص وتحديد التركيب الافتراضي لهذه المركبات باستخدام الأجهزة التالية: مطياف الأشعة تحت الحمراء وجهاز مطياف الأشعة فوق البنفسجية والمرئية وجهاز الرنين النووي المغناطيسي (الهيدروجيني-1 والكروموني-13) و خصائص فيزيائية أخرى.

تمت دراسة الأنشطة الحيوية للمركبات ضد أربعة أنواع من الغرام سلبية البكتيريا *Proteus mirabilis*, *Escherichia coli*, *pneumonia Klebsiella* and *Pseudomonas aeruginosa* وخمسة أنواع من الغرام إيجابية البكتيريا *Staphylococcus aureus*, *Staphylococcus epidermidis*, *Bacillus subtilis*, *Micrococcus luteus*, and *Enterococcus faecalis* باستخدام طريقة الانتشار في الأجار.

جميع المركبات التي تم تحضيرها أظهرت فعالية ضد أنواع معينة من البكتيريا المستخدمة. تم أيضا مقارنة الفعالية ضد البكتيريا المستخدمة للمركبات التالية: (1-6) مع حمض الروزمارينك والقواعد النيتروجينية الحرة لدراسة مدى التغير في فعالية هذه المركبات عند ارتباطها في مركبات معقدة. أظهر المركبين 5 و6 فعالية ضد البكتيريا أعلى من حمض الروزمارينك والقواعد النيتروجينية الحرة لهذان المركبان. بالإضافة الى قياس سرعة تحلل bis-(4-nitrophenyl) phosphate عند درجات حرارة و تراكيز وقيم pH مختلفة واستنادا الى الدراسة كانت سرعة التحلل للمركبات التالية 1, 3, 4 كالتالي:

1: (5.2 at 25 °C), 3: (4.2 at 37 °C), 4: (8.3 at 41°C).

cellular components such as nucleic acid, proteins, lipids-membranes, metabolites, and polysaccharides, Table 1.^{1,3,4}

Table 1: Example of essential metal-containing biomolecules and their functional biological system.⁹

Category	Biological function	Examples (metal ion involved)
Nonproteins	metal transport and structural	siderophores (Fe); skeletal (Ca, Si)
Proteins	photo-redox	chlorophyll (Mg)
	oxygen transport	hemocyanin (Cu)
Enzymes	structural	Zn fingers (Zn)
	electron transfer	cytochromes (Fe); azurin (Cu)
	oxidation of phenol	catechole oxidase (Cu)
	oxido – reductases	phenoxazinone synthase (Cu); nitrogenases (Fe, Mo, V)
	isomerases and synthesases	vitamin B12 coenzymes (Co)

Despite the great diversity that is shown, yet life cannot continue with only these basic elements.¹ Over 20 additional elements are important for most species to do their function.¹ The six elements are required for conduction of nerve impulses, regulation of gene expression, hydrolysis and formation of adenosine tri-phosphate (ATP), control of cellular processes and signaling, and catalysis of many key reactions of metabolic.^{1,3} The goal of biological inorganic chemistry is to study and understand the roles of metallic and nonmetallic elements that play in a biological system.¹

The concentration and distribution of several metals among the different cell compartments as well as their incorporation into metalloproteinase is hardly controlled.⁵⁻⁷ For a healthy phenotype, a correct balance of the equilibrium in these control processes is needed.⁴ However, less than half of the known metals are considered to be toxic to humans and animals and there are some of the metals found to be carcinogens to humans and animals including Cr, As, Ni, Cd, and Be.^{8,9}

1.2. Zinc Metal Chemistry

Zinc is considered as the most common element in the earth's crust and trace element in the body of human, having atomic weight 65.37 and atomic number 30 and is essential in the living world.¹⁰ The zinc(II) cation does not undergo oxidation-reduction reactions because its filled d-shell, which is in contrast to other transition metal ions, such as copper and iron.⁴ Moreover, because of its small radius to charge ratio (i.e. 0.83 Å, coordination number (CN) = 6) Zn^{2+} has Lewis acid characteristics and consequently forms strong covalent bonds with O, N, and S donors.¹¹ The electron configuration of Zn^{2+} complexes prefer octahedral geometry, still CN = 4 and CN = 5 geometries are also possible and found in literature.¹¹

1.3. Zinc Metal in the Human Body

About 2-4 grams of zinc are distributed in the human body, Figure 2.¹³

The large amount of zinc is found in the organs (such as brain, kidney, and liver), tissues, bones, fluids, as well as cells.¹⁴ The highest concentrations of Zn is found in the prostate and parts of the eye.¹⁴

Zinc is considered as the 2nd most abundant transition metal in organisms after iron and is considered the only metal that appears in all six classes of enzyme (hydrolases, oxidoreductases, lyases, transferases ligases and isomerases).^{11,13,14}

The reactivity of the enzyme and its function is determined by both geometric and binding characteristic of Zn^{2+} complexes with ligand as well as three primary Zn^{+2} ligand binding sites are known as catalytic, structural, and co-catalytic, Figure 3.¹⁶

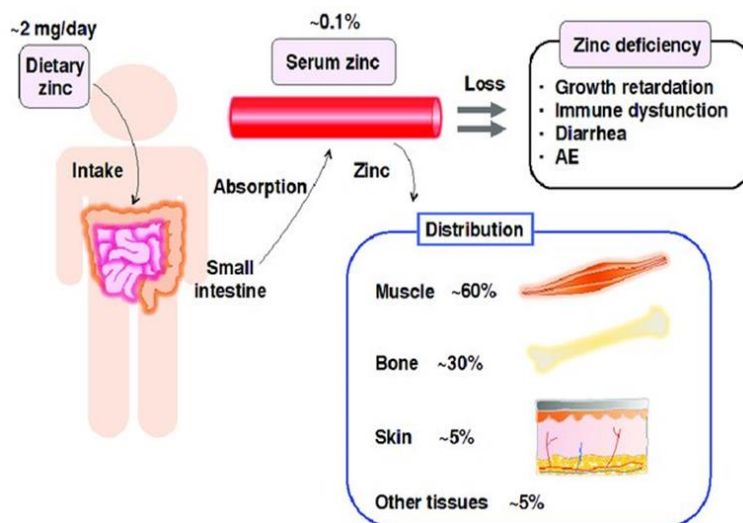


Figure 2. Schematic representation for the storage and distribution of zinc in the human body.¹⁵

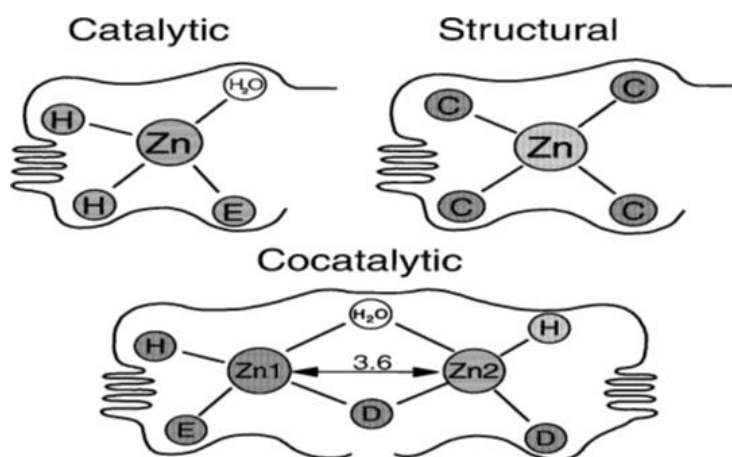


Figure 3. Catalytic, structural, and cocatalytic zinc binding sites in enzymes. The letters D, E and H refer to the amino acids, aspartic acid, glutamic acid and histidine, respectively.¹⁶

For catalytic Zn sites, Zn is directly participating in the catalytic function of the enzyme.¹⁶ In general, a catalytic zinc ions are coordinated to the amino acid of histidine (His), aspartic acid (Asp), glutamic acid (Glu), and cysteine (Cys).^{11,16} Because of its ability to disperse charge through hydrogen bonding of its free nitrogen atom, His is being the predominant amino acid chosen.^{11,16}

In structural Zn sites, there are four protein ligands (frequently cysteine) in the structural site with no bounded water molecule.¹⁶ Alcohol dehydrogenases are considered the first enzymes that have been identified to have a structural zinc site as well as the regulatory subunit of aspartate carbamoyltransferase.¹⁶ In cocatalytic sites, Zn ion can be used for structural, regulatory, and catalytic roles.¹¹

At such sites, two or three Zn ions found in close proximity and are coordinated to amino acid residues, especially glutamic acid (Glu) or aspartic acid (Asp), but His and may be a water molecule are also found, but not Cys.¹⁶ Zinc binding sites also found in a wide range of other membrane lipids, proteins, and molecules of DNA/RNA, Figure 4.¹⁶

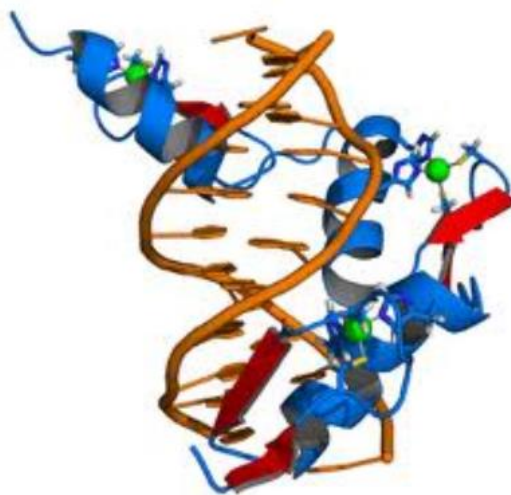


Figure 4. The Zn ion (green), coordinated by two histidine side chains in Zn fingers.

1.4. Biological Role of Zinc

Zinc metal has various biological roles from enzymatic catalysis to playing an essential role in cellular neuronal systems.¹⁰ Zinc plays essential role in cellular metabolism.¹³ About 10% of human body proteins bind zinc potentially, as well as to hundreds that transport and traffic zinc.¹³ It was estimated that about 200 enzymes and more require zinc for the catalytic activity of these enzymes, in addition to playing an important role in the immune system, DNA synthesis and cell division, wound healing, protein synthesis, and several other specialized functions, as tissue growth, sperm formation, bone

mineralization, cognitive functions, photoreception, and neurotransmission.^{13,17-19}

In addition, zinc is protect cells against oxidative stress, usually by acting on superoxide dismutase and catalase.²⁰ Several studies showed that zinc is also involved in the modulation of apoptosis, and cell death program.²¹ It has been shown in many cell lines that zinc can stop apoptosis induced through different factors and that cells maintained under conditions of zinc deficiency can undergo apoptosis spontaneously.²¹⁻² The DNA fragmentation is suppressed by zinc ions, in which its considered as one of the characteristics of apoptosis, through inhibiting the calcium/magnesium-dependent endonuclease.^{24,25}

Moreover, researches proved that Zn(II) has an essential anti-bacterial and anti-viral effects²⁶, and the high concentration of zinc ion may lead to some anti-bacterial properties.²⁷ In addition, zinc is contributed to the inhibition of the growth of many bacteria, such as *Escherichia coli*, *Enterococcus faecalis* and some types of soil bacteria.²⁸ Moreover, zinc is needed for correct smell and sense of taste, and participate in the growth and development of fetal during pregnancy, childhood, and adolescence.¹³

For communication with other cells, cells in the prostate, the salivary gland, intestine, and immune system use zinc ion signaling.¹³ In the brain, in specific synaptic vesicles by glutamatergic neurons zinc is stored, and it can modify brain excitability.²⁹ It plays a critical role in synaptic plasticity and consequently in learning.^{13,29}

1.5. Natural Foods that Contain Zinc

Foods and diets having carbohydrates were found to be lower in zinc content, whereas foods with high protein content are expected to be rich in zinc content, Table 2.³⁰ High percentage of zinc (0.40 to 6.77 mg per 100 g) is obtained from foods that derived from meat.³⁰ About 0.30 to 2.54 mg per 100 g of zinc is found in the grain group, 0.36 to 0.49 mg per 100 g in dairy product, 0.12 to 0.60 mg per 100 g in vegetables, and 0.02 to 0.26 mg per 100 g in fruits.³⁰

Table 2. Zinc content of some foods.³¹**High Ranking Plant-Based Zinc Sources**

Food Source	Zinc Content (mg)
Wheat germ (1/4 cup)	3.3 mg
Tahini (2 tbsp.)	2.8 mg
Pumpkin seeds (2 tbsp.)	2.1 mg
Oatmeal (1 cup cooked)	1.5 mg
White Beans (1/2 cup cooked)	1.5 mg
Tofu (1/2 cup)	1.3 mg
Sunflower Seeds (2 tbsp.)	.9 mg

High Ranking Animal-Based Zinc Sources

Food Source	Zinc Content (mg)
Oysters (100 grams)	78.5 mg
Beef and Lamb Liver (100 grams)	12.8 mg
Beef and Lamb (100 grams)	12.4 mg
Pork and chicken (100 grams)	5.1 mg

According to previous studies, the major sources of zinc in human food are foods of animal's origin.¹⁰ Oyster is expected to be rich in zinc and copper complexes.³² Other good sources of protein are turkey meat, beef liver, lean red meat, and poultry red muscle meat.¹⁰ Zinc is also provided through cheddar cheese, egg yolk, and skimmed milk powder.¹⁰

1.6. Intake of Zinc

The recommended human daily intake of zinc intake is from 4.7 to 18.6 mg.³³ According to the US Department of Agriculture 1994–1996 Continuing Survey of Food Intakes by Individuals, the mean daily intake of zinc for men and women less than 20 years, are 13.5 and 9.0

mg, respectively³³; for those who are above (60 years) were 12.0 mg in men and 8.0 mg in women³⁴, for children 1-5 years old ranges from 6.6 mg to 9.1 mg.³⁵ Insufficient zinc intake has been linked to an increased risk of zinc deficiency.³⁶ Limited food availability, food preferences, and poverty factors are contributing to high risk.³⁶ Widespread deficiency of zinc has significant impact on health and productivity.³⁶ Prevention of zinc deficiency is considered a serious challenge.³⁶

1.7. Excess of Zinc

An excess intake of zinc can lead to overweight, and increases the risk of other linked diseases such as diabetes in adolescents, by measuring the amount of hemoglobin in the blood and is also related to happening of hard anemia.^{37,38} Fermentation of the nutrients in the upper part of gastrointestinal tract to a lesser extent, extra energy is formed by the body, and this is lead to better growth of body, in the presence of sufficient amount of zinc oxide in the food.¹⁰ When zinc intake is high, the pancreas enzymatic activity increases.¹⁰ Excess zinc is not only related to copper deficiency but also cytopenias that typically resolved by the removal of surplus zinc sources.³⁹ The

primary metabolic defect is hyperzincemia, whereas the copper deficiency is considered as the secondary phenomenon.⁴⁰

1.8. Zinc Metal in Medicine

Medicinal inorganic chemistry plays a crucial role in studying and examining the properties of metal ions for the designing of new drugs, Table 3.⁴¹ Almost all drugs that are available in the market are non-metal organic substances.⁴¹ Recently, medicinal chemistry offers potential for the development of metal complexes to use them as a drugs or diagnostic agents.^{41,42} Medicinal inorganic chemistry offers real capabilities to pharmaceutical industries, that have traditionally been controlled by organic chemistry only, for the exploring of new novel drugs with new mechanisms of action.^{41,43} It presents, real potential was done for the discovery and design of new novel therapeutic and diagnostic agents and thus for the understanding and treatment of diseases that are currently intractable, Figure 5.^{41,44}

Table 3. A summary for some metals used in medicine.⁴¹

Metals	Medicinal Usage
Ti	Anticancer drug therapy
Fe	MRI contrast agent
Cr	Insulin receptor activation
Au	Antiarthritic drugs therapy
Zn	Anti-inflammatory agent
Pt	Anticancer therapy, diabetes and Alzheimer's
Mn	MRI contrast agent, SOD mimics

Medicinal inorganic chemistry is of extreme importance as metal-based compounds have the potential for the design of therapeutic agents and diagnostic medicine not readily found in an organic compounds.⁴¹ The exploring and development of the antitumor cisplatin compound, *cis*-[Pt(NH₃)₂Cl₂] played an important role in establishing the field of medicinal inorganic chemistry, Figure 6.⁴¹ Cisplatin and carboplatin (which is the second generation alternative) are still the most commonly used as chemotherapeutic agents for

cancer, greatly enhancing the survival rates of patients in the world.^{42,47}

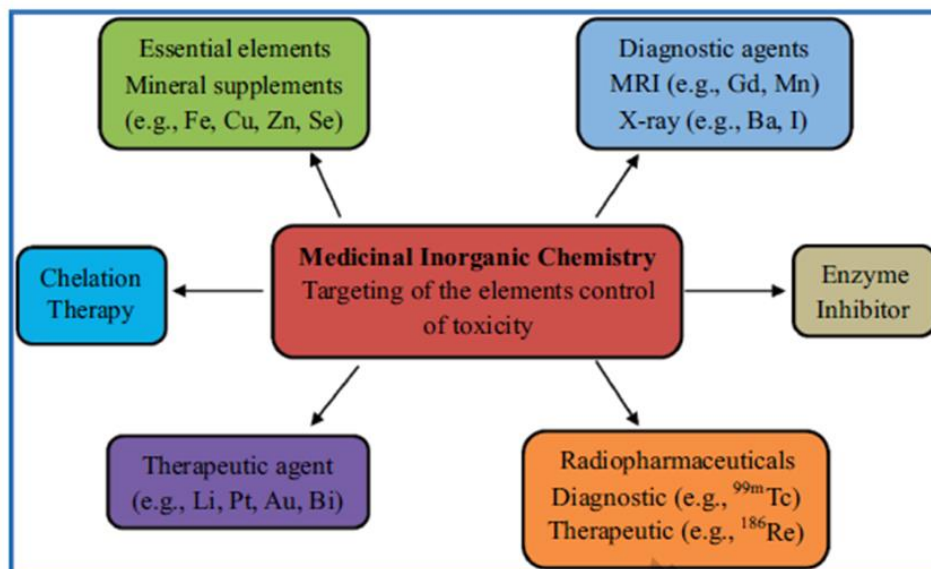


Figure 5. Some of the key areas of medicinal inorganic chemistry.⁴¹

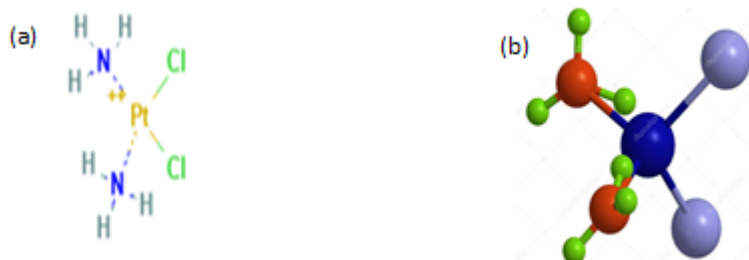


Figure 6. Molecular structure of cisplatin (a) 2D, (b) 3D, respectively.^{45,46}

Zinc is a vital element for all physiological functions, it's also a drug, that has been used as a therapeutic agent versus different diseases.¹⁰ For example, a brown colored zinc(II)-instant coffee complex, which

is a water soluble, was exhibited the highest chelating activity as well as anti-oxidative effect.¹⁰

Zinc exhibited medical treatment in gastrointestinal ailments, bacterial and microbial diseases, liver diseases, and even diabetes has confirmed beneficial effects because zinc play an important role in the synthesis, storage, and secretion of insulin. It's also maintains conformational integrity of insulin in the hexameric form, Figure

7.¹⁰

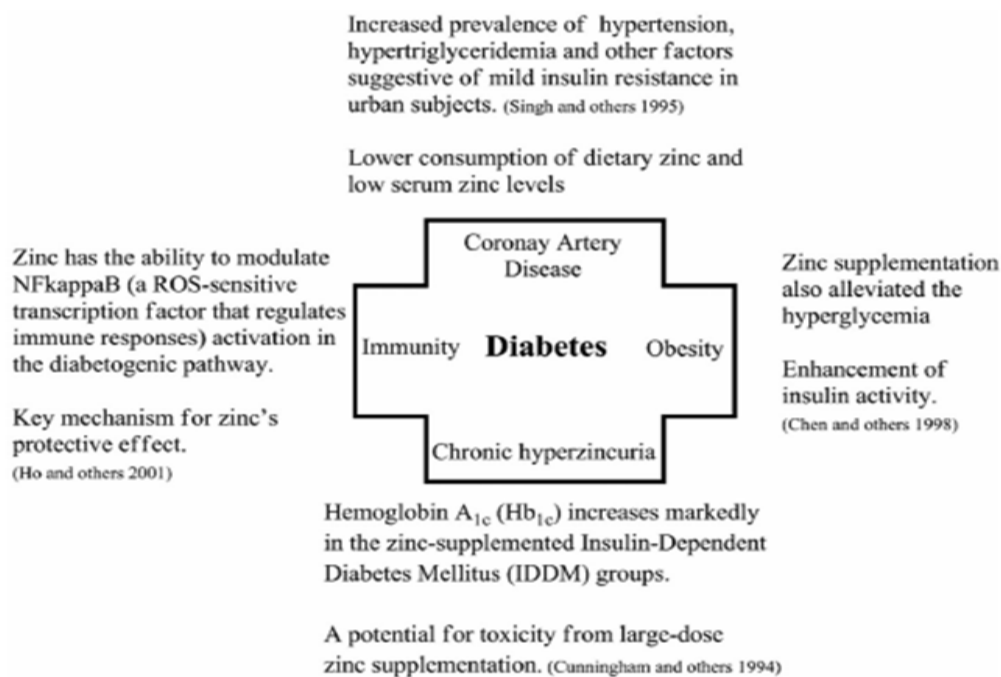


Figure 7. Role of zinc in diabetes with related disease conditions.¹⁰

1.9. Coordination Chemistry of Zinc

The coordination between zinc ion and ligand can form complexes with different stereochemistry and geometry.⁴⁸ The coordination number of zinc ion in its complexes take ranges from 2 to 8, Table 4.⁴⁸ By using both the size of the Zn^{+2} cation and the steric requirements of the ligands, the coordination number as well as the stereochemistry can be determined.⁴⁸ In general, tetrahedral and octahedral geometry are present in complexes.⁴⁸ In the biological systems, all zinc ions are found in tetrahedral coordination due to the fact the zinc is a transition metal with filled *d* valence electrons, which means a stable 18-electron complex can be produced through 4- coordination number with its ligands.^{48,49} Consequently, Zn(II) in complexes with 5- coordination numbers is expected to be unstable and considered unusual.⁵⁰⁻⁵⁴ Octahedral or trigonal prismatic geometry may appear in six-coordinate complexes.⁴⁸ Zn^{2+} can show two coordination numbers in the same compound, the maltol complex $[\text{Zn}(\text{malt})_2] \cdot 1.5\text{H}_2\text{O}$ contain both five –and six-coordinate Zn(II) ion.⁵⁵ Zn^{2+} exhibits both octahedral and trigonal bipyramidal sites in $\text{Zn}_3\text{V}_4(\text{PO}_4)_6$, and square pyramidal sites in $\text{Zn}_2(\text{VO})(\text{PO}_4)_2$,⁵⁶ while Zn^{+2} occupies trigonal

planar, tetrahedral, and trigonal bipyramidal sites in $[\text{Zn}_4(\text{thf})_4(\text{MeZn})_4(\text{O}_3\text{SiR})_4]$, where $\text{R} = -\text{N}(\text{SiMe}_3)(2,6\text{-iPr}_2\text{C}_6\text{H}_3)$.⁵⁷

Table 4. Stereochemistry of some Zn(II) compounds.⁴⁸

Coordination number	Stereochemistry	Example
2	Linear	ZnCl_2 (g), ZnEt_2
3	Planar	$[\text{ZnMe}(\text{NPh}_3)]_2$, bis(ethylxanthato) (py)Zn
4	Tetrahedral	$[\text{ZnCl}_4]^{2-}$, $[\text{Zn}(\text{NH}_3)_4]^{2+}$
5	Planar Trigonal bipyramidal 'Square' pyramidal	$[\text{Zn}(\text{TPP})]^{2+}$ $[\text{Zn}(\text{tren})\text{NCS}]^+$ $[\text{Zn}(\text{S}_2\text{CNEt}_2)_2]_2$, $[\text{Zn}(\text{acac})_2\text{OH}_2]$
6	Octahedral	$[\text{Zn}(\text{en})_3]^{2+}$
7	Pentagonal bipyramidal	$[\text{Zn}(\text{H}_2\text{dapp})(\text{H}_2\text{O})_2]^{2+}$
8	Distorted dodecahedral	$[\text{Zn}(\text{NO}_3)_4]^{2-}$

1.10. Metal Carboxylates

Carboxylic acids play an important role as a substrate in many biochemical processes.⁵⁸ Metal carboxylates are subject to research for the last decades.⁵⁹ They are used to study the anti-ferromagnetic interaction phenomenon, as a model compound of metalloenzymes, or they exhibit anti-bacterial activity.⁵⁹

The coordination of carboxylate group cannot be distinguished from the number of Raman active or infrared vibrations due to its low

symmetry.⁶⁰ Alternately, attempts have been made to relate the values of the carbon-oxygen stretching frequencies to the nature of the carboxylate coordination mode.⁶⁰

A carboxylate group, (RCOO^-), can coordinate to metals in different coordination modes, like monodentate, chelate, bidentate bridging in a *syn-syn*, *syn-anti* or *anti-anti* configuration, monoatomic alone or additional bridging and chelating bridging, Figure 8.^{60,61}

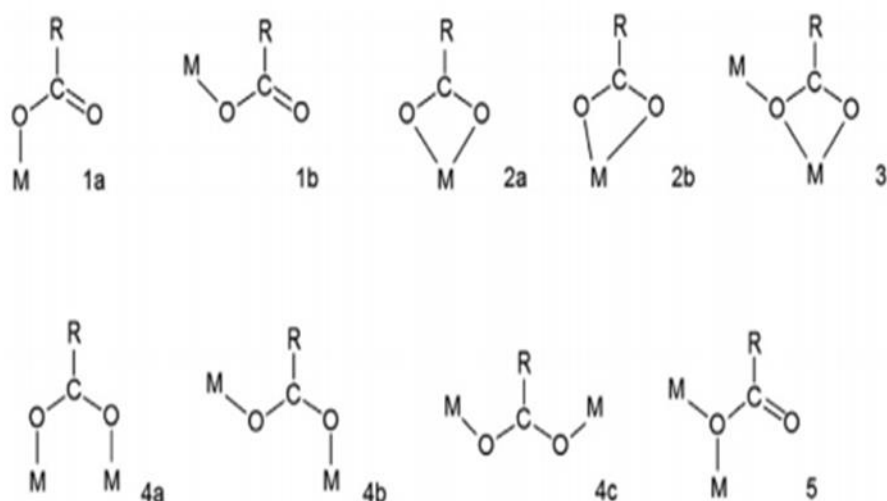


Figure 8. Coordination modes of carboxylate group: *syn* monodentate (1a), *anti* monodentate (1b), *syn-syn* symmetric chelate (2a), *syn-syn* asymmetric chelate (2b), chelating bridging (3), *syn-syn* bridging (4a), *syn-anti* bridging (4b), *anti-anti* bridging (4c), monoatomic bridging (5).

There are many factors that contribute to the determination of coordination modes including the temperature of the reaction,

the solvent used, the preparation method, and the nature of ligands used.⁶²⁻⁶⁵

The infrared spectroscopy is a useful method that used to determine the coordination mode of carboxylate in inorganic complexes.⁵⁸ The criteria that used in determining the mode of carboxylate binding is the value of the difference between the carboxylate stretches, $\Delta = \nu_{\text{as}}(\text{COO}^-) - \nu_{\text{s}}(\text{COO}^-)$, where $\nu_{\text{as}}(\text{COO}^-)$ is known as the frequency of the asymmetric carboxylate vibration in the IR spectra and $\nu_{\text{s}}(\text{COO}^-)$ is the frequency of the symmetric carboxylate vibration.⁵⁸ These criteria are used to assign the coordination modes of the carboxylate in organic compounds and biomolecules.^{60,66} In general, the following order is suggested for metal carboxylates coordination⁵⁹:

$$\Delta[\text{chelating}] < \Delta[\text{bridging}] < \Delta[\text{ionic}] < \Delta[\text{monodentate}]$$

The redistribution of the electron density occurs and the $\nu_{\text{as}}(\text{COO}^-)$ shift to higher wavenumber is noted in the monodentate mode compared to the ionic group as well as increasing the value of Δ .⁵⁹ On the contrary, the $\nu_{\text{as}}(\text{COO}^-)$ of the chelating mode shifts to the lower wavenumbers compared to the ionic group and lower the value of Δ .⁵⁹

In the bridging mode, when one divalent metal coordinates to one of the oxygen atoms of the COO^- group and the other divalent metal cation to the other one, thus the band of asymmetric carboxylate stretch ($\nu_{\text{as}}(\text{COO}^-)$) is taking place at the same location as that of the ionic group.^{59,67}

1.10.1 Zinc Carboxylate Complexes

Zinc(II) complexes of amino acid, peptide, nucleotide, and nucleoside ligands possess important biological activities.⁴⁸ The amino acid can bind through one or more nitrogen (N), oxygen (O), sulfur (S) donor atoms.⁴⁸ In metalloenzymes and metalloenzyme modes, almost all coordination environment of the Zn^{2+} ion is usually NNN, NNO, or NNS, and the water molecule occupied the fourth position (Figure 9).⁴⁸ Histidine, glutamate, and aspartate are the most common ligating residues. For example, the Zn^{2+} ion bonded to cysteine and histidine in zinc finger proteins, (Figure 10).⁴⁸

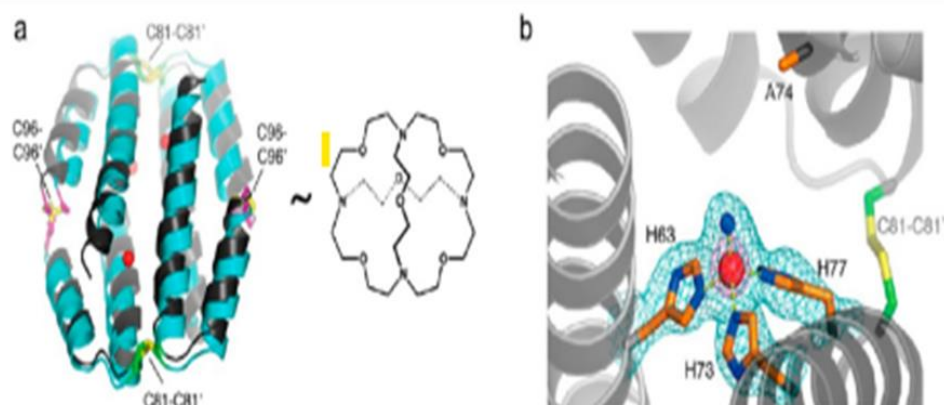


Figure 9. Overall structure and example of a Zn(II) site in a self-assembling protein crypt and templated by disulfide bonds. (a) Overlay of protein backbones of the apo and Zn(II)-bound forms of C81/C96 RIDC₁₄. (b) One of four ZnHis₃(H₂O) sites in A74/C81/C96 RIDC₁₄.

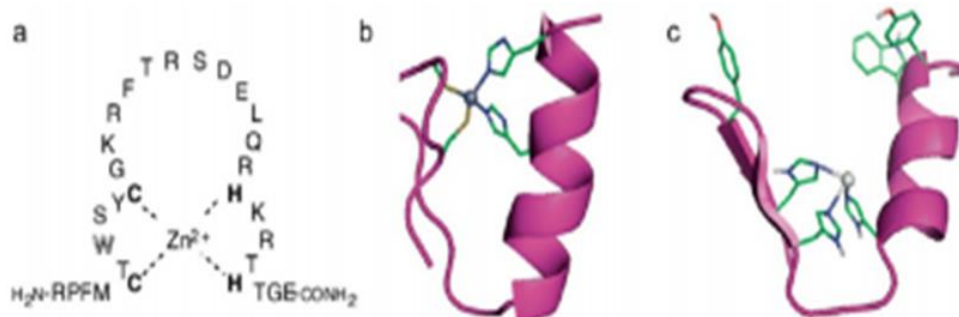


Figure 10. (a) Amino acid sequence of the zinc finger parent peptide. (b) Natural zinc finger fold ($\alpha\beta$ structure) and (c) zinc finger $\alpha\beta$ fold modified as a metallohydrolase.

From this point of view, mono and dinuclear zinc carboxylate play an essential role as biological models.⁵⁸ Regardless of the bioactive role of zinc carboxylate compounds, the design and synthesis of a carboxylic acid with metal-organic frameworks (MOFs) continue to

be excited because of their potential applications in optics, magnetism, catalyst, guest-host chemistry, and also due to their intriguing architectures.^{58,71,72} Zinc carboxylate complexes have been used as catalysts, magnetism, dye, pharmaceutical, plastic industry, liquid crystal technology, optics, paints drying agents, hydrogen storage etc.⁷³⁻⁷⁵ For example, alkoxy zinc carboxylates play an important role as catalysts for the polymerization or copolymerization of a wide range of organic monomers, Figure 11.⁷⁶

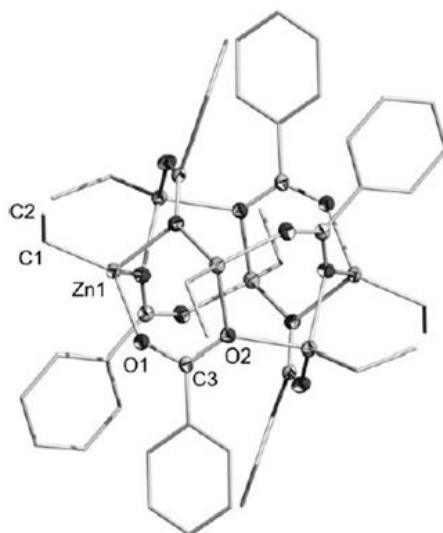


Figure 11. Molecular structure of alkoxy zinc carboxylate.⁷⁶

A common structure of zinc carboxylate complexes is that in which two Zn atoms are bounded by three *syn-syn* bridging carboxylate ligands to produce a binuclear unit with the general formula $[\text{Zn}_2\text{O}_2\text{CR}_3]^+$, where R = alkyl or aryl.⁷⁷ Linear (3,1) polymer is

formed when these units are linked to one another through a *syn-anti* binding carboxylate ligand. For example, zinc crotonate, benzoate, methacrylate, 3,3-dimethylacrylate, and o-chlorobenzoate were synthesized, Figure 12.⁷⁷

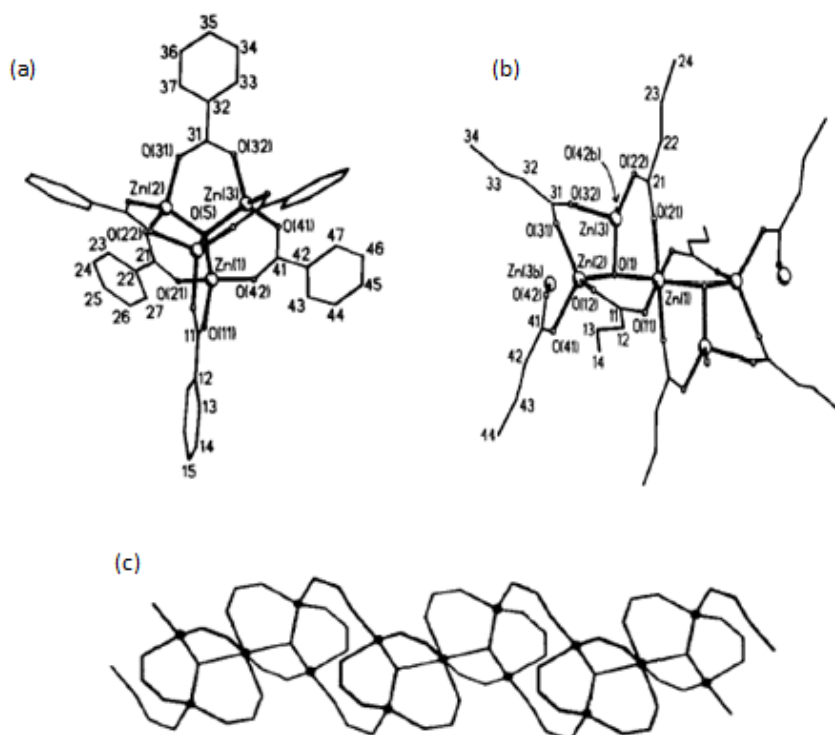


Figure 12. The basic unit of (a) zinc benzoate structure. (b) zinc crotonate unit. (c) zinc crotonate polymer.⁷

Zinc carboxylates complexes exhibit coordination modes like those of metal carboxylates that were previously prepared, Figure 13.⁷⁸

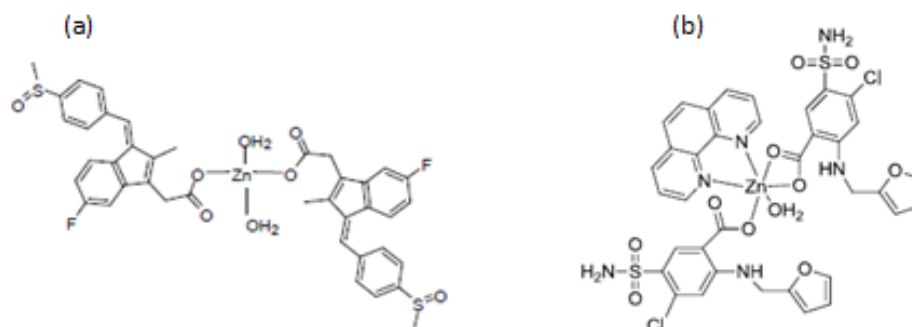


Figure 13. The bonding mode of carboxylates with metals (a) monodentate, $[\text{Zn}(\text{sul})_2 \cdot 2\text{H}_2\text{O}]^{73}$ (b) bidentate chelate, $[\text{Zn}(\text{furo})_2(\text{quin})_2]^{75}$. (sul = sulindac, furo= furosemide, quin= quinoline).

1.10.2 Zinc Complexes with Nitrogen Ligands

There are many nitrogen donor ligands such as, *bis*-pyrazole (pz), bipyridine (bpyr), and 1,10- phenanthroline (phen) derivatives have been utilized in the synthesis of several metal complexes, that are considered useful in many applications from biological to nanostructured materials, especially the development of anti-cancer, anti-bacterial, anti-malarial complexes.⁷⁹ According to previous studies, these nitrogen donor ligands can play an important role in the anti-cancer activities that might lead to the electronic interactions between the π -electrons in the rings and the metal center.⁷⁹ Sometimes the use of these nitrogen-chelating ligands in the synthesis of anti-cancer metal complexes have few or no attention on the anti-cancer

activities in an individual way, so some derivatives of common nitrogen donor ligands are synthesized and their anti-cancer activities are studied.⁸⁰ So, many nitrogen-based ligands have been prepared and their biological activity were studied.⁸¹ According to these and other studies, heterocyclic nitrogen ligands played an essential role in coordination chemistry.⁸¹ Heterocyclics which contain more than one nitrogen atoms are essential part in a large variety of biochemical processes.^{82,83} In general, many nitrogen-based ligands have been used in complexation with transition metals such as, 4,4'-bipyridine (4,4'-bipy), 1,10-phenanthroline (phen), 2,9-dimethyl-1,10-phenanthroline (2,9-dmphen), 1,2-dimethylimidazole (1,2-dmimidazole), and 2-amino-6-picoline (2-am-6-picoline), Figure 14.⁸⁴

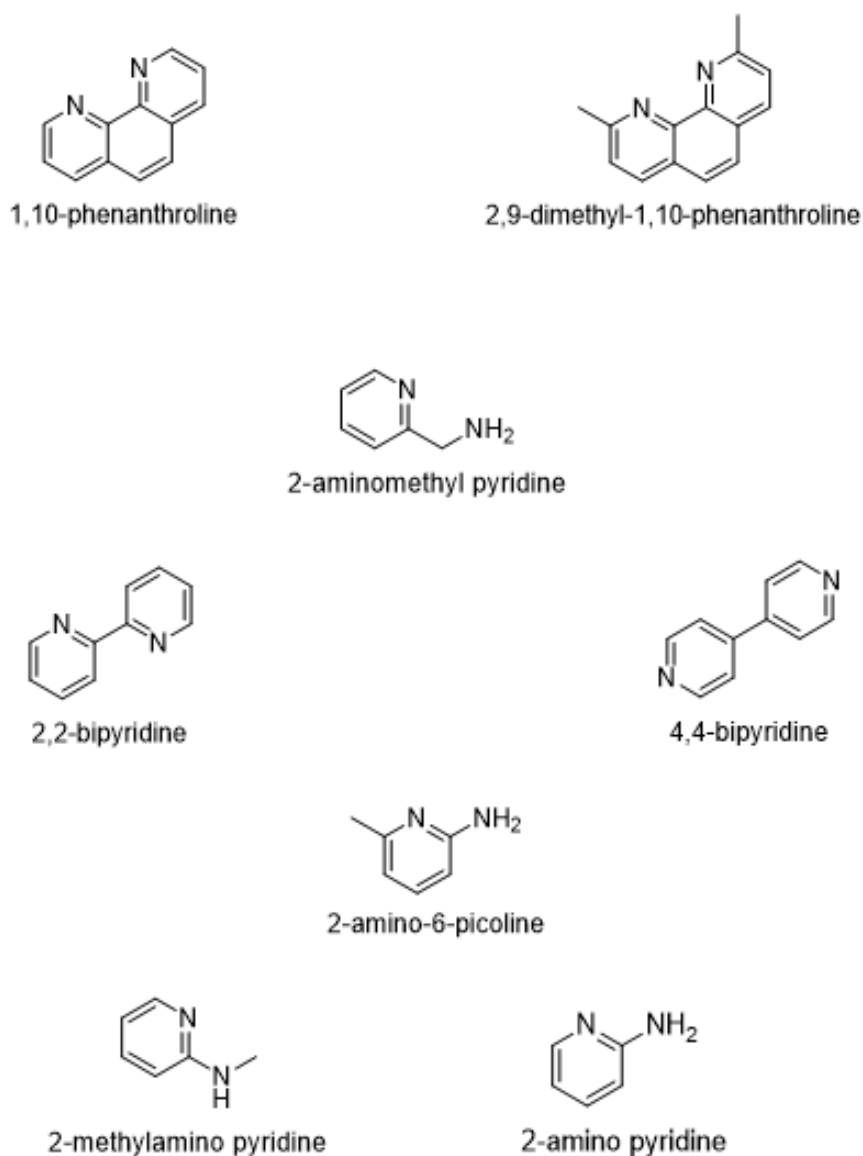


Figure 14. Heterocyclic N-donor ligands.

Zinc(II) complexes with N-donor ligand are attracting a great attention due to their pharmaceutical effects since they can catalyze many enzymatic activities in biological systems, for example, aliphatic Zn(II) carboxylates with nitrogen-based ligands.^{84,85} Recently,

aromatic metal carboxylates with nitrogen-based ligands have been synthesized and their anti-bacterial and anti-malarial activities and many other biological applications were studied.⁸⁴

1.11. Rosmarinic Acid

Polyphenolic compounds are usually referred to as a diverse group of phytochemicals that are widely found in plants, such as vegetables, fruits, tea, olive oil, tobacco and so on.⁸⁶ Structurally, these compounds have an aromatic ring bearing one or more hydroxyl groups and their structures may range from that of a simple phenolic molecule to that of a complex high-molecular mass polymer.⁸⁷ They have been exhibited an important role against several diseases and health risks, including hyperglycemia, hepatotoxicity, tumor cell proliferation, carcinogenesis, apoptosis, ischaemic heart disease, depression, bronchial asthma, peptic ulcer atherosclerosis, cataract, poor sperm motility, metastasis, and spasmogenic disorders, in addition to roles as a powerful antioxidant, anti-carcinogenic, anti-microbial, anti-allergy, anti-inflammatory, cardioprotective and vasodilatory effects.^{87,88} One of the most important polyphenol compounds is rosmarinic acid (RA).⁸⁸

Rosmarinic acid (RA) is known as α -O-caffeoyl-3,4-dihydroxyphenyllactic acid and as an ester of caffeic acid as well as is present in nature as a bioactive phenolic compound, Figure 15.⁸⁹⁻⁹¹ The fundamental sources of RA belong to the families called Lamiaceae and Boraginaceae.⁹² It was formally extracted for the first time in 1958 from the rosemary (*Rosmarinus officinalis*) which belongs to the Lamiaceae family.⁹³ RA is considered one of the essential active components that present in several medicinal plants (such as *Salvia Officinalis*, *Thymus Vulgaris*, *Symphytum Officinale*, *Melissa Officinalis*) within the mentioned families.⁹²

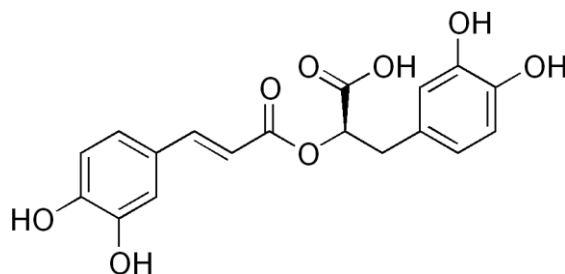


Figure 15. The chemical structure of rosmarinic acid ($C_{18}H_{16}O_8$).

Rosmarinic acid molecule has highly lipophilic and slightly hydrophilic properties, which is usually found in the form of a red-orange powder.⁹² It is mostly soluble in organic solvents.⁹² Its melting point is 171-175° and its molar mass is 360.32 g/mol.⁹²

According to recent studies, RA possesses several biological activities including, anti-bacterial, anti-oxidant, anti-cancer, anti-aging, anti-diabetic, anti-allergic, hepatoprotective, cardioprotective, nephroprotective, anti-viral, anti-inflammatory, and anti-depressant activities, Figure 16.⁹⁴⁻⁹⁷

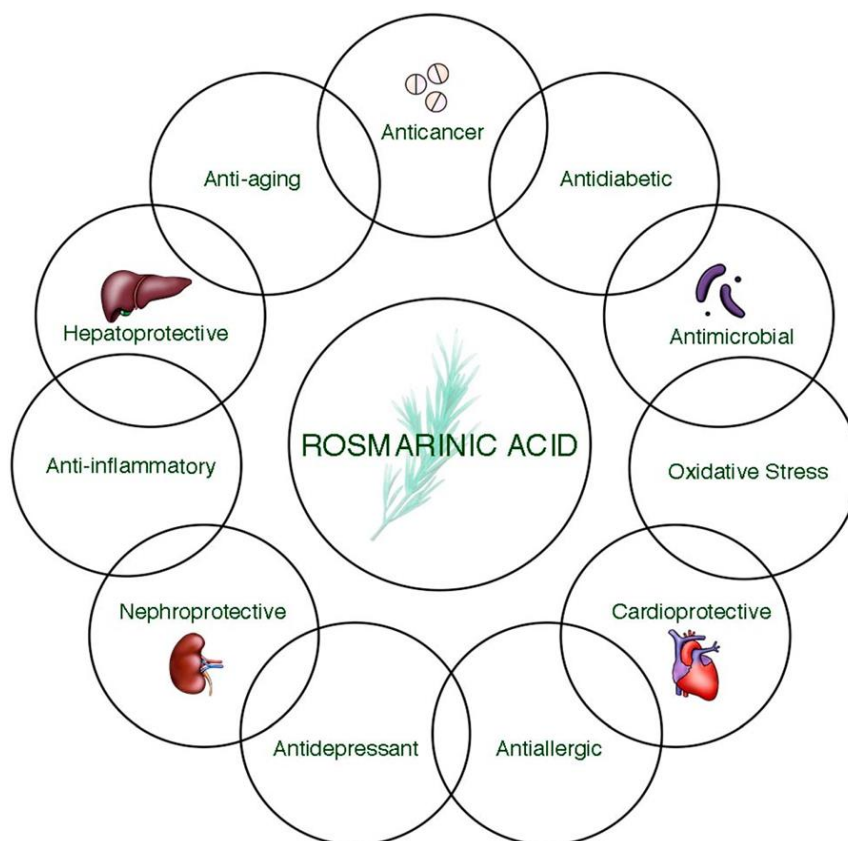


Figure 16. Potential functions of rosmarinic acid.⁸⁸

RA is considered to be an effective candidate as a natural feed additive/supplement and pharmaceutical plant-based products.⁸⁸ RA behaves like a good anti-oxidant by protecting the cell membrane and

decrease the induction of oxidative reactive oxygen species (ROS) through improving the activity of the antioxidant defense mechanism by multiple enzymes throughout the body.⁸⁸ In addition, RA has an advantageous role in improving growth and enhancing productive and reproductive performance as a result of its potential effect on nutrient absorption.⁸⁸ It showed many nutritional benefits by reducing lipid peroxidation in eggs, meats, and sera. Also, RA as a natural antioxidant exhibited many healthy and pharmacologic activities including, anti-spasmodic, anti-fungal, immune modulatory in addition to the activities that previously mentioned in Figure 16.⁸⁸

The modes of action and potential activities of RA (antimicrobial & antioxidant) are shown in Table 5.

In the present work Zn(II) rosmarinic acid complex will be prepared and then will reacts with different bioactive nitrogen donor ligands. The prepared complexes will be characterized by different techniques, and their anti-bacterial activities will be tested against Gram-negative and Gram-positive bacteria.

Table 5. Bioactive effects of rosmarinic acid.

Bioactive Effects	Mechanism
Antimicrobial (<i>In vivo</i>)	Exert anti-microbial activity against Enterobacteriaceae, lactic acid bacteria, Pseudomonas spp., psychotropic, yeast, and mold. ⁹⁸ Show anti-bacterial activity against <i>S.aureus</i> . ⁹⁹ Decreased counts of pathogenic bacteria such as <i>E.coli</i> . ^{100,101}
Antioxidant (<i>In vitro & in vivo</i>)	Anti-oxidant Reduced the production of hydrogen peroxide (H ₂ O ₂) and superoxide (O ₂ ⁻) radicals. ¹⁰² Up regulated catalase, heme oxygenase-1, and superoxide dismutase, reduced malondialdehyde. ¹⁰³

1.12. Anti-bacterial Activity Study

The discovery of new anti-microbial agents is important because of the resistance gained by several pathogenic microorganisms, due to the incorrect dosage used of anti-biotic.¹⁰⁴ Over 13 millions of people die due to the emergence of new infectious diseases and the re-emergence caused by microorganisms' resistance to available antibiotics.¹⁰⁵ Consequently, the discovery of new drugs is needed.¹⁰⁴

The bioinorganic chemistry, which deals with the study of the role of transition metal complexes in biological systems during the last decades, great attention has been given to the synthesis of new metal complexes and testing their ability for anti-bacterial activity.¹⁰⁴ Metal ions are needed for many essential functions in the biological system.¹⁰⁴ In general, coordination complexes or metal complexes have been used in medicine and pharmaceutical fields owing to their broad bioactivities of anti-fungal, and anti-bacterial.¹⁰⁴ Metal ions are needed for many essential functions in the biological systems.¹⁰⁴ In general, coordination complexes or metal complexes have been used in medicine and pharmaceutical fields owing to their broad bioactivities of anti-fungal, and anti-bacterial.¹⁰⁶ They have been tested against many pathogenic fungi and bacteria with promising results.¹⁰⁴ Recent studies showed that metal complexes act as anti-tumor, anti-viral, anti-HIV, and they are used in diabetes treatment.¹⁰⁴ Also, some metal complexes have been used as diagnostic agents and drugs to treat a variety of diseases and conditions.¹⁰⁴ In the biological systems, the importance of metal ions is well known. The coordination of transition metal complexes with nitrogen donor ligands, which

showed better anti-microbial activity and a broad range of pharmacological activity compared to the free ligands, .¹⁰⁷

To check the enhanced anti-bacterial activity of the free ligands, .the anti-bacterial activities of the prepared zinc RA complexes in the presence of nitrogen donor ligands will be tested against Gram-negative (*Escherichia coli*, *Klebsiella pneumonia* and *Proteus mirabilis*) and Gram-positive (*Micrococcus luteus*, *Staphylococcus aureus* and *Bacillus subtilis*) bacteria will be tested by measuring the inhibition zone diameters (mm).

1.13. Kinetic Measurements of BNPP Hydrolysis

Bis-p-nitrophenyl phosphate (BNPP) is a kind of phosphodiester compound and it can be used to examine the formation or the cleavage of the P-O bond. At physiological pH, phosphodiester compound are kinetically highly stable and show high resistance to hydrolytic cleavage. The half-life time ($t_{1/2}$) of BNPP compound in water at 20 °C is two thousand years, while at 50 °C (in water) is 53 years.¹⁰⁸⁻¹¹⁰

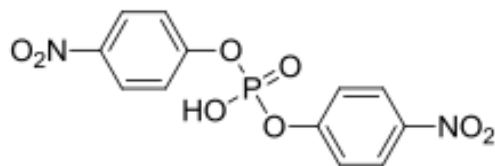


Figure 17. Structure of BNPP.

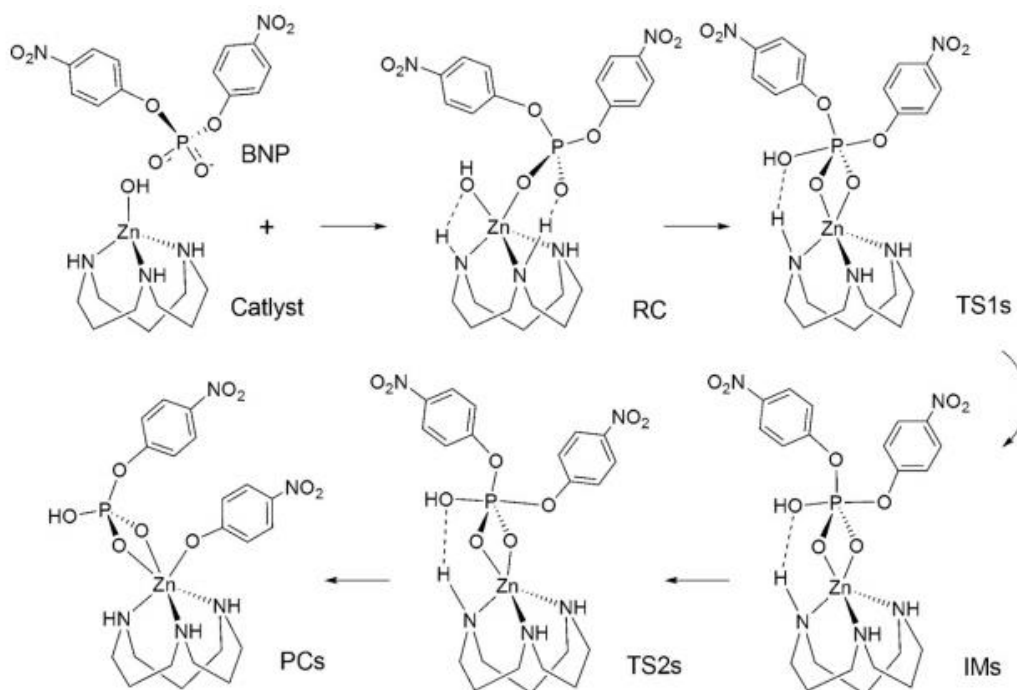
The hydrolysis of phosphodiester is important in biological and industrial processes.^{111,112} Many researches have concentrated on studying and developing biomimetic models for metalloenzymes with high efficiency and selectivity to achieve environmentally-save and great economy processes.¹¹³⁻¹¹⁶ The metal ions play an important role in catalytically active sites in phosphate ester hydrolysis.¹¹⁷⁻¹¹⁹ Therefore, Co(III), Cu(II), Zn(II), Ni(II) and La(III) complexes have been served as metalloenzyme models in phosphate ester hydrolysis.¹²⁰⁻¹²⁴

In general, metal ions with suitable Lewis acidity and high reactivity were preferred in the synthesis of chemical enzymes.¹²⁵ Zinc complexes are highly efficient because of its suitable Lewis acidity, rapid exchange of ligands, harmless and reduction inert. In addition, zinc(II) ion has no LFSE achieve the requirement of structure in

reactions.^{126,127} The mononuclear zinc(II):OH⁻ complex of 1,5,9-triazacyclododecane (Zn:([12]aneN₃)) was used to study the hydrolysis mechanism of the DNA analog BNPP. The proposed mechanism for the cleavage of BNPP catalyzed by mononuclear Zn(II):OH⁻ complex of Zn:([12]aneN₃) is shown in Scheme 1.¹²⁸

The stepwise and concerted reaction paths have the same starting reactant RC but their transition states TS differ. When the nucleophilic hydroxyl ion attacks the P atom in BNPP transition state TS1s is produced subsequently and both of the phosphoryl oxygens bind zinc center. The distance between O1 atom and the zinc center becomes longer and the intermediate IMs forms. The bond length in MIs is 1.744Å and 1.878Å for P-O1 and P-O5, respectively. The five oxygen atoms binding to P atom produce a quasi-trigonal bipyramid structure with two elongated polar. In TS2s the bond length of P-O5 is increase to 1.938Å and vibrations corresponding to the imaginary frequency in TS2s predict a tendency of cleaving the P-O5 bond. The O5 leaving group departs form P atom and turns to bind with zinc center keeps a six-coordination number with both of the phosphoryl oxygen atoms binding to it.¹²⁸

Scheme 1. The possible mechanism for the cleavage of BNPP catalyzed by mononuclear Zn(II):OH⁻ complex of Zn:([12]aneN₃).¹²⁸



The calculation of K_{obs} constant for the hydrolysis of BNPP depend on the initial rate (V_0) method according to the following equation $(\text{rate})_0 = (dc/dt)_0 = (dA/dt)_0/\epsilon$ and $(\text{rate})_0 = k_{\text{obs}} [\text{ML}]_0$ where $(\text{rate})_0$ is initial rate, A is absorbance, c is a concentration and $[\text{ML}]_0$ is the initial concentration of the complex. The rate of release of p-nitrophenol from BNPP hydrolysis was determined at 400 nm by using UV-Vis spectrophotometer.⁷⁵

1.14. Aim of the Project.

The main objectives of the present work is the synthesis, characterization and anti-bacterial activity of new Zn(II) rosmarinic acid complexes with 2-aminopyridine (2-ampy), 2-aminomethylpyridine (2-ammethylpy), 2,2'-bipyridine (2,2'-bipy), 4,4'-bipyridine (4,4'-bipy), 1,10-phenanthroline (phen), 2,9-dimethyl-1,10-phenanthroline (2,9-dmphen), and 2-(methyl amino)pyridine (2-methylampy).

These complexes will be characterized by different techniques such as IR, UV-Vis, ¹H-NMR spectroscopic techniques, and other physical properties. The *in-vitro*, biological activities for the characterized complexes i.e. anti-bacterial and the hydrolysis of BNPP *bis*-(p-nitrophenyl phosphate will be screened and tested.

2. EXPERIMENTAL

2.1. Chemicals, reagents, and biological species

All chemicals, solvents, and reagents used for the synthesis of the desired complexes were purchased from commercial sources (such as, Sigma Aldrich) and used without further purification. Biological species: *Bacillus subtilis*, *Klebsiella pneumonia*, *Escherichia coli*,

Staphylococcus aureus, *Micrococcus luteus*, *Proteus mirabilis*, *Enterococcus faecalis*, *Pseudomonas aeruginosa* and *Staphylococcus epidermidis* were obtained from the Biology and Biochemistry Department at Birzeit University.

2.2. Instrumentation

Infrared (IR) spectra were recorded in the 200-4000 cm^{-1} region using a Varian 660 FT-IR Spectrometer using KBr pellets. Melting points were determined in capillary tubes using MPA120 EZ-Melt apparatus. UV-Vis spectra were recorded using Hewlett Packard 8453 photo diode array spectrophotometer in the 200-800 nm regions using suitable solvent for each complex prepared. NMR spectra were recorded on a Varian Unity Spectrometer operating at 300 MHz for ^1H measurements and 400 MHz for the $^{13}\text{C}\{^1\text{H}\}$ measurements. Spectra were recorded in DMSO. Chemical shifts are given in ppm downfield from the internal standard Me_4Si , and coupling constants are given in Hz. Melting points were determined in glass capillary tubes with EZ-Melt apparatus without any correction.

2.3. Synthesis and characterization of zinc with rosmarinic acid complexes

All zinc rosmarinic acid complexes were prepared at room temperature (RT).

2.3.1 Synthesis of zinc with rosmarinic acid [Zn(RA)_n] (1)

Appropriate amount of zinc chloride (0.1967g, 1.443 mmol) in 10 ml of methanol was added to a solution of rosmarinic acid (1.012 g, 2.808 mmol) in 50 ml of methanol containing sodium hydroxide (0.1539 g, 3.848 mmol). The pale yellow mixture was stirred for 3 h. Then the mixture was filtered and the filtrate was reduced under vacuum using rotary evaporator. Anhydrous ether was added to wash the pale yellow precipitate and the crude product was re-crystallized from mixture of methanol and water to give complex **1** as a pale yellow solid in 60.75 % yield.

[Zn(RA)_n](1): 60.75% yield, m.p. (> 250) °C. IR (cm⁻¹): 3233.69, 1686.90, 1596.86, 1522.68, 1445.50, 1358.19, 1252.67, 1158.77, 1114.62, 1069.23, 975.57, 852.67, 809.78, 592.06, 524.83, 437.55, and 285.11. ¹H-NMR (DMSO, δ (ppm)): 7.35 (d, ³J_(H-H) = 15.8 Hz, 1H, CH), 7.01 (s, 1H, CH), 6.92 (d, ³J_(H-H) = 7.2 Hz, 1H, CH), 6.72 (d, ³J_(H-H) = 6.5 Hz, 1H, CH), 6.65 (d, ³J_(H-H) = 1.8 Hz, 1H, CH), 6.58 (d,

$^3J_{(H-H)} = 8.0$ Hz, 1H, CH), 6.47 (dd, $^3J_{(H-H)} = 1.8$ Hz, 1H, CH), 6.16 (d, $^3J_{(H-H)} = 15.6$ Hz, 1H, CH), 4.87 (d, $^3J_{(H-H)} = 8.2$ Hz, 1H, CH), 2.99 (d, $^3J_{(H-H)} = 11.9$, 2H, CH₂), 2.73 (dd, $^3J_{(H-H)} = 14.2$, 2H, CH₂). $^{13}\text{C}\{^1\text{H}\}$ NMR (DMSO, δ (ppm)): 37.55 (CH₂), 75.80 (O-C=O), 115.07 (CH), 115.35 (CH), 115.84 (CH), 116.35 (CH), 117.03 (CH), 120.19 (CH), 121.47 (CH), 129.4 (C-CH₂), 129.94 (C-CH₂), 144.04 (C-OH), 144.98 (C-OH), 145.33 (C-OH), 146.22 (CH), 148.92 (C-OH), 166.61 (C=O), 173.00 (C=O). UV-Vis (H₂O, λ (nm)): 197, 218, 287, and 324.

2.3.2 Synthesis of zinc rosmarinic acid with 2-(methylamino) pyridine complex [Zn(RA)_n(2-(methylamino) py)_m] (2)

Aqueous solution of 2-(methylamino) py (0.2185 g, 2.025 mmol) was gradually added to a stirred aqueous solution of complex **1** (0.7866 g, 1.0 mmol). The mixture was stirred for 3.5 h. Then the mixture was filtered off and the filtrate was reduced under vacuum using rotatory evaporator. Anhydrous ether was added to wash the brown precipitate and the crude product was re-crystallizes from methanol to give complex **2** as a beige solid in 37.10 % yield. The complex was characterized by using IR-spectroscopy, UV-spectroscopy and ^1H -NMR spectroscopy.

[Zn(RA)_n(2-(methylamino) py)_m] (2): 37.10% Yield, M.p. 175 °C, IR (cm⁻¹): 3113.83, 1661.44, 1591.11, 1518.77, 1441.93, 1392.37, 1255.76, 1159.37, 1116.66, 1066.09, 1030.51, 979.00, 855.44, 813.01, 761.79, 592.10, 516.09, 455.39, and 208.78. ¹H-NMR (DMSO, δ (ppm)): 7.98 (d, ³J_(H-H) = 8.1 Hz, 1H, CH), 7.93 (d, ³J_(H-H) = 7.5 Hz, 1H, CH), 7.44 (d, ³J_(H-H) = 9.9 Hz, 1 H, CH), 7.37 (d, ³J_(H-H) = 9.9 Hz, 1H, CH), 7.32 (d, ³J_(H-H) = 7.2 Hz, 1H, CH), 7.04 (s, 1H, CH), 6.75 (d, ³J_(H-H) = 8.4 Hz, 1H, CH), 6.66 (s, 1H, CH), 6.61 (d, ³J_(H-H) = 7.5 Hz, 1H, CH), 6.50 (d, ³J_(H-H) = 7.5 Hz, 1H, CH), 6.42 (t, ³J_(H-H) = 5.4 Hz, 1H, CH), 6.22 (d, ³J_(H-H) = 15.6 Hz, 1H, CH), 4.95 (t, ³J_(H-H) = 4.8 Hz, 1H, CH), 2.98 (d, ³J_(H-H) = 11.7 Hz, 2H, CH₂), 2.86 (d, ³J_(H-H) = 11.7 Hz, 2H, CH₂), 2.72 (d, ³J_(H-H) = 3.3 Hz, 3H, CH₃). UV-Vis ((H₂O and MeOH in 1:1 ratio), λ (nm)): 201, 238, 289, and 323.

2.3.3 Synthesis of zinc rosmarinic acid with 2,2'-pyridine complex [Zn(RA)_n(2,2'-bipy)_m] (3)

2, 2'-bipy (0.0780 g, 0.499 mmol) in 20 methanol was added to a solution of complex **1** (0.393 g, 0.50 mmol) in 25 ml of methanol. The clear solution was stirred for 3 h. Then the mixture was filtered and the filtrate was reduced under vacuum using rotatory evaporator. Anhydrous ether was added to deposit the yellowish precipitate and

the crude product was re-crystallized from a mixture of absolute ethanol and water to give complex **3** as a yellowish solid in 63.86 % yield. The complex was characterized by using IR-spectroscopy, UV-spectroscopy and $^1\text{H-NMR}$ spectroscopy.

[Zn(RA)_n(2,2'-bipy)_m](3): 63.86% Yield, M.p. 159 °C (decomposed). IR (cm^{-1}): 3080.19, 2102.53, 1694.99, 1592.80, 1515.33, 1439.81, 1393.02, 1252.72, 1155.43, 1115.32, 1064.28, 1017.97, 977.24, 855.13, 811.48, 762.40, 735.36, 649.22, 626.41, 521.60, 411.57, and 218.74. $^1\text{H-NMR}$ (DMSO, δ (ppm)): 8.71 (d, $^3J_{(\text{H-H})} = 4.2$ Hz, 2H, CH), 8.42 (d, $^3J_{(\text{H-H})} = 7.5$ Hz, 2H, CH), 7.98 (s, 2H, CH), 7.95 (d, $^3J_{(\text{H-H})} = 7.8$ Hz, 1H, CH), 7.49 (s, 2H, CH), 7.37 (d, $^3J_{(\text{H-H})} = 15.6$ Hz, H, CH), 7.03 (s, 1H, CH), 6.75 (d, $^3J_{(\text{H-H})} = 7.8$ Hz, 1H, CH), 6.66 (s, 1H, CH), 6.60 (d, $^3J_{(\text{H-H})} = 4.2$ Hz, 1H, CH), 6.48 (d, $^3J_{(\text{H-H})} = 6.0$ Hz, 1H, CH), 6.18 (d, $^3J_{(\text{H-H})} = 7.8$ Hz, 1H, CH), 4.91 (d, $^3J_{(\text{H-H})} = 9.6$ Hz, 1H, CH), 2.99 (d, $^3J_{(\text{H-H})} = 13.2$ Hz, 2H, CH_2), 2.77 (dd, $^3J_{(\text{H-H})} = 13.2$ Hz, 2H, CH_2). UV-Vis (MeOH, λ (nm)): 200, 222, 233, 284, and 328.

2.3.4 Synthesis of zinc rosmarinic acid with 4,4'-pyridine complex [Zn(RA)_n(4,4'-bipy)_m] (4)

4, 4'-bipy (0.2648 g, 1.695 mmol) in 20 ml methanol was added to a solution of complex **1** (0.300 g, 0.833 mmol). The mixture was stirred for 3 h. Then the mixture was filtered and the filtrate was reduced under vacuum using rotatory evaporator. Anhydrous ether was added to deposit the brown precipitate and the crude product was re-crystallized from a mixture of methanol and water to give complex **4** as a yellowish solid in 84.52 % yield. The complex was characterized by using IR-spectroscopy, UV-spectroscopy and ¹H-NMR spectroscopy.

[Zn(RA)_n(4,4'-bipy)_m](**4**): 84.52% Yield, M.p.157 °C (decomposed), IR (cm⁻¹): 3104.24, 2108.93, 1685.59, 1589.02, 1520.71, 1445.23, 1403.92, 1256.23, 1160.37, 1066.48, 976.60, 853.57, 806.99, 592.09, 522.63, and 453.57. ¹H-NMR (DMSO, δ (ppm)): 8.71 (d, ³J_(H-H) = 4.5 Hz, 4H, CH), 7.83 (d, ³J_(H-H) = 5.1 Hz, 4H, CH), 7.36 (d, ³J_(H-H) = 15.9 Hz, 1H, CH), 7.02 (s, 1H, CH), 6.92 (d, ³J_(H-H) = 8.4 Hz, 1H, CH), 6.73 (d, ³J_(H-H) = 8.1 Hz, 1H, CH), 6.64 (s, 1H, CH), 6.58 (d, ³J_(H-H) = 16.8 Hz, 1H, CH), 6.47 (d, ³J_(H-H) = 7.8 Hz, 1H, CH) 6.17 (d, ³J_(H-H) = 15.9 Hz, 1H, CH), 4.86 (d, ³J_(H-H) = 7.5 Hz, 1H, CH), 2.98 (d, ³J_(H-H) =

13.2 Hz, 2H, CH₂), 2.77 (d, $^3J_{(H-H)} = 13.2$ Hz, 2H, CH₂). UV-Vis (H₂O and MeOH in 1:1 ratio, λ (nm)): 195, 219, 254, 273, and 327.

2.3.5 Synthesis of zinc rosmarinic acid with 2,9-dimethyl-1, 10-phenanthroline complex [Zn(RA)_n(2,9-dmp)_m] (5)

2, 9-dmp (0.1050 g, 0.5041 mmol) was dissolved in 10 ml MeOH, and added to a stirred methanol solution of complex **1** (0.3945 g, 0.5019 mmol). The solution was stirred for 5 h. Then the mixture was filtered and the filtrate was reduced under vacuum using rotatory evaporator. Anhydrous ether was added to deposit the yellowish precipitate. The solvent was allowed to decant to give yellowish solid in 40 % yield. The complex was characterized by using IR-spectroscopy, UV-spectroscopy and ¹H-NMR spectroscopy.

[Zn(RA)_n(2,9-dmp)_m] (5): 40.00% Yield, M.p. 80 °C (decomposed).

IR (cm⁻¹): 3448.98, 3059.91, 2957.16, 2921.56, 1669.85, 1615.92, 1593.63, 1500.39, 1430.53, 1362.89, 1268.16, 851.41, 814.80, 783.90, 756.26, 732.13, 638.37, 548.09. ¹H-NMR (DMSO, δ): 8.75 (t, $^3J_{(H-H)} = 8.1$ Hz, 2H, CH), 7.98(d, $^3J_{(H-H)} = 8.1$ Hz, 2H, CH), 7.60 (d, $^3J_{(H-H)} = 7.5$ Hz, 1H, CH), 7.36 (d, $^3J_{(H-H)} = 15.9$ Hz, 1H, CH), 7.04 (s, 1H, CH), 6.92 (d, $^3J_{(H-H)} = 8.1$ Hz, 1H, CH), 6.75 (d, $^3J_{(H-H)} = 7.8$ Hz, 1H, CH), 6.67 (s, 1H, CH), 6.57 (d, $^3J_{(H-H)} = 4.2$ Hz, 1H, CH), 6.47 (d,

$^3J_{(H-H)} = 6.6$ Hz, 1H, CH), 6.17 (d, $^3J_{(H-H)} = 16.2$ Hz, 1H, CH), 4.91 (d, $^3J_{(H-H)} = 8.1$ Hz, 1H, CH), 3.00 (d, $^3J_{(H-H)} = 15.3$ Hz, 2H, CH₂), 2.79 (d, $^3J_{(H-H)} = 15.3$ Hz, 2H, CH₂). UV-Vis (DMSO, λ (nm)): 286, 306, and 324.

2.3.6. Synthesis of zinc rosmarinic acid with 2-aminopyridine complex [Zn(RA)_n(2-ampy)_m] (**6**)

Aqueous solution of 2-aminopyridine (0.1886 g, 2.004 mmol) was gradually added to a stirred aqueous solution of complex **1** (0.7870 g, 1.001 mmol). The solution was stirred for 3 h. Then the mixture was filtered off and the filtrate was reduced under vacuum using rotatory evaporator. Anhydrous ether was added to wash the brown precipitate and the crude product was re-crystallizes from methanol to give complex **6** as a beige solid in 41 % yield. The complex was characterized by using IR-spectroscopy, UV-spectroscopy and ¹H-NMR spectroscopy.

[Zn (RA)_n (2- ampy) m] (**6**): 40% Yield, M.p. 180 °C (decomposed).

IR (cm⁻¹): 3081.55, 2098.26, 1667.99, 1587.08, 1517.10, 1485.70, 1441.13, 1382.46, 1255.56, 1156.66, 1118.33, 981.32, 853.39, 816.65, 765.45, 620.75, 550.49, 514.87, 415.53. ¹H-NMR (DMSO, δ (ppm)): 8.70 (d, $^3J_{(H-H)} =$ Hz, 1H, CH), 7.85 (s, 2H, NH₂), 7.45 (t, $^3J_{(H-H)} =$ Hz,

1H, CH), 7.35 (d, $^3J_{(H-H)} = \text{Hz}$, 1H, CH), 7.01 (s, 1H, CH), 6.90 (d, $^3J_{(H-H)} = \text{Hz}$, 1H, CH), 6.70 (d, $^3J_{(H-H)} = \text{Hz}$, 1H, CH), 6.64 (s, 1H, CH), 6.60 (d, $^3J_{(H-H)} = \text{Hz}$, 1H, CH), 6.50 (d, $^3J_{(H-H)} = \text{Hz}$, 1H, CH), 6.40 (t, $^3J_{(H-H)} = \text{Hz}$, 1H, CH) 6.20 (d, $^3J_{(H-H)} = \text{Hz}$, 1H, CH), 4.99 (d, $^3J_{(H-H)} = \text{Hz}$, 1H, CH), 2.99, 2.80 (d, $^3J_{(H-H)} = \text{Hz}$, 2H, CH₂). UV-Vis (H₂O and MeOH in 1:1 ratio, λ (nm): 233, 289, 321, and 427.

2.4. *In-vitro* Biological Activity

In order to show any participating roles of DMSO in the biological screening study, separate study was carried out with DMSO alone, and exhibited hardly any activity against any bacterial and fungal strains.¹²⁹ The tests were carried out in triplicate.

2.4.1. Agar -well diffusion method

The nitrogen donor ligand metal complexes were tested for antibacterial activity against five Gram- positive bacteria (*M. luteus*, *B. subtilis*, *S. aureus*, *S. epidermidis*, and *E. faecalis*) and four Gram-negative bacteria (*E. coli*, *P. mirabilis*, *K. pneumoniae*, and *P. aeruginosa*) using the agar-well diffusion method. The nutrient agar powder was added to distilled water and brought it to boil to dissolve completely and then sterilization was carried out at 121 °C for 15 minutes in an autoclave. 10 ml aliquots of nutrient agar was inoculated

with the test bacteria and incubated at 37 °C for 24 h. In the sterile saline solution (0.9% of NaCl), single bacteria colonies were dissolved until the cell suspension's turbidity in the range of the McFarland 0.5 turbidity standard. By using the sterile cotton swab the bacterial inocula were put on the sterile surfaces of the nutrient agar. The required numbers of holes were cut by using sterile plastic borer. Using a micro pipette, 25 µl of the test complex (12 mg/ml in DMSO) dissolved in an appropriate solvent was transferred into appropriately labeled holes. The same concentrations of the standard antimicrobial agents: gentamycin 12 mg/ml, erythromycin 12 mg/ml and the solvent (DMSO) as controls were used. The plates were incubated at 37 °C for 24 h. The diameter of the zones of inhibition is measured in millimeter by using caliper. The results were recorded as average of the three trails and compared with standard antimicrobial drug.

2.4.2. Tube dilution method

The broth dilution methods is used to determine the lowest concentration of the tested antimicrobial agent (minimal inhibitory concentration, MIC) to stop growth of bacteria. The complexes **1-6** were selected for the MIC test against *P. aeruginosa*. The standard

antimicrobial agents: gentamycin 2 mg/ml, ampicillin 2 mg/ml and the solvent (DMSO) as controls were used.

For broth dilution method, often determined in sterile 96-well microtitre plates, bacteria are inoculated into a liquid growth medium (broth) in the presence of different concentration of the complexes prepared and antibiotics agent. Growth is obtained after incubation for a defined period of time (16-24 h.) and the value of MIC is assessed.

2.5. Kinetic studies of the hydrolysis reaction of BNPP

The kinetics of the hydrolysis of BNPP in the catalytic system containing nitrogen-donor ligand and zinc(II) with rosmarinic acid **1-3** were performed at different pH, temperature, and concentrations by a spectrophotometric method.

HEPES buffer, (4-(2-hydroxyethyl)-1-piperazineethanesulfonic acid) was utilized to maintain the pH constant. The buffer system were prepared by adding 0.0012 g (50 μ M) to minimum amount of deionized water then the pH was adjusted to the desired value by using NaOH or HCl, then the BNPP (0.0034 g) was dissolved in the buffer system and the volume of the solution was completed to 100 ml in the 100 ml volumetric flask.

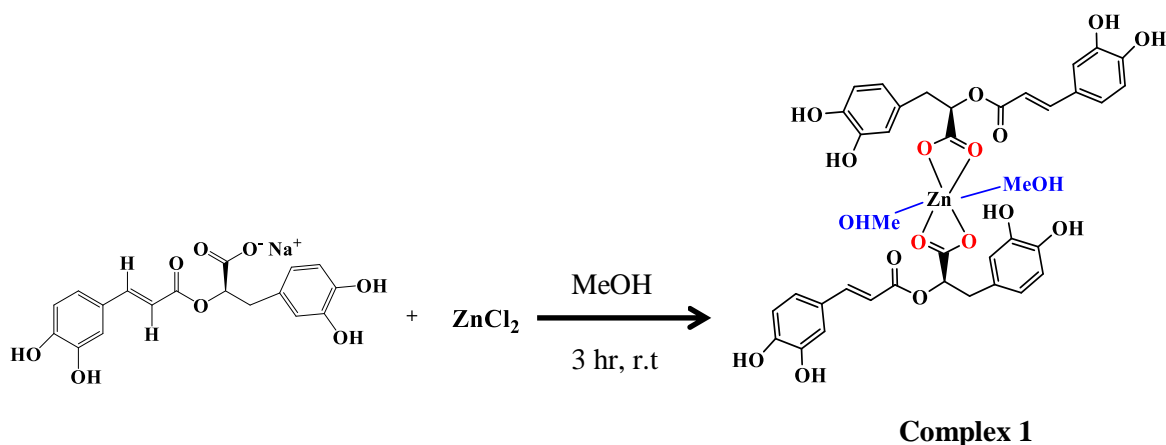
The prepared zinc (II) complexes **1-3** were utilized as catalyst in the BNPP hydrolysis process, these complexes were dissolved in DMSO solvent with different concentrations. A 1.5 ml of the zinc complex was added to 1 cm cuvette in the spectrophotometer with a temperature control system. A buffer solution of BNPP was added into the cuvette, the absorbance of the produced p-nitrophenol from the BNPP hydrolysis at wavelength of 400 nm was recorded. The kinetic experiments were carried in triplicates.

3. RESULTS AND DISSCUTION

3.1. Synthesis of zinc rosmarinic acid complexes

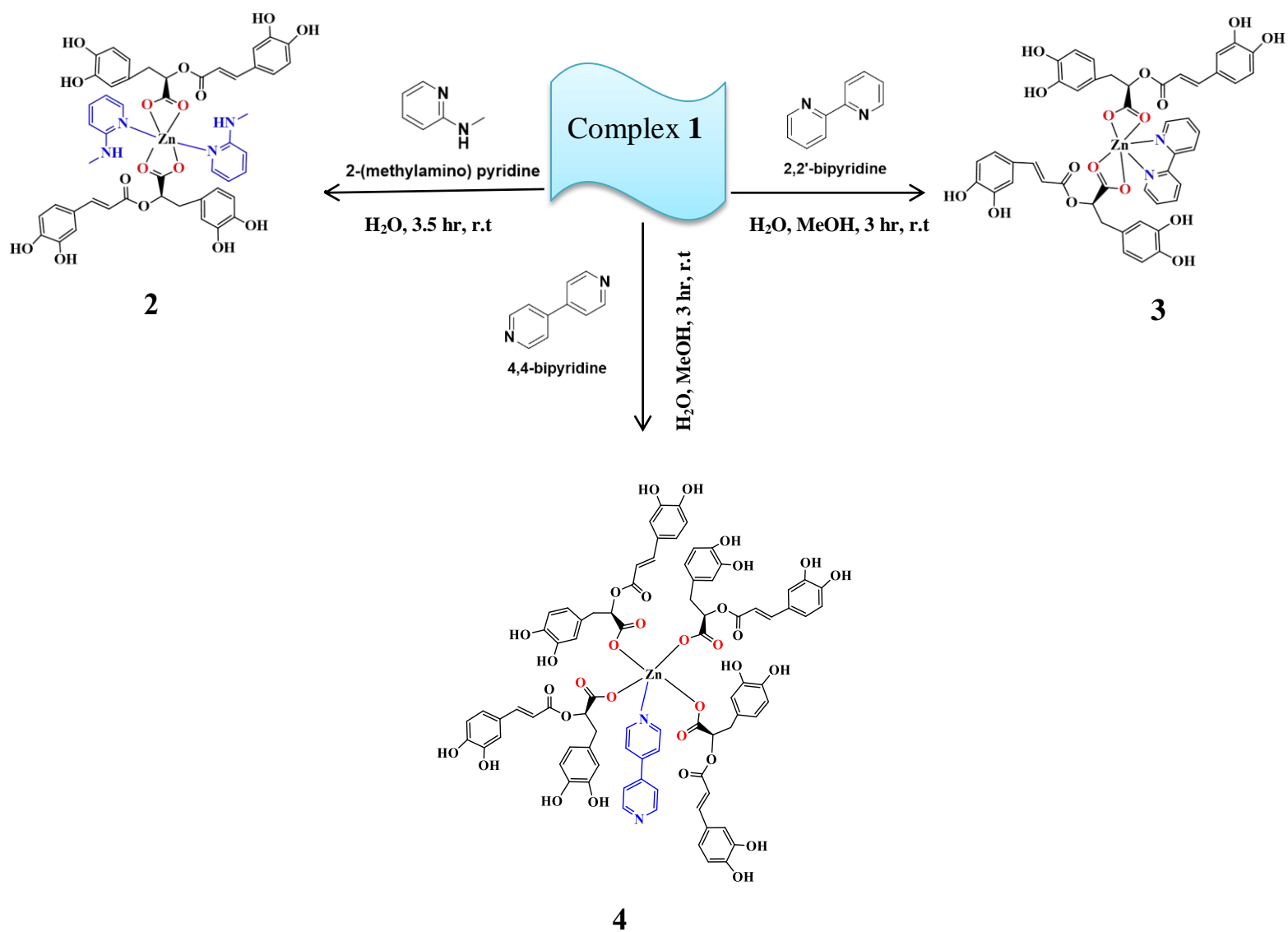
Zinc rosmarinic acid complex $[(Zn(RA)_n]$ was obtained at room temperature by adding 0.5 equivalent of $ZnCl_2$ to a solution mixture of 1 equivalent of rosmarinic acid and 1.1 equivalent of NaOH as shown in Scheme 2. The white to faint beige solid complex was obtained in 60.75% yield.

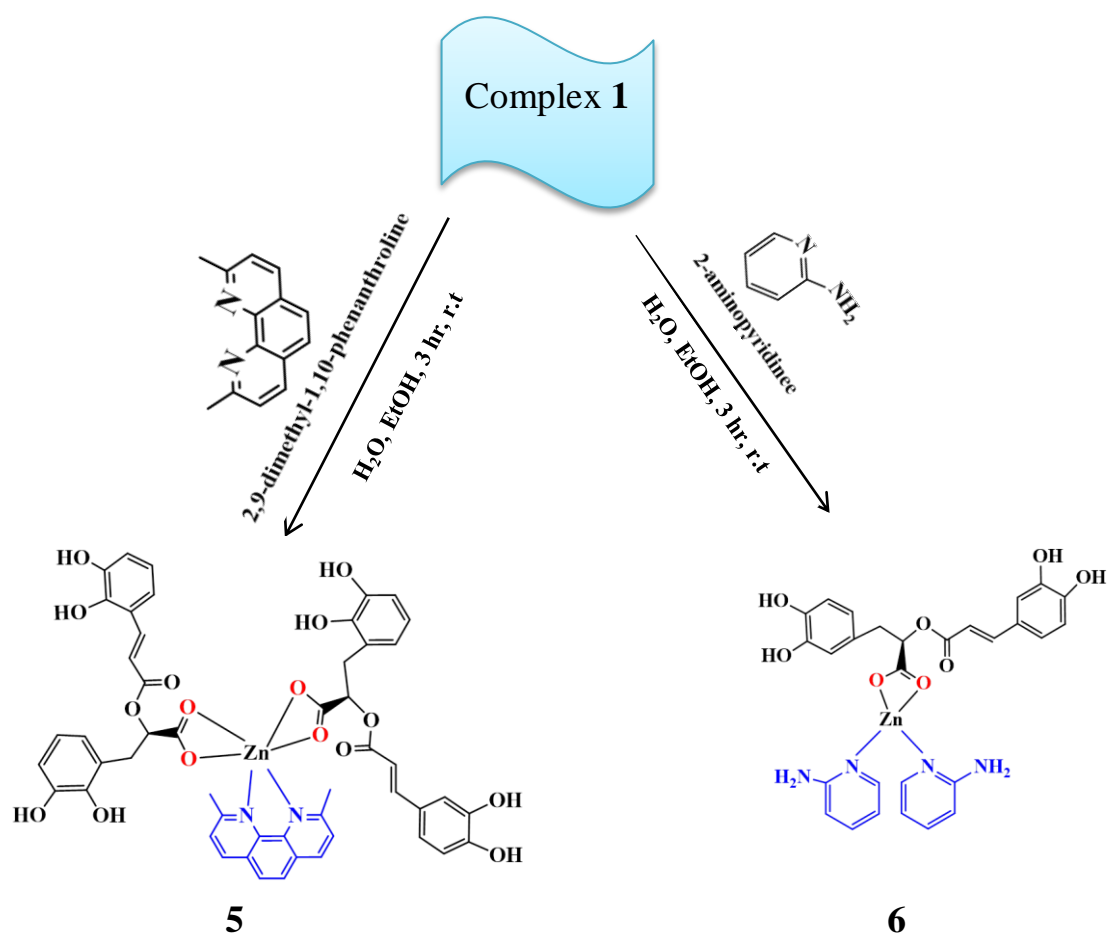
Scheme 2. Proposed structure of $[(\text{Zn}(\text{RA})_n]$.



A series of novel mixed ligand zinc complexes were prepared by adding N-donor ligands such as (2-amethylpy), (2,2'-bipy), (4,4'-bipy), (2,9-dmphen), and (2-ampy) to complex **1**, as shown in Schemes 3 and 4. The ligand solution was added to the reaction mixture of $\text{Zn}(\text{RA})_n$ precursor. The addition of ligand resulted in either precipitation of complexes and the complexes were filtered, dried, and obtained as dry powder or the complexes were soluble in the solvent and separated from solvent by evaporation.

Scheme 3. Synthesis of complexes 2-4.



Scheme 4. Synthesis of complexes **5** and **6**.

The physical properties and the percent yields of complexes **1-6** are listed in Table 6.

Table 6. Analytical and physical data of the ligands and their complexes.

Compound	Color	% Yield	m.p (°C)	Solubility
[Zn(RA) ₂ (MeOH) ₂] (1)	Pale yellow	60.75	>250	Water, DMF, DMSO, and slightly soluble in methanol
[Zn(RA) ₂ (2-(methylamino)py)] (2)	Beige	37.10	175	Methanol, DMSO, DMF
[Zn(RA) ₂ (2,2'-bipy)] (3)	Yellowish	63.86	185	Methanol, DMSO, DMF
[Zn(RA) ₄ (4,4'-bipy)] (4)	Yellowish	84.52	157	DMSO and DMF
[Zn(RA) ₂ (2,9-dmp)] (5)	Yellowish	40.00	80	DMSO and DMF
[Zn(RA)(2-ampy) ₂] (6)	Brown	40.00	180	DMSO and DMF

3.2. ^1H and $^{13}\text{C}\{^1\text{H}\}$ NMR spectral results

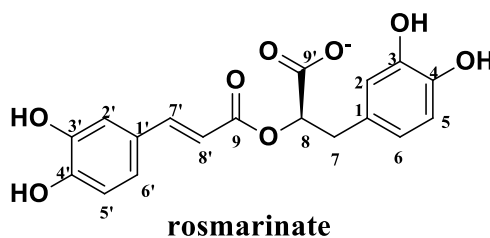
The ^1H and ^{13}C NMR of the diamagnetic Zn(II) complex (**1**) was examined and compared with that of Na_{RA} and RA as shown in Tables 7 and 8. The intensities of ^1H NMR signals exhibited clear correlation with the proposed structures. From the ^1H NMR spectra of rosmarinic acid and sodium rosmarinate the calculated chemical shifts for H3, H4, and H3', and H4' protons are in the range of 4.30-5.47 ppm, whereas in complex **1** spectrum the corresponding signals are not found. The phenolic proton signals is usually a sharp singlet (H2 and H2') in the range of 6.56-7.01 ppm. The presence of two group attached to each other in the ortho position strongly influences the chemical shift of phenolic protons (signals are in the range of 12-10 ppm). This is due to the formation of intramolecular hydrogen bonds. In the ^1H NMR spectrum of complex **1**, the decrease in chemical shifts in comparison to sodium rosmarinate is observed in the case of H2, H5, H6, H7, H8, H2', H5', H7', and H8' protons, while H6' chemical shift was unchanged. In general, only slight changes are noticed when the spectra of complex **1** and sodium rosmarinate, were compared.

Table 7. ^1H NMR spectral data for **1**, Na_{RA} , and RA.

H Number. ^a	^1H NMR ^b 1	^1H NMR ^c Na_{RA}	^1H NMR ^c RA
2	6.65 (d, 1H, 1.8)	6.68	6.59
3	-	-	-
4	-	-	-
5	6.58 (d, 1H, 8.0)	6.61	6.54
6	6.47 (dd, 1H, 1.8)	6.50	6.47
7a	2.73 (dd, 2H, 14.2)	2.78	2.85
7b	2.99 (d, 2H, 11.9)	3.03	2.93
8	4.87 (d, 1H, 8.2)	4.89	5.03
2'	7.01 (s, 1H)	7.05	6.88
3'	-	-	-
4'	-	-	-
5'	6.72 (d, H, 6.5)	6.76	6.61
6'	6.92 (d, 1H, 7.2)	6.92	6.79
7'	7.35 (d, 1H, 15.8)	7.38	7.39
8'	6.16 (d, H, 15.6)	6.19	6.11

*ppm downfield related to TMS as internal standard (CDCl_3).

a: Confirming to following atoms numbers (R = rosmarinate):



b: The data are stated as : chemical shift (multiplicity, integration, and coupling constant ($J_{\text{H-H}}$)). c: Reference (130).

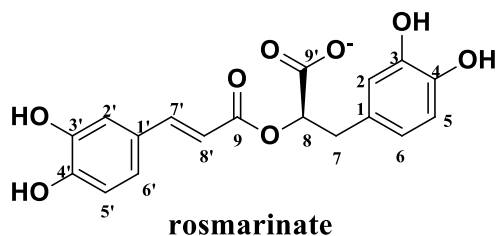
In the ^{13}C -NMR spectra there are resonances attributed to the carbon of aromatic rings (C1–C6) and (C1'–C6'), the double bond (C7'–C8'), the ester group C9 and carboxyl group C9'. ^{13}C NMR spectra of rosmarinic acid and complex **1** show the highest value of chemical shift for C9' carbon atom (171.30-173.01 ppm), slightly lower values of chemical shifts are observed for C9 atom (166.50-166.61 ppm). In the ^{13}C NMR spectrum of complex **1** the chemical shifts observed for C3, C4 and C3', C4' nuclei as well as for C7' are in the range 144.04-148.93 ppm. The lowest chemical shift in complex **1** is observed for C7 of CH₂ group (37.55 ppm). The chemical shifts for C8 atom are 75.81 ppm. The highest changes in complex **1** spectrum in comparison to acid spectrum are noticed for C4' and C4. The increase in chemical shifts in complex **1** spectrum in comparison to acid spectrum is observed in the case of C2', C8', C9, C1, C4, C7, C8, and C9 atoms. In contrast, a decrease is noticed for C3', C4', C5', C6', C7', C2, C3, C5, and C6 atoms.

Table 8. ^{13}C -NMR spectral data for **1**, Na_{RA}, and RA.

C Number. ^a	$^{13}\text{C}\{^1\text{H}\}$ NMR ^b 1	$^{13}\text{C}\{^1\text{H}\}$ NMR ^c Na _{RA}	$^{13}\text{C}\{^1\text{H}\}$ NMR ^c RA
1	129.95	129.83	129.40
2	117.04	116.06	117.50
3	145.33	144.98	146.10
4	148.93	143.63	145.20
5	116.36	115.11	116.50
6	121.48	119.67	121.80
7	37.56	37.25	37.40
8	75.81	75.95	75.00
9	173.01	173.07	167.4
1'	-	125.48	127.60
2'	115.07	114.73	114.50
3'	144.99	146.00	146.80
4'	144.04	148.73	149.70
5'	115.84	116.70	116.20
6'	121.48	120.82	123.10
7'	146.23	144.39	147.60
8'	115.36	115.49	115.20
9'	166.61	166.30	168.50

*ppm downfield related to TMS as internal standard (CDCl_3).

a: Confirming to following atoms numbers (R = rosmarinate):



b: The data are: chemical shift. c: Reference (130)

In summary, comparison of the ^1H NMR spectra of complex **1** and sodium rosmarinate exhibited a slight upfield shift of the former due to complex formation. In addition, the OH resonance in the spectra of complex **1** was absent indicating the coordination with the zinc metal center as shown in Figure 18. While the C=O resonance in complex **1** was shifted downfield from 171.30 (RA) to 173.01 ppm in the ^{13}C NMR (Figure 19) showing a deshielding effect due to pull the electron density from the carboxylate group to the zinc ion. The ^1H NMR spectral data for **2-6** and their parent N-donor ligands are listed in Tables 9-13. The results are in agreement with the proposed structures shown in Schemes 2 and 3. Figure S1-S5 of complexes **2-6** ^1H -NMR spectra are shown in **Appendix A**.

Tables 9-13 show the resonance chemical shifts of the complexes **2-6**, some of the resonance chemical shifts of these complexes are slightly upfield shifted and others are downfield shifted compared to the same resonance in H-RA which may be to complexation with Zn metal cation. The OH group was absent in the spectra of complexes **2-6** may be also indicating the complexation with the zinc metal center.

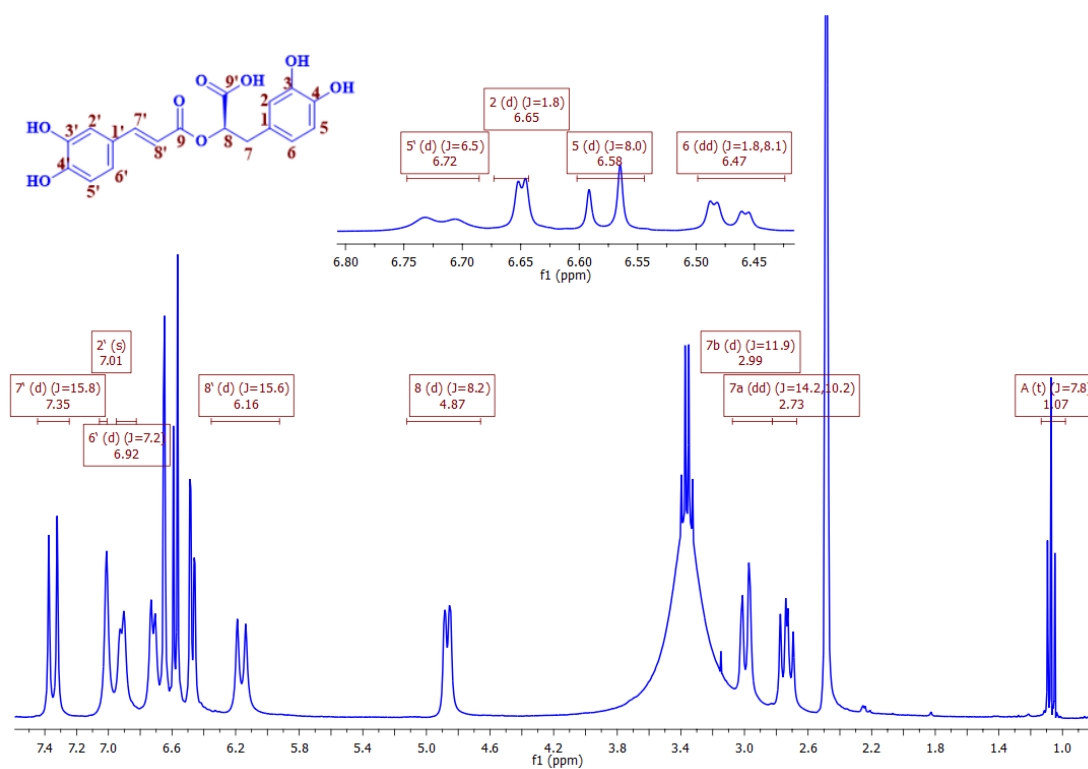


Figure 18. $^1\text{H-NMR}$ spectra of complex 1.

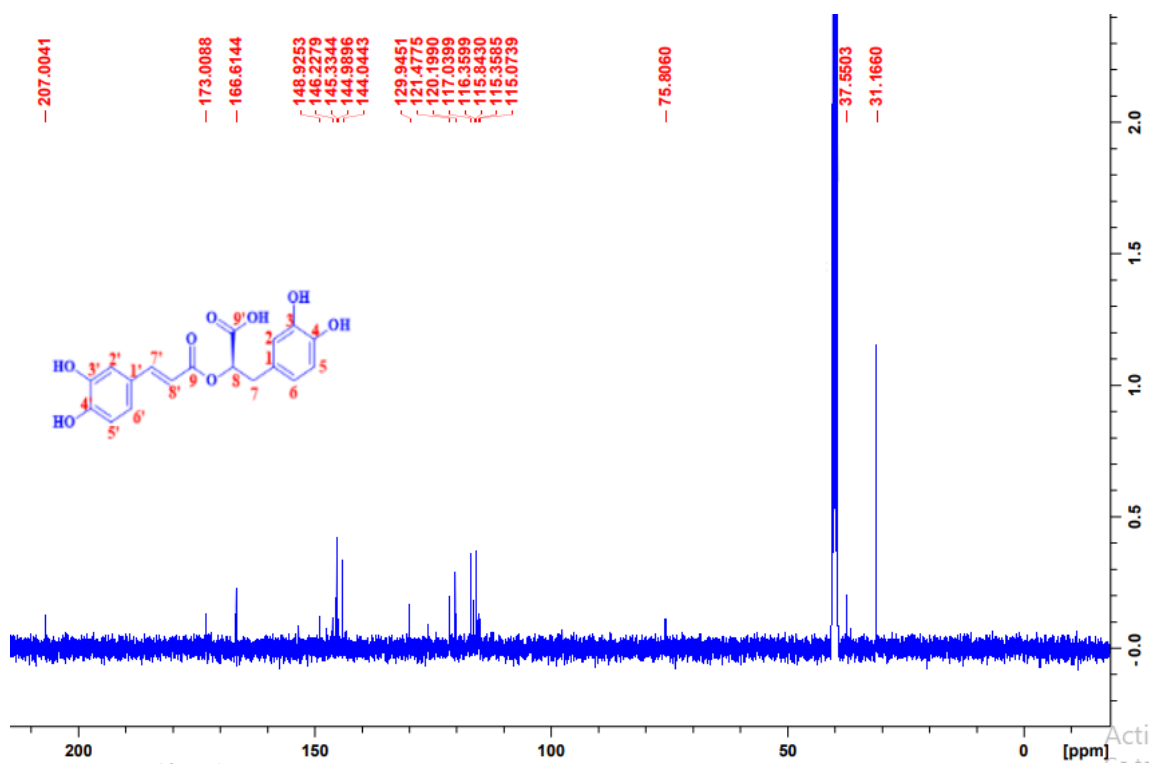


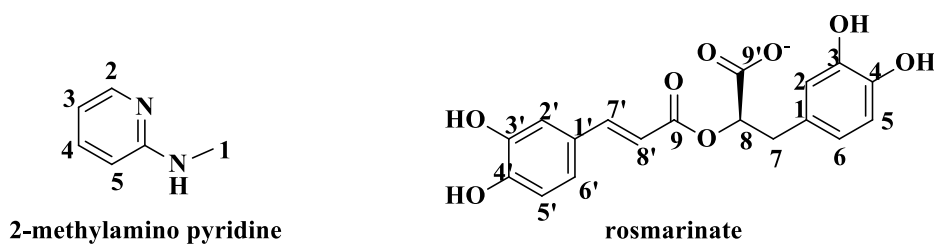
Figure 19. $^{13}\text{C}\{^1\text{H}\}$ -NMR spectra of complex 1.

Table 9. ^1H NMR spectral data for **2**, and 2-(methylamino)py.

H Number. ^a	^1H NMR ^b 2	^1H NMR ^c 2-(methylamino)py
2R	6.66 (s, 1H)	-
5R	6.61 (d, 1H, 7.5)	-
6R	6.50 (d, 1H, 7.5)	-
7a R	2.86 (dd, 2H, 11.7)	-
7b R	2.98 (d, 2H, 11.7)	-
8R	4.95 (d, 1H, 4.8)	-
2'R	7.04 (s, 1H)	-
5'R	6.75 (d, 1H, 8.4)	-
6'R	7.98 (d, 1H, 8.1)	-
7'R	7.32 (d, 1H, 7.2)	-
8'R	6.22 (d, 1H, 15.6)	-
1	2.72 (d, 3H, 3.3)	2.72
2	7.93 (d, 1H, 7.5)	8.07
3	6.42 (t, 1H, 5.4)	6.62
4	7.44 (d, 1H, 9.9)	7.86
5	7.37 (d, 1H, 9.9)	7.13

*ppm downfield related to TMS as internal standard (CDCl_3).

a: Confirming to following atoms numbers (R = rosmarinate):



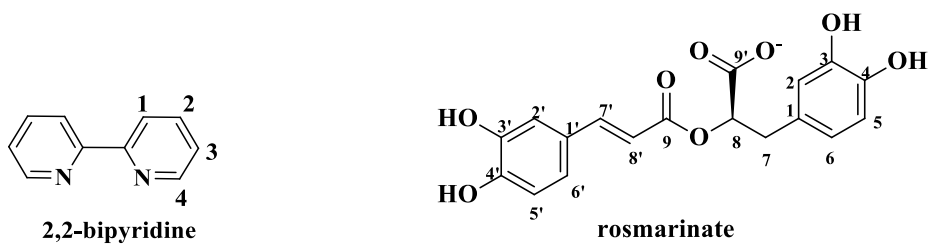
b: The data are stated as: chemical shift (multiplicity, integration, $J_{\text{H-H}}$ (Hz)). c: Reference (131).

Table 10. ^1H NMR spectral data for **3**, and 2,2'-bipy.

H Number. ^a	^1H NMR ^b 3	^1H NMR ^c 2,2'-bipy
2R	6.66 (s, 1H)	-
5R	6.60 (d, 1H, 4.2)	-
6R	6.48 (d, 1H, 6.0)	-
7a R	2.77 (dd, 2H, 13.2)	-
7b R	2.99 (d, 2H, 13.2)	-
8R	4.91(d, 1H, 9.6)	-
2`R	7.03 (s, 1H)	-
5`R	6.75 (d, 1H, 7.8)	-
6`R	7.95(d, 1H, 7.8)	-
7`R	7.37 (d, 1H, 15.6)	-
8`R	6.18(d, 1H, 7.8)	-
1	8.42 (d, 2H, 7.2)	8.496
2	7.49 (s, 2H)	7.124
3	7.98 (s, 2H)	7.658
4	8.71(d, 2H,4.2)	8.587

*ppm downfield related to TMS as internal standard (CDCl_3).

a: Confirming to following atoms numbers (R = rosmarinate):



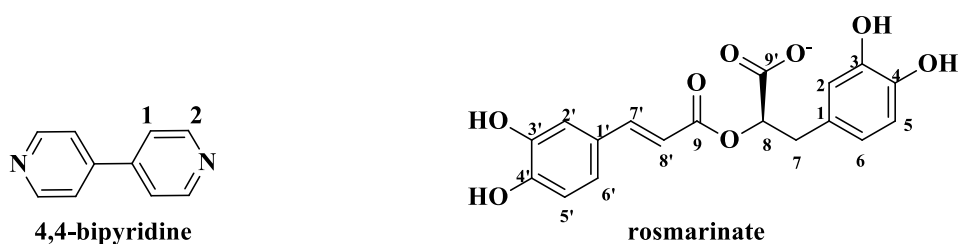
b: The data are stated as: chemical shift (multiplicity, integration, $J_{\text{H-H}}$ (Hz)). c: Reference (132).

Table 11. ^1H NMR spectral data for **4**, and 4,4'-bipy.

H Number. ^a	^1H NMR ^b 4	^1H NMR ^c 4,4'-bipy
2R	6.64(s, 1H)	-
5R	6.58 (d, 1H, 16.8)	-
6R	6.47 (d, 1H, 7.8)	-
7a R	2.77 (dd, 2H, 13.2)	-
7b R	2.98 (d, 2H, 13.2)	-
8R	4.86(d, 1H, 7.5)	-
2`R	7.02 (s, 1H)	-
5`R	6.73 (d, 1H, 8.1)	-
6`R	6.92 (d, 1H, 8.4)	-
7`R	7.36(d, 1H, 15.9)	-
8`R	6.17 (d, 1H, 15.9)	-
1	8.71 (d, 4H, 4.5)	8.75
2	7.82 (d, 4H, 5.1)	7.99

*ppm downfield related to TMS as internal standard (CDCl_3).

a: Confirming to following atoms numbers (R = rosmarinate):



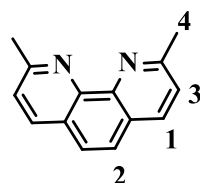
b: The data are stated as: chemical shift (multiplicity, integration, $J_{\text{H-H}}$ (Hz)),c: Reference (133).

Table 12. ^1H NMR spectral data for **5**, and 2,9-dmphen.

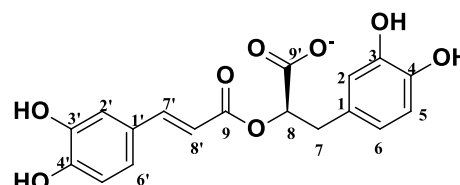
H Number. ^a	^1H NMR ^b 5	^1H NMR ^c 2,9-dmphen
2R	6.67 (s, 1H)	-
5R	6.57 (d, 1H, 4.2)	-
6R	6.47 (d, 1H, 6.6)	-
7a R	2.79 (d, 2H, 15.3)	-
7b R	3.00 (d, 2H, 15.3)	-
8R	4.91 (d, 1H, 8.1)	-
2`R	7.04 (s, 1H)	-
5`R	6.75 (d, 1H, 7.8)	-
6`R	6.92 (d, 1H, 8.1)	-
7`R	7.36(d, 1H, 15.9)	-
8`R	6.17(d, 1H, 16.2)	-
1	2.45 (s, 6H)	2.53
2	7.60 (d, 2H, 7.5)	7.12
3	7.98 (d, 2H, 8.1)	7.92
4	8.75 (t, 2H, 8.1)	8.587

*ppm downfield related to TMS as internal standard (CDCl_3).

a: Confirming to following atoms numbers (R = rosmarinate):



2,9-dimethyl-1,10-phenanthroline



rosmarinate

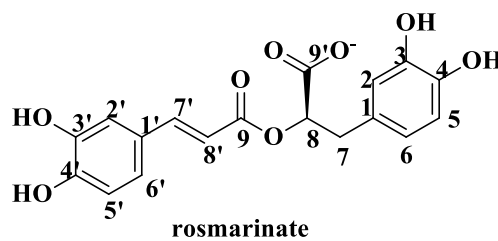
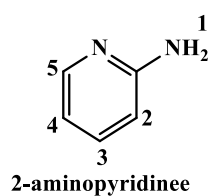
b: The data are stated as: chemical shift (multiplicity, integration, and $J_{\text{H-H}}$ (Hz)).c: Reference (134).

Table 13. ^1H NMR spectral data for **6**, and 2-ampy.

H Number. ^a	^1H NMR ^b 6	^1H NMR ^c 2-ampy
2R	6.64 (s, 1H)	-
5R	6.60 (d, 1H)	-
6R	6.50 (d, 1H)	-
7a R	2.80 (d, 2H)	-
7b R	2.99 (d, 2H)	-
8R	4.99 (d, 1H)	-
2`R	7.01 (s, 1H)	-
5`R	6.70 (d, 1H)	-
6`R	7.90 (d, 1H)	-
7`R	7.35 (d, 1H)	-
8`R	6.19 (d, 1H)	-
1	7.85 (s, 2H)	7.74
2	6.40 (d, 1H)	6.70
3	7.45 (d, 1H)	7.55
4	5.85 (s, 1H)	6.62
5	8.70 (d, 1H)	8.07

*ppm downfield related to TMS as internal standard (CDCl_3).

a: Confirming to following atoms numbers (R = rosmarinate):



b: The data are stated as: chemical shift (multiplicity, and integration). c: Reference (135).

The ^1H NMR spectral data for complex **2** shows that the ligand resonances (8.07, 7.13, 6.62, and 2.72 ppm) were observed at 7.93, 7.37, 6.42, and 2.72 ppm in the complex. The significant shift of the $-\text{CH}-$ proton from 7.86 in the free ligand ppm to 7.44 ppm in the complex was observed.

The spectrum of complex **3** shows that the ligand resonances (8.587, 8.50, 7.66, and 7.12 ppm in the ligand) were observed at 8.69, 8.45, 8.04, and 7.53 ppm in the complex, respectively.

In the ^1H NMR spectra of complexes **4-6** the upfield shifts compared to the corresponding free ligands chemical shifts are observed in the case of H1 and H2 in **4**, H1 in **5**, H2, H3, and H4 protons in **6**. In comparison, an increase is noted for H2 in **5** and H1 and H5 in **6**.

Particularly, NMR is a powerful technique that can give useful information regarding the determination of the binding modes of the carboxylate group. Both NMR and IR techniques are providing complementary data for diagnosing the binding modes of the carboxylate groups. It is well-known that the ^{13}C chemical shift of the carbonyl carbon (COO^-) depends on both the coordination number of metal ions and on the coordination modes. The chemical shifts of

carbonyl carbon $\delta_{(\text{COO}^-)}$ in metal carboxylates are in the following order:

$$\delta_{(\text{COO}^-)} \text{ Bidentate chelating} > \delta_{(\text{COO}^-)} \text{ bidentate bridging} > \delta_{(\text{COO}^-)} \text{ monodentate.}$$

However, the $^{13}\text{C}\{^1\text{H}\}$ NMR chemical shifts may be influenced by different factors that form a little but not equal shift of signals. In order to determine the carboxylate binding mode of Zn(II) rosmarinate complex **1**; it was essential to use an internal standard in $^{13}\text{C}\{^1\text{H}\}$ NMR spectra. It can be noticed that the chemical shift of the C7 of the rosmarinate group is less affected due to the complexation and metal environment. This suggestion is in confirmation with the small change showed in the chemical shift values for the C7 in zinc rosmarinate complex **1**. The small change in this chemical shift may be due to external effects such as temperature or concentration. Therefore, the $^{13}\text{C}\{^1\text{H}\}$ NMR chemical shifts of the carbonyl group (COO^-) have been calculated using the C7 chemical shift value as a reference. $\delta'(\text{COO}^-) = [\delta(\text{COO}^-) - \delta(\text{C7})]$. $\delta'(\text{COO}^-)$ is 135.46 for complex **1**. Using the results of $\Delta\nu(\text{COO}^-)$ and $\delta' ^{13}\text{C}(\text{COO}^-)$ for zinc rosmarinate complexes, the binding mode of the rosmarinate in complex **1** can be assumed as chelating bidentate.

3.3. Infrared spectra

IR spectroscopy has confirmed to be suitable technique to determine the method of bonding of the ligand to the metal ion.¹²⁹ The determination of the nature of coordinating atoms is made on the basis of the comparison of the IR spectra of the parent ligand and the complexes.^{84,129} The FT-IR spectra of the complexes show all the absorption peaks from the ligands and other new absorption peaks showing coordination of the ligands with metal ions through nitrogen and oxygen atoms.¹³⁶ The carboxylate binding mode has often been determined from the magnitude of the observed difference between the symmetric and asymmetric carboxylate stretching frequencies, [$\Delta = \nu_{\text{as}}(\text{COO}^-) - \nu_{\text{s}}(\text{COO}^-)$].^{129,137} The differences between $\nu_{\text{as}}(\text{COO}^-)$ and $\nu_{\text{s}}(\text{COO}^-)$ of rosmarinate group complexes **1-6** are given in Tables 14 and 15 with $\Delta\nu(\text{COO}^-)$ values = 151.36, 149.18, 152.99, 148.4, 145.95, and 152.61 for complexes **1-6** respectively, supporting the chelating bidentate coordination mode of carboxylate groups.

Table 13 shows the bands assignment and their corresponding wave numbers for RA, Na_{RA}, and complex **1**. The IR spectrum for complex **1** exhibits two (COO⁻) stretching frequencies symmetric and asymmetric, $\nu_{\text{s}}(\text{COO}^-)$ at 1445.50 cm⁻¹ and $\nu_{\text{as}}(\text{COO}^-)$ at 1596.86 cm⁻¹.

The difference between them is $\Delta\nu(\text{COO}^-) = 151.36 \text{ cm}^{-1}$) which is less than ($\Delta\nu(\text{COO}^-) = 183.31\text{cm}^{-1}$) of Na_{RA} indicating chelating bidentate coordination modes between the zinc cation and rosmarinic acid (Figure 20). Figure S6-S10 of complexes **2-6** IR spectra are shown in **Appendix B**.

Table 14. Important IR spectral data of the RA, $\text{Na}_{\text{(RA)}}$ and complex **1**.

Assignments	RA	$\text{Na}_{\text{(RA)}}$	Complex 1
$\nu(\text{C-H})_{\text{ar}}$	3163.39	2975.62	3190.45
$\nu(\text{C=C})$	1645	1684.24	1686.90
$\nu(\text{C=O})_{\text{carb}}$	1709.23	-	-
$\nu(\text{COO}^-)_{\text{asym}}$	-	1585.65	1596.86
$\nu(\text{COO}^-)_{\text{sym}}$	-	1402.34	1445.50
$\nu(\text{C-O})$	-	1159	1158.77
$\nu(\text{C-C})_{\text{ring}}$	1517.50	1508.92	1522.68
$\Delta\nu(\text{COO}^-)$	-	183.31	151.36
$\nu(\text{Zn-O})$	-	-	-

In general, The peaks appearing in the (430-520) cm^{-1} range correspond to $\nu(\text{M-O})$ as weak ones.¹³⁸⁻¹⁴⁰ In complex **2**, $\Delta\nu(\text{COO}^-) = 149.18 \text{ cm}^{-1}$ is less than $\Delta\nu(\text{COO}^-)$ of Na_{RA} , indicating chelating bidentate coordination of the carboxylate groups. Also in complexes **3-6**, $\Delta\nu(\text{COO}^-) = 152.99, 148.4, 145.95, 152.61, \text{ and } \text{cm}^{-1}$ respectively and all are less than $\Delta\nu(\text{COO}^-)$ of Na_{RA} ($\Delta\nu(\text{COO}^-) = 183.31 \text{ cm}^{-1}$), that indicate chelating bidentate coordination mode of the carboxylate groups.

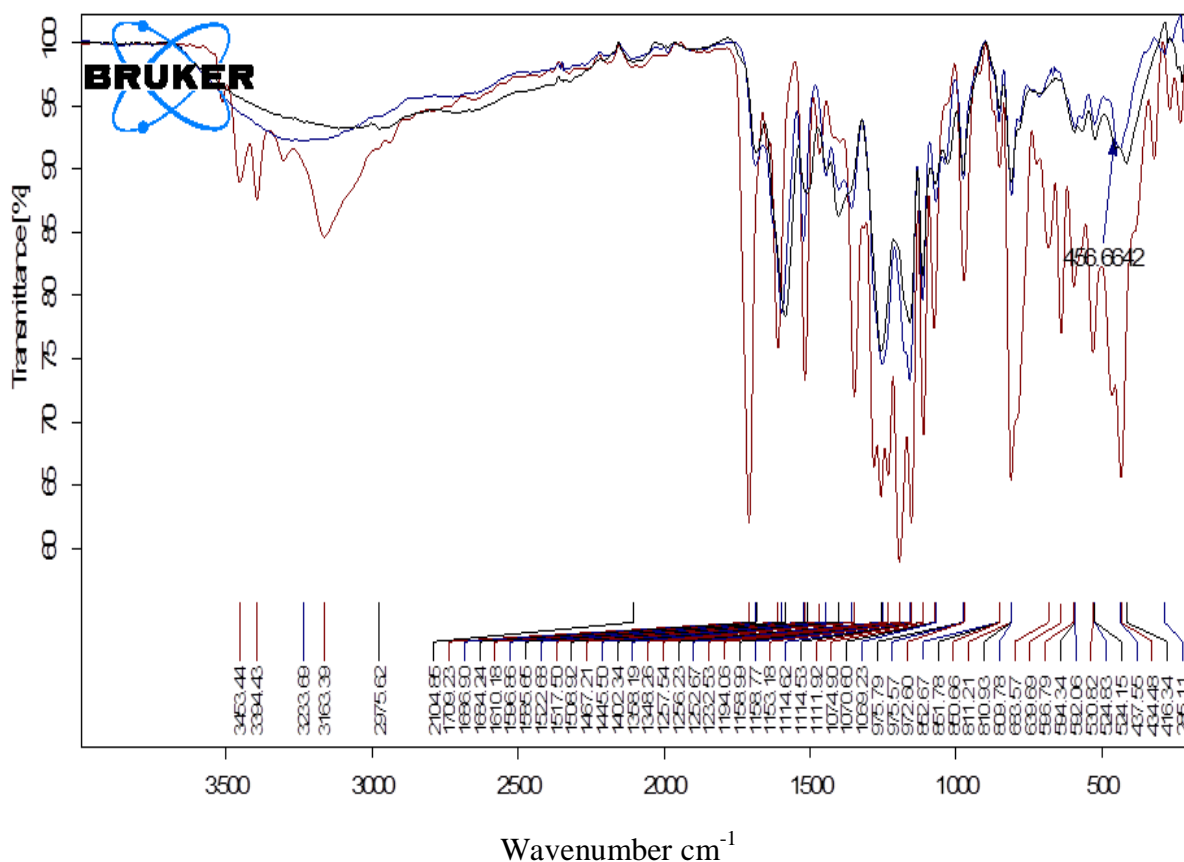


Figure 20. IR spectra of RA (red), Na_{RA} (black), and complex **1**(blue).

Table 15. Important IR spectral data (in cm^{-1}) of complexes **2-6**.

Assignments	Complex 2	Complex 3	Complex 4	Complex 5	Complex 6
$\nu(\text{C-H})_{\text{ar}}$	3113.83	3080.19	3014.24	3448.98	3081.55
$\nu(\text{C}=\text{C})$	1661.44	1694.99	1685.59	1669.85	1167.99
$\nu(\text{C}=\text{O})_{\text{carb}}$	-	-	-	-	-
$\nu(\text{COO}^-)_{\text{asym}}$	1591.11	1592.80	1589.02	1593.63	1587.08
$\nu(\text{COO}^-)_{\text{sym}}$	1441.93	1439.81	1445.23	1430.53	1441.13
$\nu(\text{C-O})$	1159.37	1155.43	1160.37	1268.16	1156.66
$\nu(\text{C-C})_{\text{ring}}$	1518.77	1515.33	1520.71	1500.39	1517.10
$\Delta\nu(\text{COO}^-)$	149.18	152.99	143.79	163.10	145.95
$\nu(\text{Zn-O})$	-	-	-	-	-

3.4. Electronic Absorption Spectral Results

As shown in Figure 21, UV–Vis spectra of RA and its metal complex in water measured in the range of 200–500 nm show two distinct regions. The lower wavelength in the range of 200–400 nm is specific

for the electronic intra-ligand transitions.¹²⁹ The higher wavelength region is specific for d–d transition.¹²⁹ The observed absorption bands and their assignments are shown in Table 16.

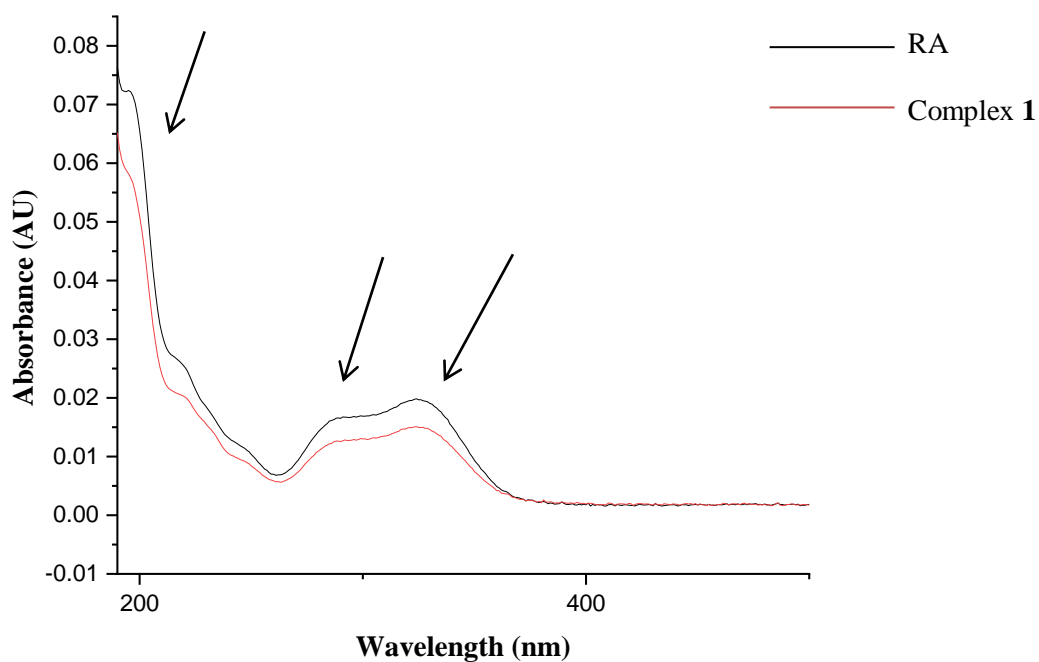


Figure 21. UV-Vis spectra of RA and complex 1.

Table 16. Electronic spectral data (nm) of the RA and complex 1.

Compound	$\sigma \rightarrow \sigma^*$	$\pi \rightarrow \pi^*$	$n \rightarrow \pi^*$	d–d
Rosmarinic acid	197	324	287	-
[Zn(RA) _n] (1)	197	324	261	-

RA exhibits a band at 287 nm assignable to $n-\pi^*$ transition, which is changed in the spectra of their metal complexes. In addition, in the spectrum of RA there are two bands at 197 nm and 324 nm, which may be attributed to $\sigma \rightarrow \sigma^*$ and $\pi \rightarrow \pi^*$ transitions, respectively.

Absorption spectra of all complexes **2-6** were performed in suitable solvent and were similar to those of the parent N-donor ligands with only small changes caused by coordination to the zinc cation, Table 17. Figure S11-S15 of complexes **2-6** UV-Vis spectra are shown in **Appendix C**.

Thus almost all bands exhibited by the complexes are due to the ligands bands. Complex **1** exhibited no UV-Vis band maximum between 400-800; which is in agreement with the spectra of RA. However, there is a spatial configuration of d^{10} track in the metal ion Zn(II) and the d orbitals are completely filled; thus no d-d electronic transition bands will be shown for all complexes.

Table 17. Electronic spectral data (nm) of the ligands and their complexes.

Compound	$\sigma \rightarrow \sigma^*$	$\pi \rightarrow \pi^*$	$n \rightarrow \pi^*$	d-d
[Zn(RA) _n (2-(methylamino)py) _m] (2)	201	324	288	-
2-(methylamino)py	195	306	242	-
[Zn(RA) _n (2,2'-bipy) _m] (3)	200	328	284	-
2,2'-bipy	201	280	236	-
[Zn(RA) _n (4,4'-bipy) _m] (4)	195	327	273	-
4,4'-bipy	203	270	243	-
[Zn(RA) _n (2,9-dmp) _m] (5)	194	326	273	-
2,9-dmp				
[Zn(RA) _n (2-ampy) _m] (6)	233	321	289	-
2-ampy	195	298	240	-

3.5. Bioassay Antibacterial Activity

The ligands and their metal complexes were screened for their antibacterial activity by using the agar-well diffusion method. Both gentamycin and erythromycin were used as standard antibacterial agent. The concentration was 12 mg ml⁻¹ in DMSO with a volume of 25 μ L per well. The values of antibacterial activity are obtained by

calculating the average of the three trials and are expressed as average \pm standard deviation. Figure **22** shows the agar diffusion plates.

The results obtained are presented in Tables 18 and 19. The negative control, DMSO, did not exhibit any inhibition zone against all the tested bacteria. The first positive control, gentamycin, showed an average inhibition zone (mm) of 35.6, 26.3, 33.3, 25.0, 25.6, 28.0, 38.6, 18.6, and 36.0 against *M. luteus*, *B. subtilis*, *S. aureus*, *E. coli*, *P. mirabilis*, *K. pneumoniae*, *S. epidermidis*, *E. faecalis*, and *P. aeruginosa*, respectively. Also, the second positive control, erythromycin, showed an average inhibition zone (mm) of 38.6, 38.3, 38.7, 20.0, 14.3, 21.7, 39.5, -, 19.0 0 against *M. luteus*, *B. subtilis*, *S. aureus*, *E. coli*, *P. mirabilis*, *K. pneumoniae*, *S. epidermidis*, *E. faecalis*, and *P. aeruginosa*, respectively.

As shown in Tables 17 and 18 agar the well-diffusion analysis results revealed that complex **1** showed antibacterial activity against the test bacteria of *P. aeruginosa*, *K. pneumoniae*, and *M. luteus* with average inhibition zones of 31.0 mm, 15.0 mm, and 10.0 mm, respectively. However, it showed more significant antibacterial activity against the of *P. aeruginosa* strains compared with the other test strains.

Table 18. Results of antibacterial bioassay against Gram- positive bacteria (concentration used in 12 mg ml⁻¹ of DMSO)^a

Compound	<u>Diameter of zones showing complete inhibition of growth (mm)^b</u>				
	<i>M. luteus</i>	<i>B. subtilis</i>	<i>S. aureus</i>	<i>S. epidermidis</i>	<i>E. faecalis</i>
Gentamycin	35.6 ± 1.0	26.3 ± 1.1	33.3 ± 0.5	38.6 ± 4.6	18.6 ± 3.2
Erythromycin	38.6 ± 0.5	38.3 ± 3.8	38.7 ± 0.5	39.5 ± 0.6	-
ZnCl ₂	-	-	-	-	-
DMSO	-	-	-	-	-
RA	-	-	-	-	-
Complex 1	-	-	-	-	-
2- (methylamino) py	-	16.7 ± 3.5	21.0 ± 6.0	15.7 ± 3.5	-
Complex 2	9.7 ± 1.0	-	21.7 ± 2.7	-	-
2,2'-bipy	34.3 ± 7.0	17.6 ± 3.2	-	28.3 ± 2.7	-
Complex 3	-	-	-	-	-
4,4'-bipy	-	-	-	-	-
Complex 4	-	-	-	-	-
2,9-dmp	-	-	-	-	-
Complex 5	15.0 ± 0.0	15.7 ± 1.0	11.3 ± 1.1	-	12.0 ± 0.8
2-ampy	-	-	13.3 ± 2.7	-	-
Complex 6	9.0 ± 0.0	-	19.0 ± 1.6	-	18.6 ± 0.9

^a Gentamycin and erythromycin were used as a standard antibacterial agent, ^b the data expressed as average ± sta. deviation (N = 3), - dashes showing zero inhibition of growth, all tested bacteria were resistance to DMSO.

Complex **2** showed good antibacterial activity against Gram-negative bacteria: *P. aeruginosa* and *E. coli* with average inhibition zones of 32.0 mm and 18.3 mm, respectively. For the Gram-positive bacteria, *M. luteus*, complex **2** showed weaker inhibition activity with IZD of 9.7 mm. The complexes **1-4** did not show any antibacterial activity against *E. faecalis* and *B. subtilis*.

Complex **3** showed good inhibition activity against all screened Gram-negative bacteria except for *E.coli* with IZD ranging between 16.0-23.0 mm. For the Gram positive bacteria, *M. luteus*, complex **3** showed antibacterial activity with average inhibition zone of 15.0 mm.

Complex **4** showed more significant antibacterial activity against the strains of *P. aeruginosa* and *P. mirabilis* with average inhibition zones of 22.0 mm and 21.3 mm, respectively. This complex showed weak inhibition activity against *M. luteus*, *E. coli*, and *K. pneumoniae* with average inhibition zones of 8.0 mm, 10.3 mm, and 12.7 mm respectively.

Table 19. Results of antibacterial bioassay against Gram- negative bacteria (concentration used in 12 mg ml⁻¹ of DMSO)

Compound	<u>Diameter of zones showing complete inhibition of growth (mm)</u>			
	<i>E. coli</i>	<i>P. mirabilis</i>	<i>K. pneumoniae</i>	<i>P. aeruginosa</i>
Gentamycin	25.0 ± 0.9	25.6 ± 1.4	28.0 ± 1.8	36.0 ± 3.2
Erythromycin	20.0 ± 0.9	14.3 ± 2.7	21.7 ± 1.1	19.0 ± 1.6
ZnCl ₂	-	-	-	-
DMSO	-	-	-	-
RA	15.0 ± 0.0	-	-	11.6 ± 0.5
Complex 1	-	-	15.0 ± 0.0	31.0 ± 1.4
2- (methylamino) py	-	-	-	13.0 ± 2.0
Complex 2	18.3 ± 1.4	9.5 ± 2.1	-	32.0 ± 1.0
2,2'-bipy	24.0 ± 4.2	26.0 ± 1.4	28.0 ± 2.4	-
Complex 3	16.0 ± 4.0	22.3 ± 0.5	14.7 ± 0.5	23.0 ± 2.6
4,4'-bipy	11.3 ± 0.5	-	12.5 ± 2.1	-
Complex 4	10.3 ± 0.5	21.3 ± 1.1	12.7 ± 1.1	22.0 ± 2.0
2,9-dmp	-	-	-	-
Complex 5	19.5 ± 0.6	-	9.5 ± 0.6	22.0 ± 2.0
2-ampy	-	-	-	-
Complex 6	24.0 ± 0.9	10.5 ± 0.6	-	18.0 ± 2.0

Complexes **5** and **6** did not show antibacterial activity against *S. epidermidis*. These complexes showed good antibacterial activity

against *P. aeruginosa* and *E. coli* with IZD ranging between 18.4-24.0 mm. For the Gram-positive bacteria, complex **6** showed good inhibition of growth against *S. aureus* (19.0 mm). On the other hand, complex **5** showed weak inhibition towards *S. aureus*. The ligands generally exhibited moderate antibacterial activity against three or four species and insignificant activity against two or three species.

A cursory view of the data indicates the following trends in the activity of complex **3** under investigation against *M. luteus*, *P. mirabilis*, and *K. pneumonia*:

Parent ligand (2,2'-bipy) > complex **3**

The parent ligand (2,2'-bipy) was found to be more active than complex **3**. The complexes **2** and **6** showed substantially enhanced antibacterial activity against *P. aeruginosa* compared with the parent ligand.

The minimum inhibition concentration (MIC), which is known as the lowest concentration of the injected sample that inhibits the bacterial growth, was determined for complexes **1-6** and their parent ligands against *P. aeruginosa*. The data are summarized in Table 20

Table 20. *In-vitro* antibacterial activity data of complexes **1-6** at 18 mg/ml.*

Complex	1	2	3	4	5	6	L1	L2	L3	L4	L5	L6
MIC	4.5	4.5	4.5	4.5	-	9	9	2.25	2.25	4.5	9	4.5

*The data are the rounded average of three trials, - dashes indicated error, all microorganisms were resistant to DMSO. The concentration of complexes and their ligands is 18 mg/ml in DMSO. ERYC = Erythromycin (2.0 mg/ml) and AMP = Ampicillin (2.0 mg/ml). The MIC values for the ERYC and AMP are 0.25 and 0.5 mg/ml, respectively.

The complexes **2-6** showed good antibacterial activity against *P. aeruginosa* compared with the parent ligand. The MIC values for the complexes **1-4** are 4.5 mg/ml, undetermined for **5**, and 9 mg/ml for **6**.

In general, the enhancement of metal complexes in the bacterial activity can be rationalized on the basis of chelation theory.¹²⁹ Chelation decreases the polarity of the metal ion mainly because of the partial sharing of its positive charge with the donor groups and possible π -electron delocalization through the chelate ring system produced during coordination.^{129,141,142} Moreover, chelation increase the lipophilic character of the central metal atom, that favors its permeation more efficiently within the lipid layers of the cell membrane and blocking the metal binding sites in the enzymes of the

microorganism.¹⁴² Furthermore, the variation in the effectiveness of different metal complexes against different organism depends on the impermeability of the microbes or on the ribosomes of microbial cells.¹⁴³

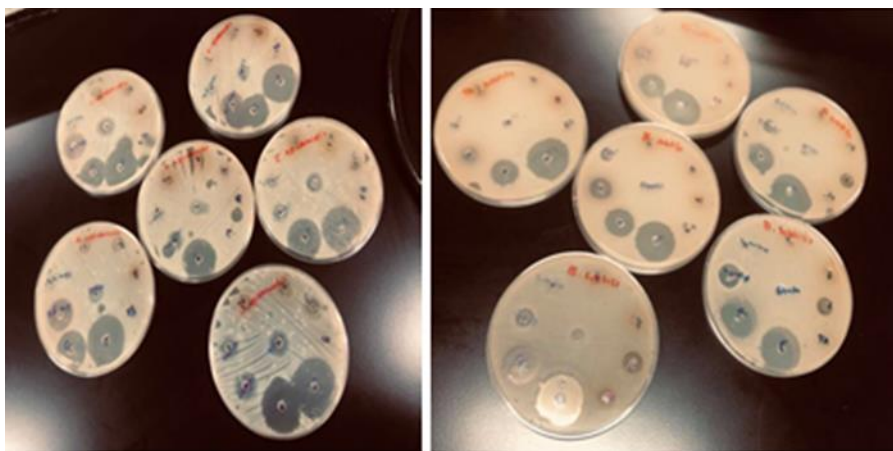


Figure 22. Agar diffusion plates.

3.6. Kinetic Measurements of BNPP Hydrolysis Results

The system made up of a nitrogen heterocyclic ligand with zinc(II) cation (complex **1**, **3**, and **4**) were used in the catalytic hydrolysis of bis(4-nitrophenyl) phosphate ester (BNPP). The rate of BNPP hydrolysis was performed at different pH, concentrations, and temperatures. The optimum conditions for hydrolysis of BNPP were determined by changing one of these factors and adjusting the other two factors constant.

3.6.1. Effects of temperature on the reactions of BNPP with complex (1)

Figure 23 shows the relationship between the absorbance and time at different temperature and constant pH and concentration of both complex **1** and BNPP. The initial rate of BNPP hydrolysis (V_0) was determined through plotting the absorbance of p-nitrophenol vs. time at 400 nm. For complex **1**, the value of V_0 are 7.0×10^{-8} , 3.0×10^{-8} , and 4.0×10^{-8} mol/L.S at $T= 25\text{ }^\circ\text{C}$, $37\text{ }^\circ\text{C}$, $41\text{ }^\circ\text{C}$, respectively. The maximum initial rate observed at $25\text{ }^\circ\text{C}$ for complex **1**.

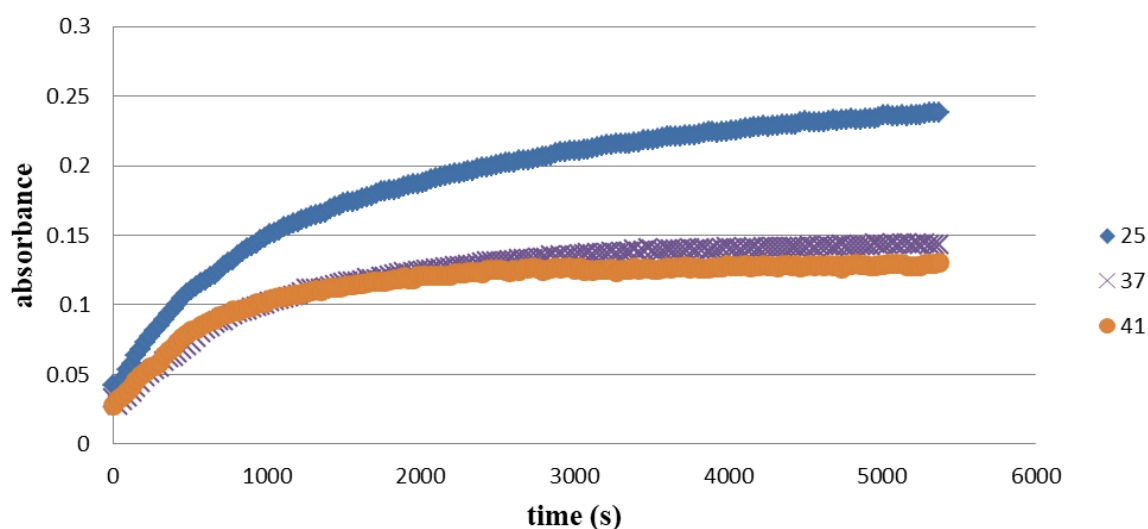


Figure 23. Plots of absorbance at 400 nm vs. time for BNPP hydrolysis by complex **1** in DMSO/HEPEs buffer solution with different temperature under the selected conditions ($\text{pH} = 7.40$, $[\text{complex } \mathbf{1}] = 5.8 \times 10^{-4}$ M, $[\text{HEPEs buffer}] = 50 \times 10^{-6}$ M and $[\text{BNPP}] = 1 \times 10^{-4}$ M).

3.6.2. Effects of pH on the reactions of BNPP with complex 1

Figure 24 shows the relationship between the absorbance and time at various solution pH values in the presence of 5.8×10^{-4} M of complex 1 and constant temperature and concentration of both complex 1 and BNPP. The values of V_0 at the pH = 6.96, 7.4, and 8.1 are 3.0×10^{-8} , 5.0×10^{-8} , and 3.0×10^{-8} mol/L.S, respectively for complex 1. The maximum initial rate observed at pH = 7.40 for complex 1.

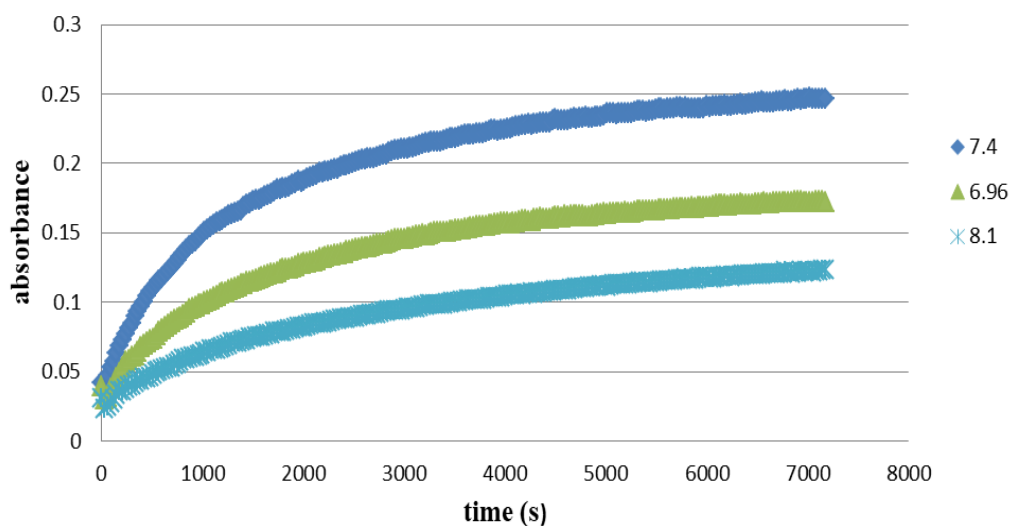


Figure 24. Plots of absorbance at 400 nm vs. time for BNPP hydrolysis by complex 1 in DMSO/HEPEs buffer solution with different solution pH values under the selected conditions ($T = 25$ °C, $[\text{complex 1}] = 5.8 \times 10^{-4}$ M, $[\text{HEPEs buffer}] = 50 \times 10^{-6}$ M and $[\text{BNPP}] = 1 \times 10^{-4}$ M).

3.6.3. Effects of temperature on the Reactions of BNPP with complex 3

Figure 25 shows the relationship between the absorbance and time at different temperature in the presence of 2.0×10^{-4} M of complex 3 and constant pH and concentration of both complex 3 and BNPP. For complex 3, the value of V_0 are 6.0×10^{-8} , 1.0×10^{-7} , and 1.0×10^{-7} mol/L.S at $T= 25$ °C, 37 °C, 43 °C, respectively. The maximum initial rate observed at 25 °C for complex 3.

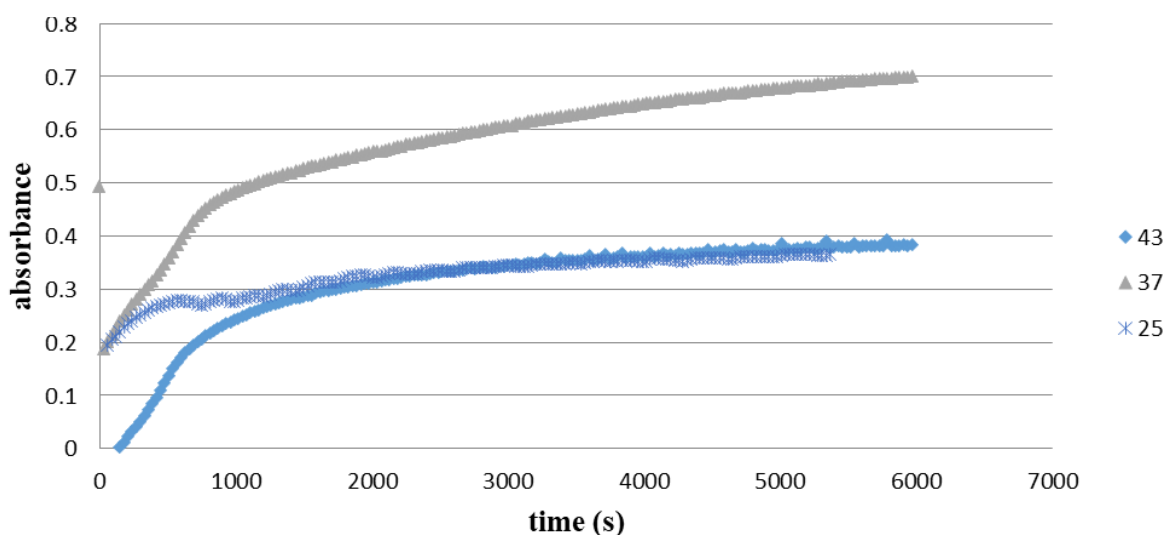


Figure 25. Plots of absorbance at 400 nm vs. time for BNPP hydrolysis by complex 3 in DMSO/HEPEs buffer solution with different temperature under the selected conditions (pH = 7.47, [complex 3] = 2.0×10^{-4} M, [HEPEs buffer] = 50×10^{-6} M and [BNPP] = 1×10^{-4} M).

3.6.4. Effects of pH on the reactions of BNPP with complex 3

Figure 26 shows the relationship between the absorbance and time at various solution pH value in the presence of 2×10^{-4} M of complex 3 and constant temperature and concentration of both complex 3 and BNPP. The values of V_0 at the pH = 6.96, 7.47, and 7.91 are 5.0×10^{-8} , 6.0×10^{-8} , and 4.0×10^{-8} mol/L.S, respectively for complex 3. The maximum initial rate observed at pH = 7.47 for complex 3.

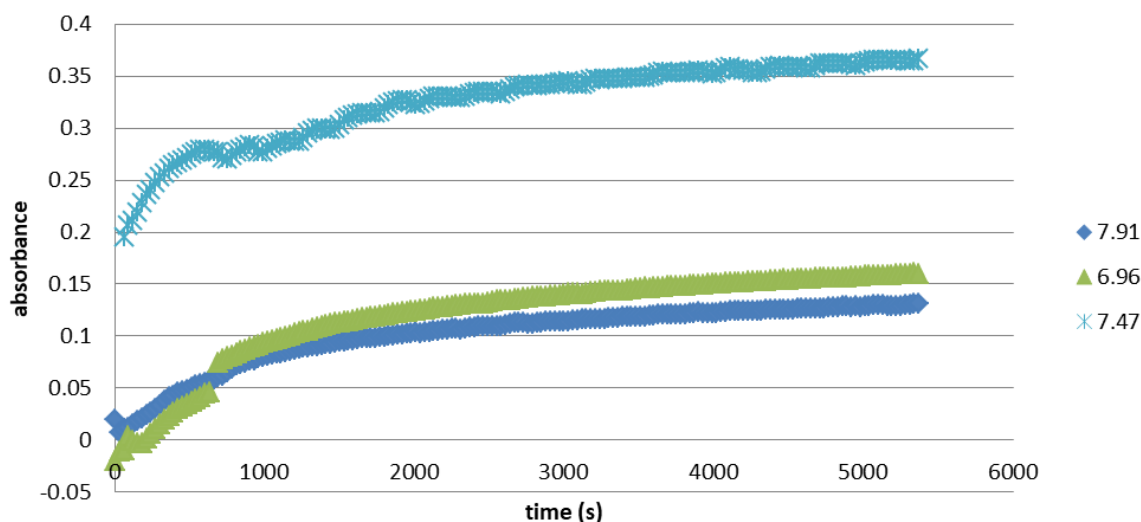


Figure 26. Plots of absorbance at 400 nm vs. time for BNPP hydrolysis by complex 3 in DMSO/HEPEs buffer solution with different solution pH values under the selected conditions ($T = 25$ °C, [complex 3] = 2×10^{-4} M, [HEPEs buffer] = 50×10^{-6} M and [BNPP] = 1×10^{-4} M).

3.6.5. Effects of complex **3** concentration on the reactions of BNPP with complex (**3**)

Figure 27 shows the relationship between the absorbance and time at different concentration of complex **3** and constant pH and temperature. The initial rates were determined to be 1.0×10^{-7} and 3.0×10^{-8} mol/L.S for 2.0×10^{-4} M and 1.0×10^{-3} M, respectively. The maximum initial rate observed at 2.0×10^{-4} M for complex **3**.

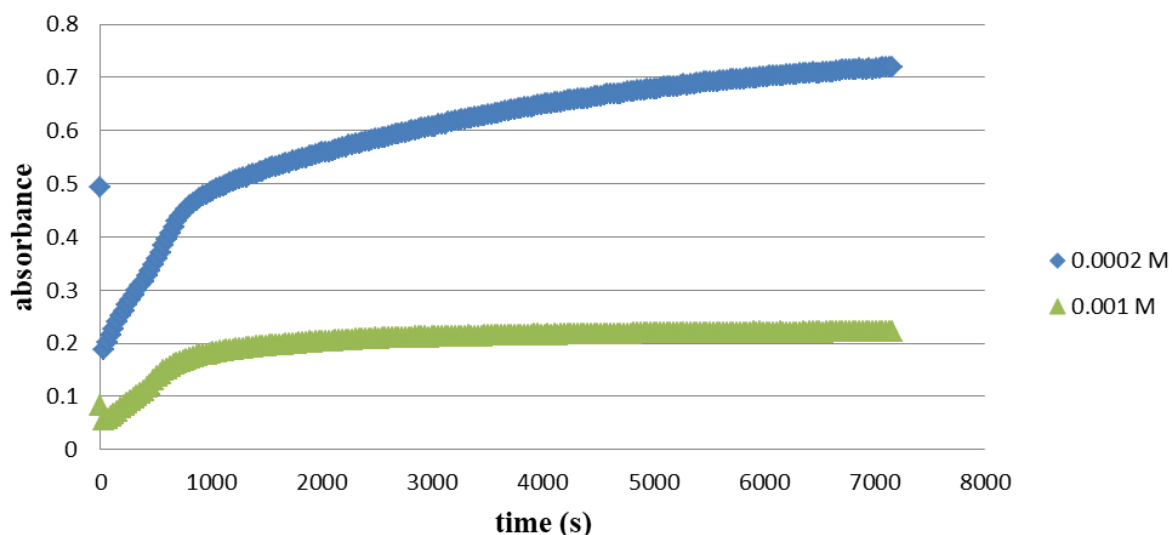


Figure 27. Plots of absorbance at 400 nm vs. time for BNPP hydrolysis by complex **3** in DMSO/HEPEs buffer solution with different concentration of complex **3** under the selected conditions (pH = 7.47, T = 37 °C, [HEPEs buffer] = 50×10^{-6} M and [BNPP] = 1×10^{-4} M).

3.6.6. Effects of complex 4 concentration on the Reactions of BNPP with complex (4)

Figure 28 shows the relationship between the absorbance and time at different concentration of complex 4 and constant pH and temperature. The initial rates were determined to be 1.0×10^{-7} and 5.0×10^{-8} mol/L.S for 5.3×10^{-7} M and 5.3×10^{-6} M, respectively. The maximum initial rate observed at 5.3×10^{-7} M for complex 4.

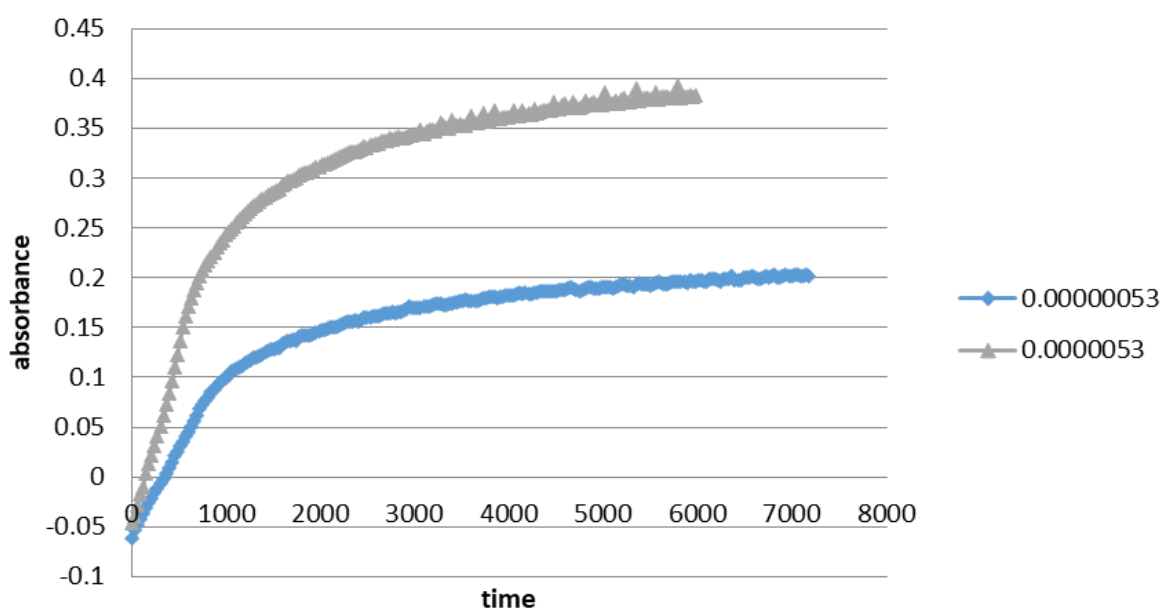


Figure 28. Plots of absorbance at 400 nm vs. time for BNPP hydrolysis by complex 4 in DMSO/HEPEs buffer solution with different concentration of complex 4 under the selected conditions (pH = 6.99, T = 41 °C, [HEPEs buffer] = 50×10^{-6} M and [BNPP] = 1×10^{-4} M).

ON the basis of Michaelis–Menten equation ($1/V_o = 1/V_{\max} + K_m/V_{\max}[\text{BNPP}]$) and experimental data, the plots $1/V_o$ versus $1/[\text{BNPP}]$ is shown in Figure 29. From the intercept of the straight lines in Figure 29, obtained via a linear fit using the least-squares method, V_{\max} values were evaluated and are listed in Table 21. The curve of Figure 29 shows a good linear relationship between the variables, with $R^2 = 0.9368$, which means the above mathematical model is reasonable. All complexes **1**, **3**, and **4** have the similar relationship.

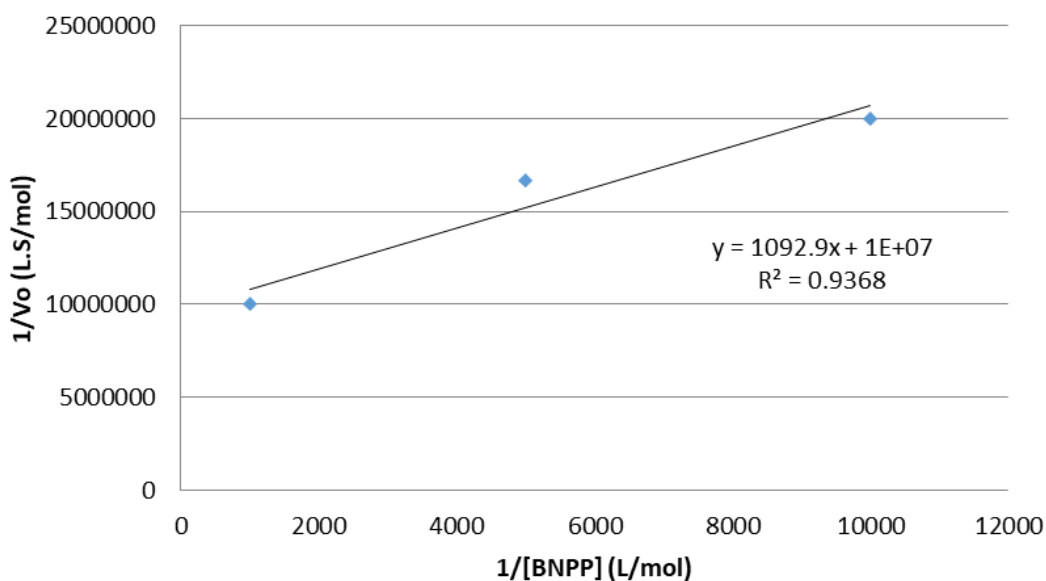


Figure 29. Second order rate for complex **3** with different $[\text{BNPP}]$ under the selected conditions (pH = 7.91, temp = 37 °C and $[\text{complex } \mathbf{3}] = 2 \times 10^{-4} \text{ M}$).

The hydrolysis rate of BNPP for the **1**, **3**, and **4** complexes as follow:
5.2 at 25 °C, 4.2 at 37 °C, and 8.3 at 41 °C, respectively.

Table 21. Kinetic parameters of the BNPP hydrolysis for complexes **1**, **3** and **4** at different BNPP concentrations.

Concentration (M)		V_o (mol/L.S)	V_{max} (mol/L.S)	K_m (mol/L)	K_{cat} (S ⁻¹) *	2-order rate K_{BNPP} (L.mol ⁻¹ .S ⁻¹)**
Complexes	BNPP					
1 (5.8×10^{-4})	1.0×10^{-4}	7.0×10^{-8}				
1 (5.8×10^{-4})	2.0×10^{-4}	9.0×10^{-8}	2.0×10^{-7}	4.6×10^{-5}	2.4×10^{-4}	5.2
1 (5.8×10^{-4})	1.0×10^{-3}	6.0×10^{-8}				
3 (2.0×10^{-4})	1.0×10^{-4}	5.0×10^{-8}				
3 (2.0×10^{-4})	2.0×10^{-4}	6.0×10^{-8}	1.0×10^{-7}	1.2×10^{-4}	5.0×10^{-4}	4.2
3 (2.0×10^{-4})	1.0×10^{-3}	1.0×10^{-7}				
4 (5.3×10^{-5})	1.0×10^{-4}	3.0×10^{-8}				
4 (5.3×10^{-5})	2.0×10^{-4}	9.0×10^{-8}	8.0×10^{-6}	1.8×10^{-2}	1.5×10^{-1}	8.3
4 (5.3×10^{-5})	1.0×10^{-3}	7.0×10^{-8}				

(*) $K_{cat} = V_{max}/[complex]$, (**) $K_{BNPP} = K_{cat}/K_m$

4. CONCLUSIONS

^1H NMR, $^{13}\text{C}\{^1\text{H}\}$ NMR, IR and UV-Vis spectrometric techniques were used to study and characterize new mixed ligand complexes of zinc rosmarinate with N-donor heterocyclic ligands. The synthesized complexes were $[(\text{Zn}(\text{RA})_2)]$ (**1**), $[\text{Zn}(\text{RA})_2(2\text{-}(\text{methylamino})\text{py})_2]$ (**2**), $[\text{Zn}(\text{RA})_2(2,2'\text{-bipy})]$ (**3**), $[\text{Zn}(\text{RA})_4(4,4'\text{-bipy})]$ (**4**), $[\text{Zn}(\text{RA})_2(2,9\text{-dmp})]$ (**5**), and $[\text{Zn}(\text{RA})(2\text{-ampy})_2]$ (**6**).

The prepared zinc complexes with rosmarinic acid in the presence of N-donor ligand were characterized by using various techniques such as IR, UV-Vis, ^1H -NMR, $^{13}\text{C}\{^1\text{H}\}$ NMR, and other physical properties. The proposed structure of complex **2** has two bidentate rosmarinate group and 2 monodentate 2-(methylamino)py ligand, complex **3** has two bidentate rosmarinate group and one bidentate 2,2'-bipy ligand, complex **4** has four monodentate rosmarinate group and one monodentate 4,4'-bipy ligand, complex **5** has two bidentate rosmarinate group and one bidentate 2,9-dmphen ligand, and complex **6** has one bidentate rosmarinate group and two monodentate 2-ampy ligand .

All prepared complexes showed antibacterial activity against different Gram-positive and Gram-negative bacteria. Complex **1** has shown higher antibacterial activity against the test bacteria of *P. aeruginosa* and *K. pneumonia* compared to RA. Complex **2** has shown good antibacterial activity against the test strains of *P. aeruginosa*, and *S. aureus* compared to pure ligand (2,2'-bipy). Complex **3** showed good inhibition activity against all tested Gram-negative bacteria. Complex **4** showed more significant antibacterial activity against the strains of *P. aeruginosa* and *P. mirabilis*. Complex **5** and **6** have shown higher antibacterial higher than their parent ligand.

The rate of the BNPP hydrolysis was determined in order to study the effect of zinc complexes on the phosphates hydrolysis. According to the obtained results the hydrolysis rate rate of BNPP for the **1**, **3**, and **4** complexes as follow: 5.2 at 25 °C, 4.2 at 37 °C, and 8.3 at 41 °C, respectively.

Rosmarinic acid has a lot of interesting biological activities. Its antioxidant activity is higher than that of vitamin E ¹³⁰ and it is the strongest in the hydroxycinnamic acid derivatives series: Rosmarinic acid > chlorogenic acid > caffeic acid > ferulic acid > coumaric acid

The antiviral, antiallergic, neuroprotective, antiinflammatory, anti-HIV, and antitumor effects of rosmarinic acid were showed in the literature.^{146,147} Therefore, further experimental work may include further biological applications of these complexes as anti-cancer agents.

5. REFERENCES

1. Bertini, I. *Biological inorganic chemistry: structure and reactivity*, **2007**.
2. Bertini, I.; Sigel, A.; Sigel, H. *Handbook on Metalloproteins*; Marcel Dekker: New York, 2001; pp 1-1800.
3. Lawrance, G. A. *Introduction to Coordination Chemistry*; Wiley, 2009.
4. Andreini, C.; Banci, L.; Bertini, I.; Rosato, A., *J. Proteome Res.*, **2006**, 5, 196–201.
5. Changela, A.; Chen, K.; Xue, Y.; Holshen, J.; Outten, C. E.; O'Halloran, T. V.; Mondragon, A., *Science*, **2003**, 301, 1383-1387.
6. Finney, L. A.; O'Halloran, T. V., *Science*, **2003**, 300, 931-936.
7. Bertinato, J.; LçAbbe, M. R., *J. Biol. Chem.*, **2003**, 278, 35071-35078.
8. Gwaltney-Brant, S. M. *In Haschek and Rousseaux's Handbook of Toxicologic Pathology (Third Edition)*; Haschek, W. M., Rousseaux, C. G., Wallig, M. A., Eds.; Academic Press: Boston, 2013.
9. Ke, Q.; Costa, M.; Kazantzis, G. *In Handbook on the Toxicology of Metals (Third Edition)*; Nordberg, G. F., Fowler, B. A., Nordberg, M., Friberg, L. T., Eds.; Academic Press: Burlington, 2007.
10. Kaur, K.; Gupta, R.; Saraf, S. A.; Saraf, S. K., *Compr. Rev. Food Sci. Food Saf.*, **2014**, 13, 358–376.
11. Broadley, M.R.; White, .P.J.; Hammond, J.P.; Zelko, I.; Lux, A., *NewPhyto* , **2007**, 173, 677-702.

12. <https://www.shutterstock.com/video/clip-1016792638-periodic-table-30-zinc-element-sign-position>.(Accessed Feb 20, 2020)
13. Osredkar, J.; Sustar, N., *J. Clin. Toxicol.*, **2011**, s3.
14. Pfeiffer, C.C.; Braverman, E.R., *Biol Psychiatry*, **1982**, 17, 513-532.
15. Takagishi, T.; Hara, T.; Fukada, T., *Int. J. Mol. Sci.*, **2017**, 18, 1–21.
16. Auld, D. S., *BioMetals*, **2001**,14, 271–313.
17. Deshpande, J.; Joshi, M.; Giri, P., *Int. J. Med. Sci. Public Heal.*, **2013**, 2, 1.
18. Vallee, B. L.; Falchuk, K. H., *Physiological Reviews*, **1993**, 73.
19. Smart, B., *J Physiol*, **1992**, 447, 587–625.
20. Truong Tran, A.Q.; Carter, J.; Ruffin, R.; Zalewski, PD., *Immunol Cell Biol* , **2001**, 79, 170–177.
21. Hyun, H. J.; et al., *Brain Res.*, **2000**, 869, 39–48.
22. McCabe, MJ.; Jiang, SA.; Orrenius, S., *Lab Invest*, **1993**, 69, 101–110.
23. Szuster-Ciesielska, A.; et al., *Toxicology*, **2000**, 145, 159–171.
24. Lohmann, RD.; Beyersmann, D., *Biochem Biophys Res Commun*, **1993** , 190, 1097–1103.
25. Wolf, C. M.; Morana, S. J.; Eastman, A., *Cell Death Differ.*, **1997**, 4, 125–129.

26. Zelenák, V.; Györyová, K.; Mlynarcík, D., *Met. Based. Drugs*, **2001**, 8, 269–274.
27. Atmaca, S.; Çicek, R.; GÜL ,K., *Tr. J. of Medical Sciences*, **1998**, 28, 595.
28. Szunyogová, E.; et al., *J. Therm. Anal. Cal.*, **2007**, 88, 355–361.
29. Bitanihirwe, B. K. Y.; Cunningham, M. G., *Synapse*, **2009**, 63, 1029–1049.
30. Osis, D.; Kramer, L.; Wiatrowski, E.; Spencer, H., *Am. J. Clin. Nutr.*, **1972**, 25, 582–588.
31. <https://thepaleodiet.com/tag/inflammation-3/>. (Accessed Mar 6, 2020)
32. Coombs, T. L., *Mar Biol*, **1974**, 28, 1–10.
33. Cotton, P. A.; Subar, A. F.; Friday, J. E.; Cook, A, J. *Am. Diet. Assoc.*, **2004**, 104, 921–930.
34. Ma, J.; Betts, N. M., *J. Nutr.*, **2000**, 130, 2838–2843.
35. Arsenault, J. E.; Brown, K. H., *Am. J. Clin. Nutr.*, **2003**, 78, 1011–1017.
36. Maret, W.; Sandstead, H. H., *J. Trace Elem. Med. Biol.*, **2006**, 20, 3–18.
37. Fiske, D. N.; McCoy, H. E.; Kitchens, C. S., *Am. J. Hematol.*, **1994**, 46, 147–150.
38. Singh, K. B.; Taneja, S. K., *Sci Vis*, **2009**, 9, 159–165.

39. Fong, T.; et al, *Haematologica*, **2007**, 92, 1429–1430.
40. Kumar. N; Ahlskog, JE., *Arch Neurol*, **2004**, 61, 604–605.
41. Sirajuddina, M.; Alib, S., *Current Pharmaceutical Design*, **2016**, 22, 6665-6681.
42. Ott I.; Gust R., *Arch. Pharm.*, **2007**, 340, 117-126.
43. Guo, Z.; Sadler, P. J., *Angew. Chem. Int. Ed.*, **1999**, 38, 1512 – 1531.
44. Abrams, M. J.; Murrer, B.A., *Science*, **1993**; 261, 725-730.
45. <https://pubchem.ncbi.nlm.nih.gov/compound/cisPlatin#section=Structures>. (Accessed Mar 7,2020)
46. <https://depositphotos.com/119958944/stock-photo-molecular-structure-of-cisplatin-3d.html>. (Accessed Mar 7,2020)
47. Storr, T.; Thompson, K. H., Orvig, C., *Chem. Soc. Rev.*, **2006**, 35, 534–544.
48. Burgess, J.; Prince, R. H., *Encycl. Inorg. Bioinorg. Chem.*, **2011**.
49. Liu, Z.; et al., *Int. J. Inorg. Chem.*, **2017**, 2017, 8.
50. Franks, M.; Gadzhieva, A.; Ghandhi, L.; et al., *Inorganic Chemistry*, **2013**, 52, 660–670.
51. Szłyk, E.; Wojtczak, A.; Surdykowski, A.; Goździkiewicz, M., *Inorganica Chimica Acta*, **2005**, 358, 467–475.

52. Newman, J. M.; Bear, C. A.; Hambley, T. W.; Freeman, H. C., *Acta Cryst.*, **1990**, C46, 44–48.
53. Song, X. W.; Gao, X. J.; Liu, H. X.; Chen, H.; Chen, C. N., *Inorg. Chem. Commun.*, **2016**, 70, 1–3.
54. Che, W.; et al., *Inorg. Chem. Commun.*, **2016**, 69, 89–93.
55. Ahmed, S.I.; et al., *Polyhedron*, **2000**, 19, 129–135.
56. Finn, R. C.; Zubieta, J.; Haushalter, R. C., *Prog. Inorg. Chem.*, **2003**, 51, 421.
57. Anantharaman, G.; Roesky, H. W.; Magull, J., *Angew. Chem., Int. Ed. Engl.*, **2002**, 41, 1226.
58. Dey, D.; et al., *J. Coord. Chem.*, **2011**, 64, 1165–1176.
59. Zeleňák, V; Vargová, Z ; Györyová, K, *Spectrochimica Acta Part A: Molecular and Biomolecular Spectroscopy*, **2007**, 66, 262-272.
60. Deacon, G. B., R. J. Phillips, *Coord. Chem. Rev.* **1980**, 3, 227–250.
61. Deeth, R. J., *Inorg. Chem.*, **2008**, 47, 6711–6725.
62. Kumar, U.; Thomas, J.; Thirupathi, N., *Inorg. Chem.*, **2010**, 49, 62–72.
63. Kumar, U.; Thomas, J.; Agarwal, M.; Thirupathi, N., *Inorg. Chim. Acta*, **2010**, 370, 122–131.
64. Clegg, W., Little, I. R., Straughan, B. P., *J. Chem. Soc., Dalton Trans*, **1986**, 6, 1283–1288.

65. Clegg, W.; Little, I. R.; Straughan, B. P., *J. Chem. Soc., Chem. Commun.*, **1985**, 2, 73–74.
66. Lewandowski, W.; Kalinowska, M.; Lewandowska, H., *Inorg. Chim. Acta*, **2005**, 358, 2155-2166.
67. Naraa, M.; et al., *FEBS Lett.*, **1994**, 349, 84-88.
68. Medina-Morales, A.; Perez, A.; Brodin, J. D.; Tezcan, F. A., *J. Am. Chem. Soc.*, **2013**, 135, 12013–12022.
69. Nomura, A.; and Sugiura, Y., *Inorg. Chem.*, **2004**, 43, 1708–1713.
70. Patel, K.; Srivastava, K. R.; Durani, S., *Bioorg. Med. Chem.*, **2010**, 18, 8270–8276.
71. Edgar, M.; Mitchell, R.; Slawin, A. M. Z.; Lightfoot, P.; Wright, P. A., *Chem. Eur. J.*, **2001**, 7, 5168.
72. Ghosh, S. K.; Bharadwaj, P. K., *Inorg. Chem.*, **2004**, 43, 6887.
73. A. Shalash, H. Abu Ali, Faculty of Graduate Studies, *Non-steroidal Zn(II) and Co(II) Sulindac Drugs and Bioactive bacterial Effect, Anti-malarial Effect and The Use as Phosphate Hydrolyzing Enzymes*, Birzeit University, **2015**.
74. Szłyk, E.; Wojtczak, A.; Surdykowski, A.; Goździkiewicz, M., *Inorganica Chim. Acta*, **2005**, 358, 467–475.
75. Raymoni, G.; Abu Ali, H. *Appl. Organomet. Chem.*, **2019**, 33, 1–16.
76. Lewiński, J.; et al., *Angew. Chem. Int. Ed.*, **2008**, 47, 573 –576.

77. Clegg, W.; et al., *Inorganica Chim. Acta*, **1991**, 186, 51–60.
78. Rardin, R. L.; Tolman, W. B.; Lippard, S. J. *New J. Chem.*, **1991**, 15, 417-430.
79. Adeniyi Adebayo, A.; Ajibade Peter, A., *Bioinorg Chem Appl*, **2018**, 2018, 1565-3633
80. Thorp, H., *Chemistry & Biology*, **1998**, 5, 125-127.
81. Abu Ali, H.; Maloul, S.; Abu Ali, I.; Akkawi, M.; Jaber, S., *J. Coord. Chem.*, **2016**, 69, 2514-2522
82. Ashish, B.; Pandeya, S. N., *Int. J. Res. Ayurveda Pharm.*, **2011**, 2, 1124.
83. Ali, I.; Lone, M.; Al-Othman, Z.; Al-Warthan, A.; Sanagi, M.; *Curr. Drug Targets*, **2015**, 24, 711-734.
84. Abu Ali, H.; Omar, S., *Journal of Coordination Chemistry*, **2017**, 70, 1-17.
85. Chen, X.M.; et al., *Polyhedron*, **1994**, 13, 2079-2083.
86. Ignat, I.; et al., *Food Chemistry*, **2011**, 126, 1821–1835.
87. Balasundram, N.; et al., *Food Chemistry*, **2006**, 99, 191–203.
88. Alagawany, M.; et al., *Animal Health Research Reviews*, **2017**, 18, 1-10.
89. Nadeem, M.; et al., *Appl. Sci.*, **2019**, 9, 3139.

90. Cao, H.; et al., *Journal of Molecular Structure*, **2005**, 719, 177–183.
91. Tepe, B., *Bioresource Technology*, **2008**, 99, 1584–1588.
92. Petersen, M.; et al., *Phytochemistry*, **2009**, 70, 1663–1679.
93. Gordo, J.; Maximo, P.; Cabrita, E.; Lourenco, A.; Oliva, A.; Almeida, J.; Filipe, M.; Cruz, P.; Barcia, R.; Santos, M.; et al., *Nat. Prod. Commun.*, **2012**, 7, 1491–1494.
94. Al-Sereiti, M. R.; Abu-Amer, K. M.; Sen, P., *Indian J. Exp. Biol.* , **1999**, 37, 124–130.
95. Zheng, W.; Wang, S. Y., *J. Agric. Food Chem.*, **2001**, 49, 5165–5170.
96. Ito, H.; Miyazaki, T.; Ono, M.; Sakurai, H., *Bioorganic Med. Chem.*, **1998**, 6, 1051–1056.
97. Takeda, H.; Tsuji, M.; Matsumiya, T.; Kubo, M., *Nihon Shinkei Seishin Yakurigaku Zasshi*, **2002**, 22, 15–22.
98. Raeisi, M.; Tabaraei, A.; Hashemi, M.; Behnampour, N. *Int. J. Food Microbiol*, **2016**, 238, 139–145.
99. Ekambaram, S. P.; Perumal, S. S.; Balakrishnan, A.; Marappan, N.; Gajendran, S. S.; Viswanathan, V., *J. Intercult. Ethnopharmacol*, **2016**, 5, 358–363.
100. Moreno, S.; Scheyer, T.; Romano, C. S.; Vojnov, A. A. *Free Radical Research*, **2006**, 40, 223–231.
101. Benedec, D.; et al., *Pak. J. Pharm. Sci.*, **2015**, 28, 2297–2303.

102. Fadel, O.; El Kirat, K.; Morandat, S., *Biochim. Biophys. Acta Biomembr.*, **2011**, 1808, 2973–2980.
103. Fernando, P.M.; et al, *Biomol Ther (Seoul)*., **2016**, 24, 75–84.
104. Hadjer, F.; Tahar, B.; Eddine, A. D.; Sofiane, D. , *J. Mater. Environ. Sci.*, **2018**, 9, 2153–2157.
105. Viganor, L.; et al., *Current Topics in Medicinal Chemistry*, **2017**, 17, 1280-1302.
106. Singh, U.; et al., *Microb. Pathog.*, 93, **2016**, 172–179.
107. Blackman, A. G., *Polyhedron*, **2005**, 24, 1-39.
108. Valle-Orta, M.; DÍaz, D.; Dubé, Inti.; Quiñonez, J.; Guerrero, R. *Journal of Physics*, **2017**, 838, 1-9.
109. Xie, J.; Li, C.; Wang, M.; Jiang, B. *Chemical Papers*, **2013**, 67(4), 365-371.
110. Xie, J.; Jiang, B.; Kou, X.; Hu, C.; Zeng, X. *Transition Metal Chemistry*, **2003**, 28, 782-787.
111. Auld, D.S. (1987) In: Page, M.I. and Williams, A. (eds), *Enzyme mechanism*. RCS, London.
112. Westheimer, F. H., *Science*, **1987**, 235, 1173.
113. Rossi, L. M.; Neves, A.; Hoerner, R., *Inorg. Chim. Acta*, **2002**, 337,366.

114. Iranzo, O.; Kovalecsky, A. Y.; Morow, J.R. et al., *J. Am. Chem. Soc.*, **1988**, 125, 1988.
115. Tonde, S. S.; Kumbhar, A. S.; Padhye, S. B. J., *Inorg. Biochem.*, **2006**, 100, 51.
116. Ferreira, D. E. C.; Almeida, W. B. D.; Neves, A. ; et al., *Phys. Chem. Chem. Phys.*, **2008**, 10, 7039.
117. Ercan, A.; Tay, W. M.; Grossman, S. H.; et al., *J. Inorg. Biochem.*, **2010**, 104, 19.
118. Paola, G. T.; Idania, V. Z.; Olga, T.; et al., *J. Org. Chem.*, **2006**, 71, 9713.
119. Chapman, W. H.; Breslow, R., *J. Am. Chem. Soc.*, **1995**, 117, 5462.
120. Vassilev, K.; Kreider, J.; Miller, P. D.; et al., *React. Funct. Polym.*, **1999**, 41, 205.
121. You, J. S.; Yu, X. Q. ; Su, X. Y; et al., *J. Mol. Catal. A: Chemical*, **2003**, 202, 17.
122. Rossi, L.M.; Neves, A.; Horner, R.; et al., *Inorg. Chim. Acta*, **2002**, 337, 366.
123. Cheng, S. Q.; Zeng, X. C.; Yu, X. Q. et al., *J. Colloid Interface Sci.*, **2000**, 224, 333.
124. Gunnlaugsson, T.; O'Brien, J.E.; Mulready, S., *Tetrahedron Lett.*, **2002**, 43, 8493
125. Feng, G.Q.; Natale, D.; Prabakaran, R.; Mareque-Rivas, J.C.; Williams, N.H., *Angew. Chem. Int. Ed.*, **2006**, 45, 7056–7059.

126. Lipscomb W.N.; N. Sträter, *Chem. Rev.* **1996**, 96, 2375–2434.
127. Mancin, F.; Tecilla, P., *New J. Chem.*, **2007**, 31,800–817.
128. Zhang, X. *et al. J. Mol. Catal. A Chem.*, **2013**, 368–369, 53–60.
129. Ran, X. ; Wang, L. ; Lin, Y. ; Hao, J. ;Cao, D., *Appl. Organometal. Chem.*, **2010**, 24, 741–747.
130. Swisłocka, R.; Regulska, E.; Karpinska, J.; Swiderski, G.; Lewandowski, W. *Molecules*, **2019**, 24.
131. Chemical Book, CAS DataBase. [http://www.chemicalbook.com/Spectrum_EN_\(504-29-0\)_1HNMR.htm](http://www.chemicalbook.com/Spectrum_EN_(504-29-0)_1HNMR.htm) (Accessed Dec 24, 2020).
132. Chemical Book, CAS DataBase. http://www.chemicalbook.com/Spectrum_EN_366-18-7_1HNMR.htm (Accessed Dec 24, 2020)
133. Chemical Book, CAS DataBase. http://www.chemicalbook.com/Spectrum_EN_553-26-4_1HNMR.htm (Accessed Dec 24, 2020).
134. Gillard, R. D.; Kane-Maguire, L. A. P.; Williams, P. A. *Transition Met. Chem.*, **1977**, 2, 55-57.
135. Elmkaddem, M. K.; Fischeister, C.; Thomas, C. M.; Renaud, J. L. *Chem. Commun.*, **2010**, 46, 925-927.
136. Iqbal, M. S.; Bukhari I. H.; Arif, M., *Appl. Organometal. Chem.*, **2005**, 19, 864–869
137. M. Darawsheh et al., *European Journal of Medicinal Chemistry*, **2014**, 82, 152-163.

138. Alabdali, A. J.; Ibrahim, F. M., *Journal of Applied Chemistry*; **2014**; Vol. 6.
139. Galani, A.; Efthimiadou, E. K.; Mitrikas, G.; Sanakis, Y.; Psycharis, V.; Raptopoulou, C.; Kordas, G.; Karaliota, A. *Inorganica Chim. Acta* **2014**, 423 (PART A), 207–218.
140. Niven, M. L.; Percy, G. C.; Nakamoto, K., *Infrared Spectra of Inorganic and Coordination Compounds*; Wiley-Interscience, **1978**; Vol. 3.
141. Chohan, Z. H.; Supuran, C. T.; Scozzafava, A.; *J. Enz. Inhib. Med.Chem.*, **2004**, 19, 79.
142. Thangadurai, T. D.; Natarajan, K., *Trans. Met. Chem.*, **2002**, 27, 485.
143. Lawrence, P. G.; Harold, P. L.; Francis, O. G.; *Antibiot. Chemther.* **1980**, 1597.
144. Fadel, O.; El Kirat, K.; Morandat, S., *Biochim. Biophys. Acta*, **2011**, 1808, 2973–2980.
145. Generali'c Mekini'c, I.; Skroza, D.; Ljubenkovic, I.; Šimat, V.; Smole Možina, S.; Katalini'c, V., *Food Technol. Biotechnol.*, **2014**, 52, 119–127.
146. Sánchez-Campillo, M.; Gabaldon, J.A.; Castillo, J.; Benavente-García, O.; Del Baño, M.J.; Alcaraz, M.; Vicente, V.; Alvarez, N.; Lozano, J.A. *Food Chem. Toxicol.*, **2009**, 47, 386–392.
147. Kim, G.D.; Park, Y.S.; Jim, Y.H.; Park, C.S., *Appl. Microbiol. Biotechnol.*, **2015**, 99, 2083–2092.

6. APPENDICES

Appendix A: $^1\text{H-NMR}$ spectra of complexes 2-6.

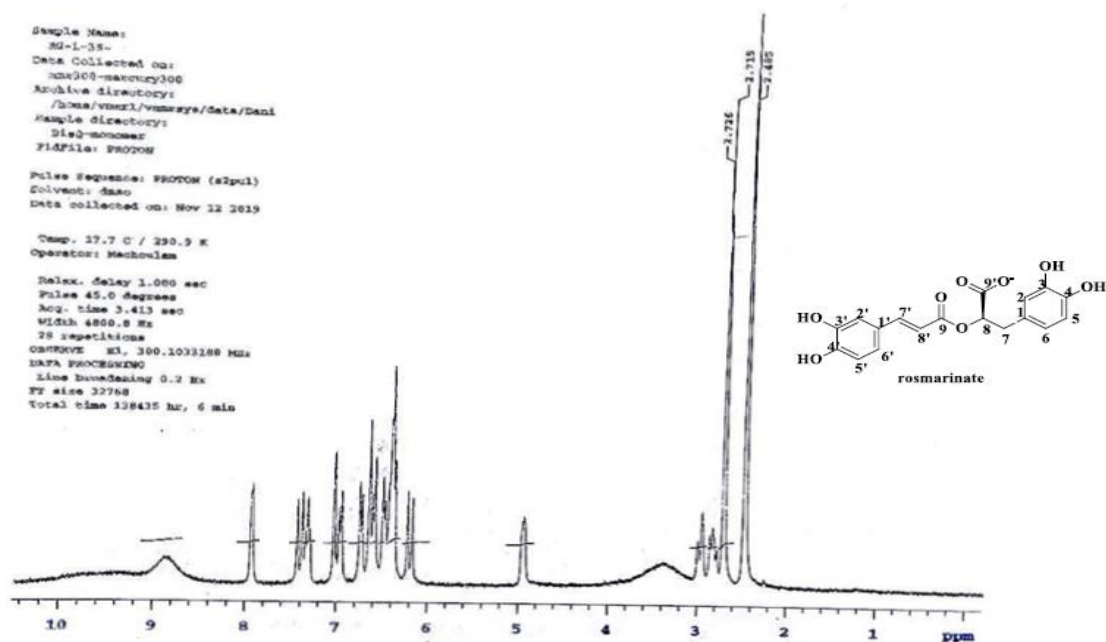


Figure S1. $^1\text{H-NMR}$ spectra of complex 2.

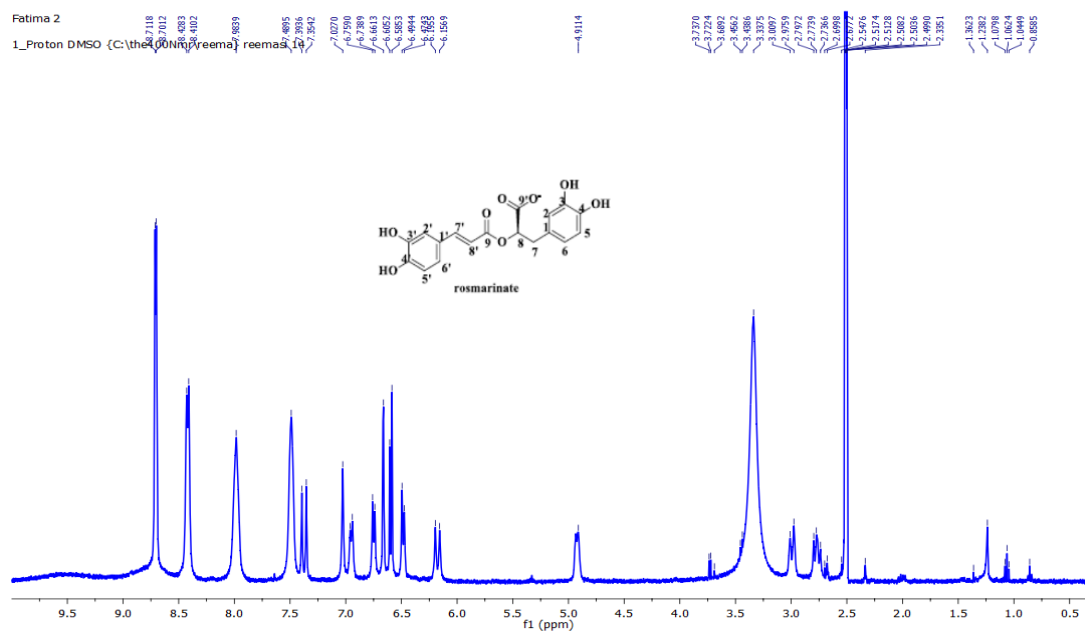


Figure S2. $^1\text{H-NMR}$ spectra of complex 3.

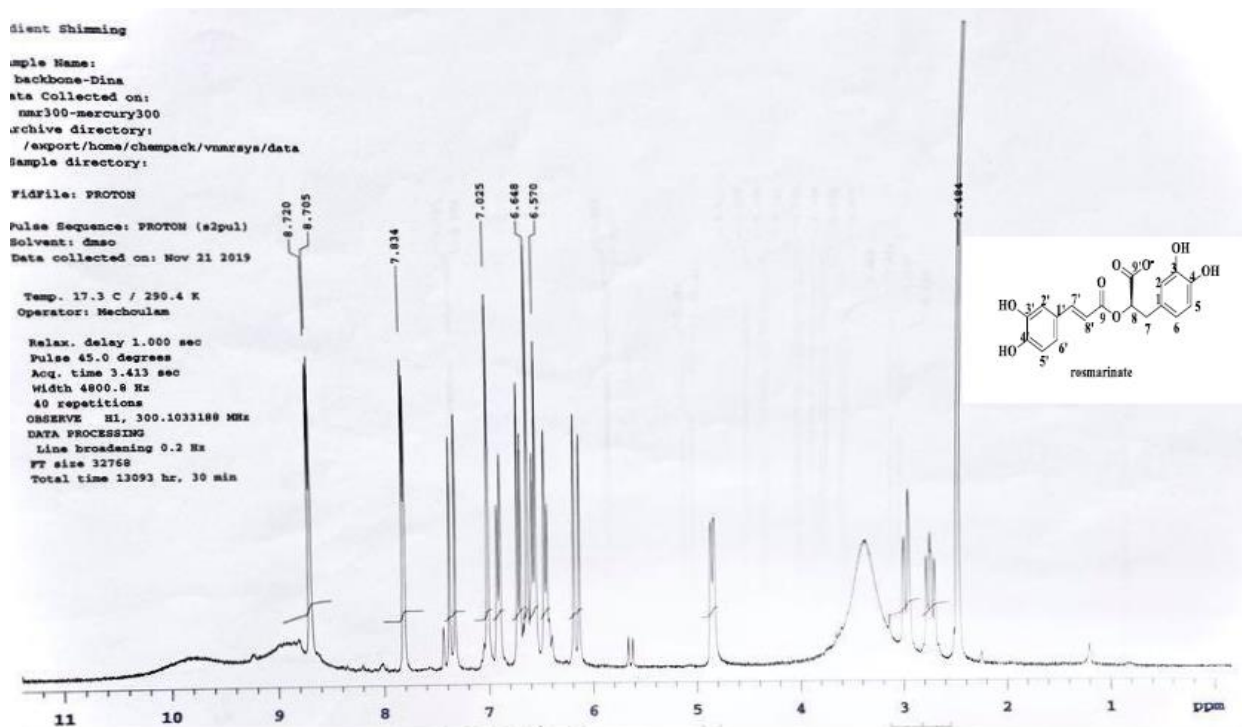


Figure S3. $^1\text{H-NMR}$ spectra of complex 4.

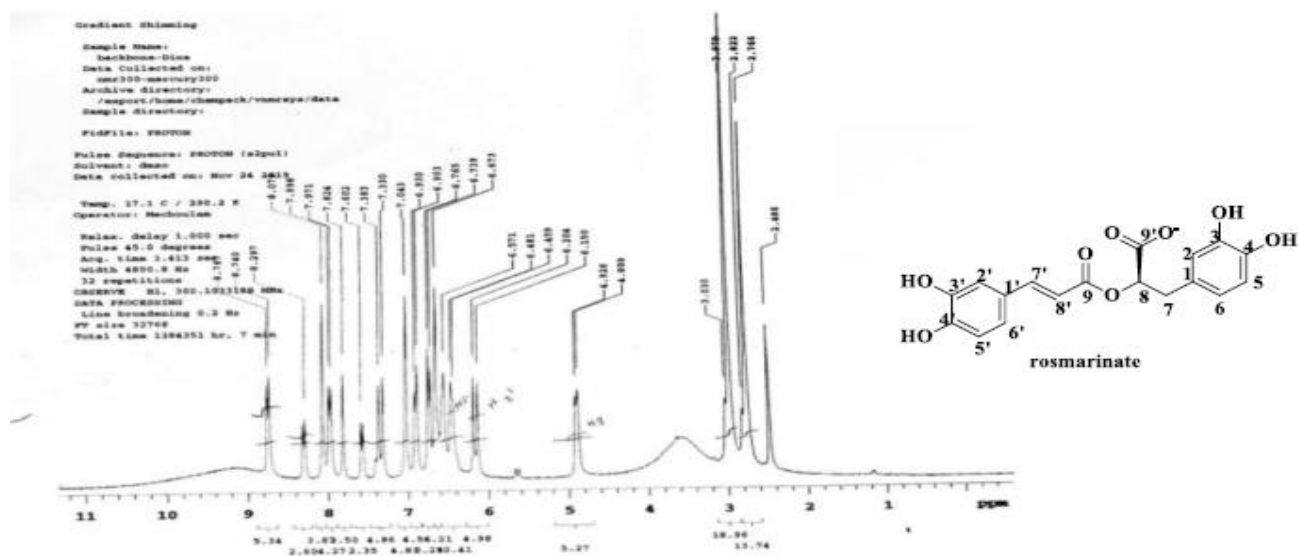


Figure S4. $^1\text{H-NMR}$ spectra of complex 5.

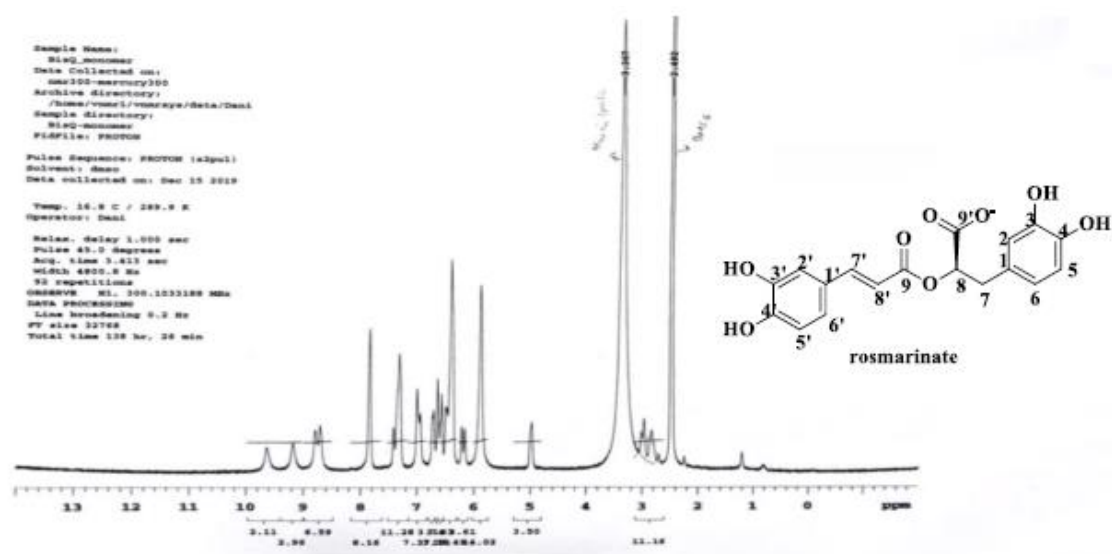


Figure S5. $^1\text{H-NMR}$ spectra of complex 6.

Appendix B: IR spectra of complexes 2-6.

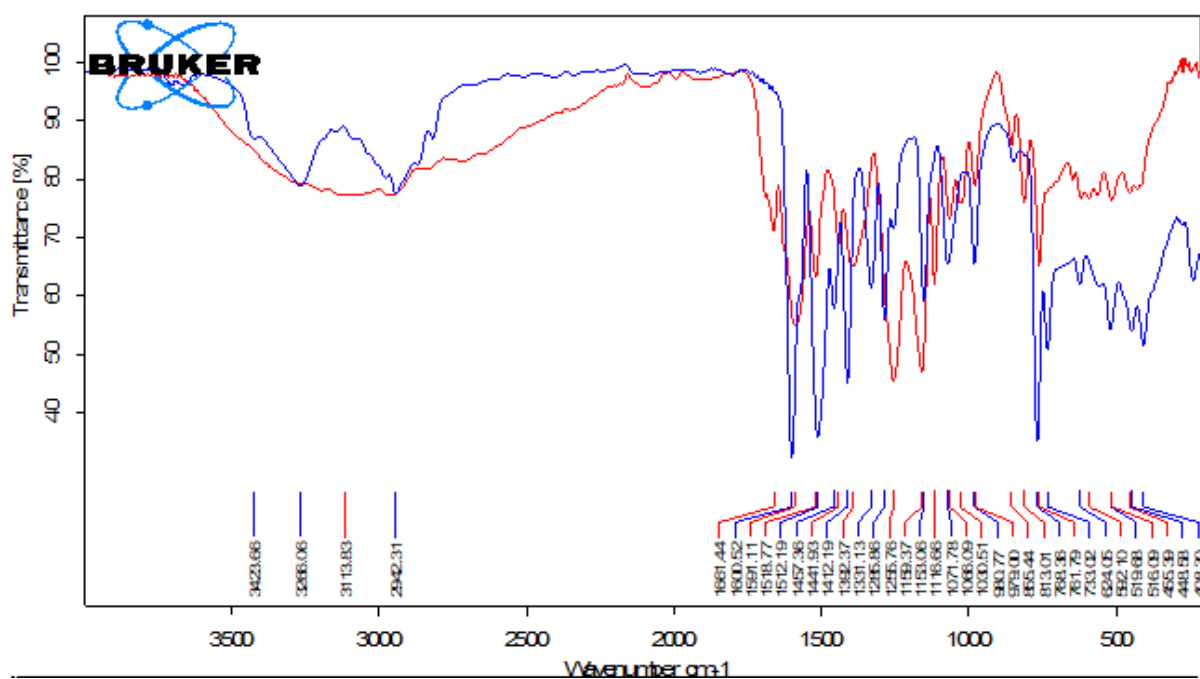


Figure S6. IR spectra of complex 2 (red) and 2-(methylamino)py (blue).

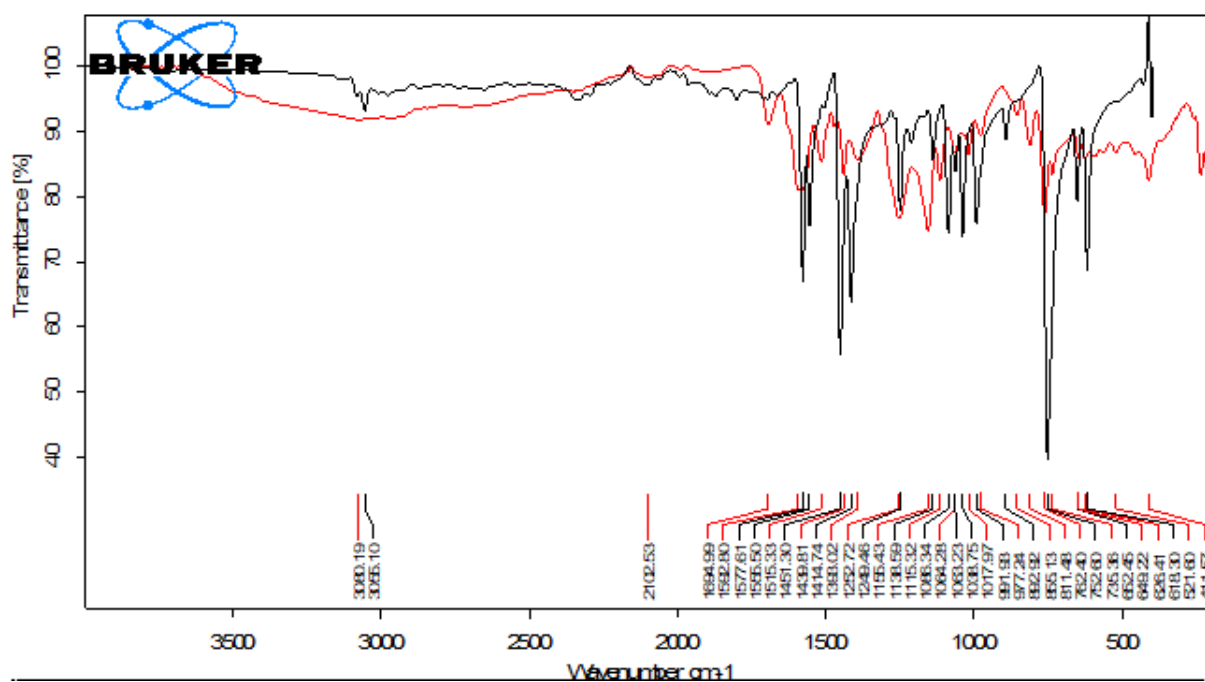


Figure S7. IR spectra of complex **3** (red) and 2,2'-bipy (black).

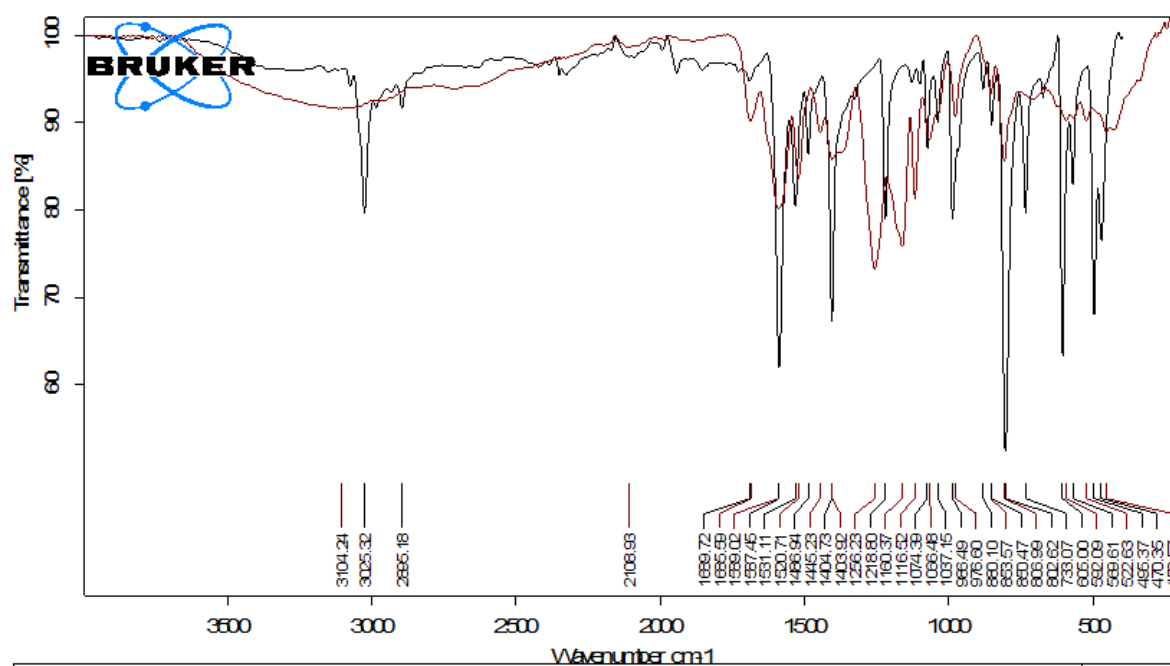


Figure S8. IR spectra of complex **4** (dark red) and 4,4'-bipyridine (black).

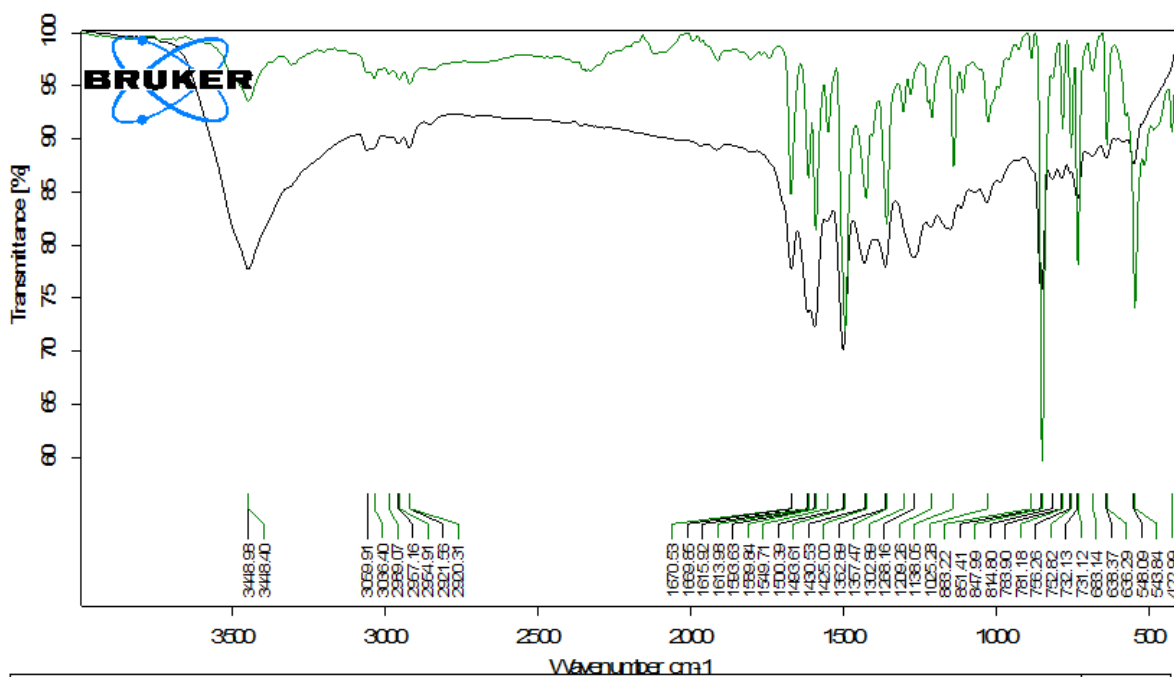


Figure S9. IR spectra of complex **5** (black) and 2,9-dmp (green).

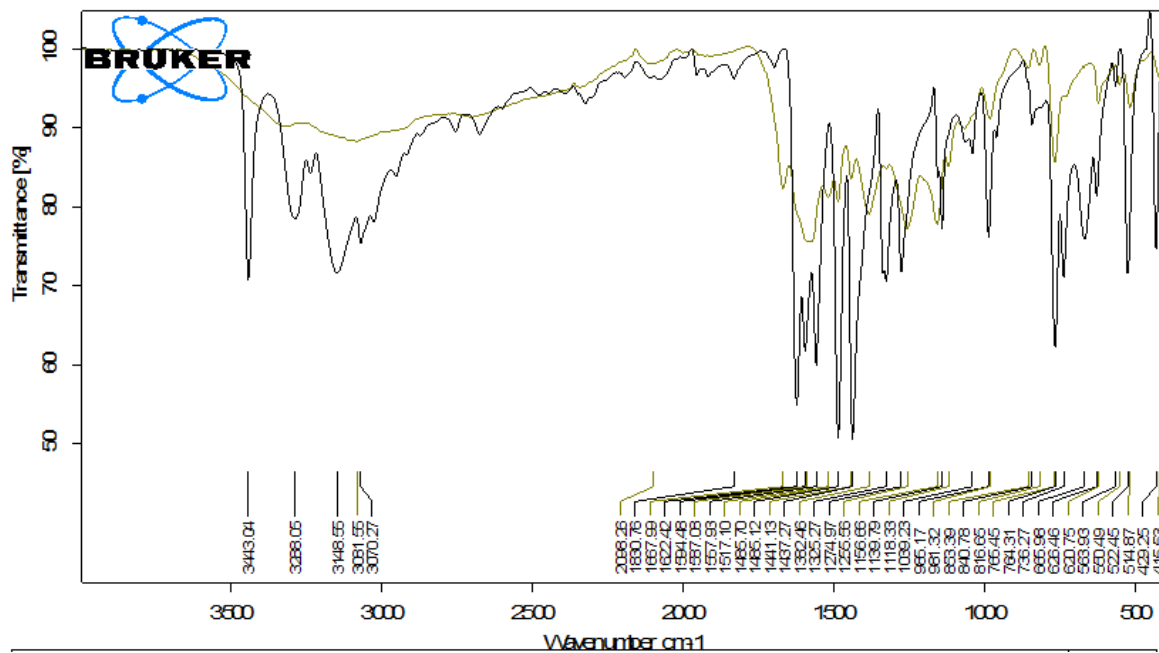
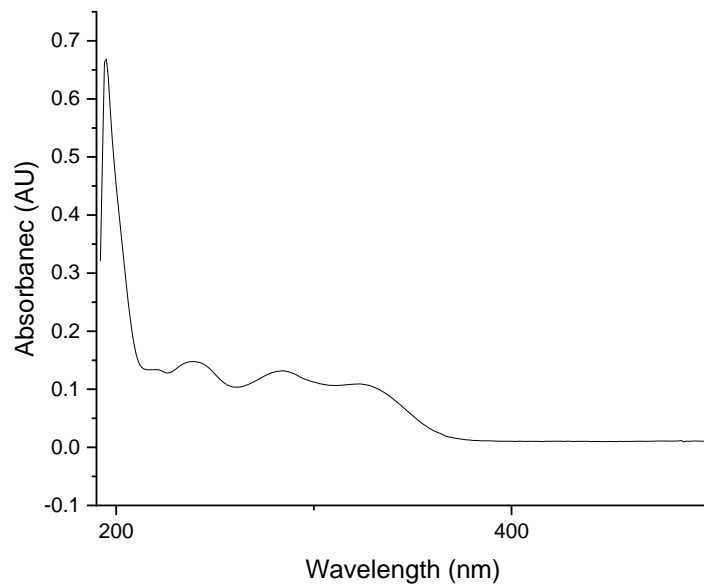
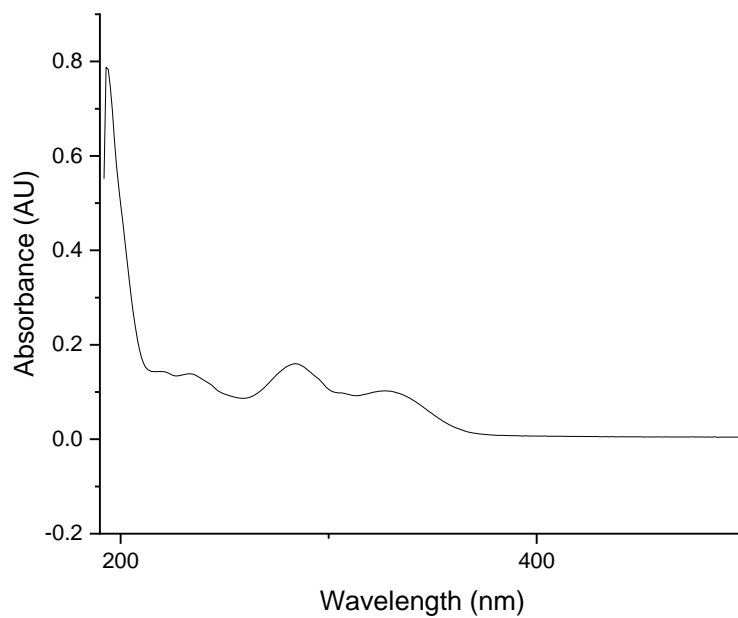


Figure S10. IR spectra of complex **6** (green) and 2-ampy (black)

Appendix C: UV-Vis spectra of complexes 2-6.**Figure S11.** UV-Vis spectra of complex **2**.**Figure S12.** UV-Vis spectra of complex **3**.

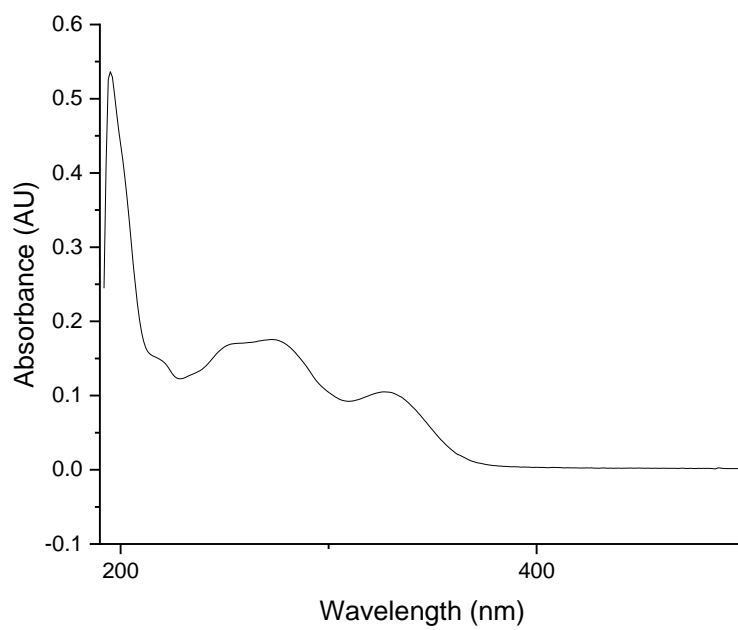


Figure S13. UV-Vis spectra of complex 4.

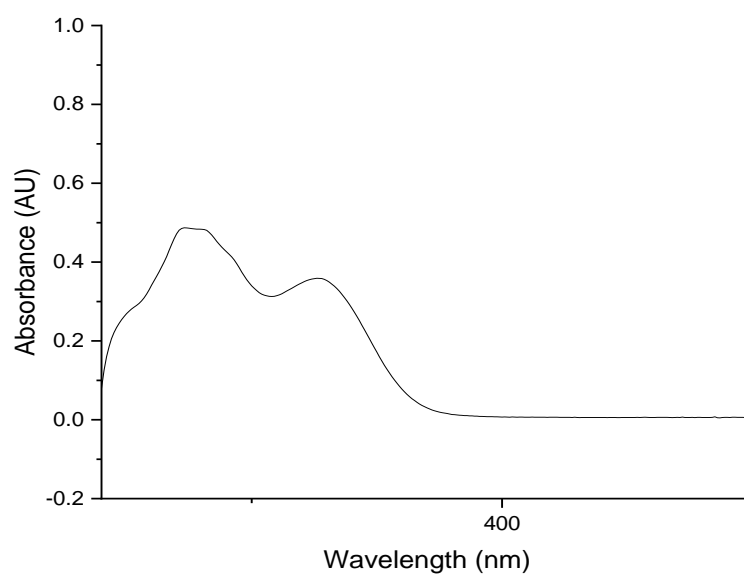


Figure S14. UV-Vis spectra of complex 5.

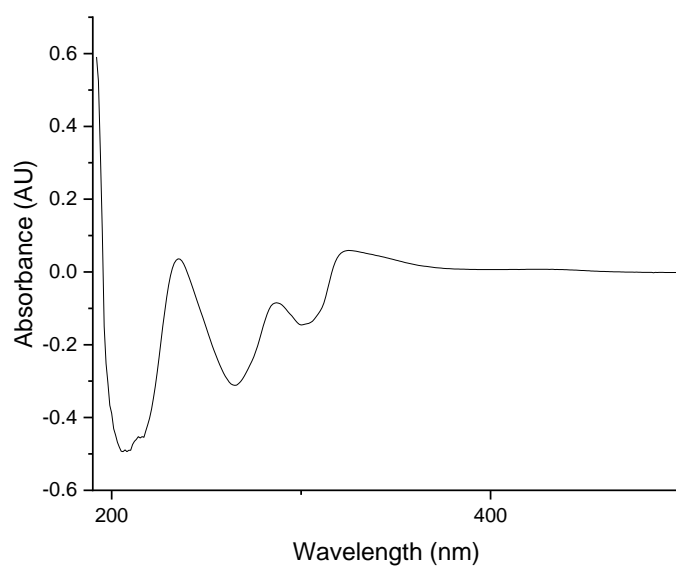


Figure S15. UV-Vis spectra of complex **6**.